

IN-PLANE SEISMIC STRENGTHENING OF BRICK MASONRY WALLS
USING RE-BARS

A THESIS SUBMITTED TO
THE GRADUATE SCHOOL OF NATURAL AND APPLIED SCIENCES
OF
MIDDLE EAST TECHNICAL UNIVERSITY

BY

MURAT ERDOĞDU

IN PARTIAL FULFILLMENT OF THE REQUIREMENTS
FOR
THE DEGREE OF MASTER OF SCIENCE
IN
CIVIL ENGINEERING

OCTOBER 2008

Approval of the thesis:

**IN-PLANE SEISMIC STRENGTHENING OF BRICK MASONRY WALLS
USING RE-BARS**

submitted by **MURAT ERDOĞDU** in partial fulfillment of the requirements for
the degree of **Master of Science in Civil Engineering Department, Middle East
Technical University** by,

Prof. Dr. Canan ÖZGEN _____
Dean, Graduate School of **Natural and Applied Sciences**

Prof. Dr. Güney ÖZCEBE _____
Head of Department, **Civil Engineering**

Assist. Prof. Dr. Ahmet TÜRER _____
Supervisor, **Civil Engineering Dept., METU**

Examining Committee Members:

Prof. Dr. Haluk SUCUOĞLU _____
Civil Engineering Dept., METU

Assist. Prof. Dr. Ahmet TÜRER _____
Civil Engineering Dept., METU

Assist. Prof. Dr. Murat Altuğ ERBERİK _____
Civil Engineering Dept., METU

Assist. Prof. Dr. Erdem CANBAY _____
Civil Engineering Dept., METU

Dr. Afşin CANBOLAT _____
Yüksel Proje Uluslararası A.Ş.

Date: 20.11.2008

I hereby declare that all information in this document has been obtained and presented in accordance with academic rules and ethical conduct. I also declare that, as required by these rules and conduct, I have fully cited and referenced all material and results that are not original to this work.

Name, Last name: Murat, ERDOĞDU

Signature :

ABSTRACT

IN-PLANE SEISMIC STRENGTHENING OF BRICK MASONRY WALLS USING RE-BARS

Erdođdu, Murat

M. Sc., Department of Civil Engineering

Supervisor: Assist. Prof. Dr. Ahmet Türer

October 2008, 116 pages

About half of the total building stock in Turkey is masonry type building [1]. Masonry buildings in Turkey, especially in rural areas, are constructed without any engineering knowledge mostly by their own residents. They generally have heavy roofs. Masonry type buildings also have thick and heavy wall materials. Heavy roof and wall material generate large inertial forces in the case of an earthquake. Brittle failure of walls leads to total failure of whole system followed by sudden collapse of heavy roof. The aim of this thesis is to understand failure mechanisms of brick masonry walls, prevent their brittle failure and allow the walls to dissipate energy during an earthquake. Furthermore, ultimate capacity increase was also targeted by using low cost and easy to obtain material.

In order to find an economical and effective way in strengthening of brick masonry walls in their in-plane direction, steel rebars were used as post-tensioning materials in brick masonry walls and house tests. Springy connections were utilized in the reinforcing and post-tensioning bars in order to prevent early loss of post-tension due to wall cracking or rebar yielding. Separate tests were conducted with and without rebars and springs in order to compare their results.

The test results indicated that the ultimate lateral load capacity of 6m long brick masonry house increased up to about 6 times with respect to its nominal value. Energy dissipation also increased up to about 10 times of the original house.

Lateral load capacity increase in 2m long rebar post-tensioned brick masonry walls were measured as about 17 times when compared with the original wall. The energy dissipation capacity was also increased about 30 times the nominal value.

A general procedure was developed to assess the vulnerability of single storey masonry houses, which calculates the earthquake demand acting on each wall segment. Comparison of capacity versus demand enables evaluation of wall segments and leads strengthening calculations if necessary. Derived formulas were used to calculate post-tensioning force and design vertical and diagonal rebars. The procedure was demonstrated using properties of an existing house and strengthening cost was found to be about 10% of the building cost.

The results of the conducted tests have shown that rebar post-tensioning of brick masonry walls is an effective and cost-efficient way of strengthening the walls in their in-plane direction and can be used as an economical and simple technique for seismically vulnerable masonry houses. Spring based connection detail has improved the post cracking performance of the walls at large deformations by keeping the wall reaction higher after ultimate strength has reached as well as increased the energy dissipation capacity of the walls.

Keywords: Earthquake, Masonry, In-plane, Rebar post-tensioning

ÖZ

TUĞLA DUVARLARIN DONATI ÇELİĞİ KULLANILARAK DÜZLEM-İÇİ YÖNDE DEPREME KARŞI GÜÇLENDİRİLMESİ

Erdoğan, Murat

Yüksek Lisans, İnşaat Mühendisliği Bölümü

Tez Yöneticisi: Yard. Doç. Dr. Ahmet Türer

Ekim 2008, 116 sayfa

Türkiye'deki yapı stokunun yaklaşık yarısı yığma türü yapılardan oluşmaktadır. Bu yapılar genellikle ev sahipleri tarafından hiçbir mühendislik bilgisi kullanılmadan inşa edilmektedir. Bu yapıların çatıları oldukça ağırdır. Ayrıca duvarlar da geniş ve ağır malzemedir oluşmaktadır. Çatı ve duvar ağırlıkları deprem esnasında yüksek atalet kuvvetleri oluşturmaktadır. Duvarlarda meydana gelen gevrek kırılmalar çatının düşmesiyle birlikte komple bir yıkıma dönüşmektedir. Bu tezin amacı, yığma duvarların yıkılma biçimlerini anlamak, deprem anında duvarlarda meydana gelen bu gevrek kırılmaları önlemek ve duvarların daha çok enerji sönümlemesini sağlamaktır. Ayrıca ucuz ve kolay bulunabilen malzemeler kullanılarak duvarın taşıma gücünü artırmak da hedeflenmiştir.

Tuğla duvarların kendi düzlemleri içinde etkili ve ekonomik bir biçimde güçlendirilmesini sağlamak için yığma duvar ve ev testlerinde ard germe olarak inşaat demirleri kullanılmıştır. Çatlak sonrasında ard germe etkisinin erken kaybolmasını engellemek için demirler üzerinde ayrıca yaylı bağlayıcılar kullanılmıştır. Testler karşılaştırma yapabilmek için boş, ard germeli ve yaylı ard germeli olarak farklı biçimlerde uygulanmıştır.

6 m uzunluğundaki ev testlerinde yapılan gözlemlere göre yatay yük kapasitesi, boş ev ile karşılaştırıldığında, yaklaşık 6 kat artmıştır. Ayrıca enerji sönümlenmesi yaklaşık 10 kat artmıştır.

Tek katlı yığma evlerin her duvarına etkiyen deprem kuvvetlerini hesaplayan ve depreme karşı yapının zayıflığını değerlendiren bir genel prosedür geliştirilmiştir. Her duvara etki eden deprem kuvveti ve duvar kapasitesinin karşılaştırılması, duvarların değerlendirilmesine ve gerekli görülmesi durumunda güçlendirilmesine olanak tanımaktadır. Geliştirilen formüller kullanılarak, güçlendirme için gerekli olan ard-germe kuvvetleri ve düşey ya da diyagonal germe çubuklarının tasarımı yapılmıştır. Prosedürün kullanımı, halihazırda bulunan bir ev örneği kullanılarak gösterilmiştir ve bu ev için güçlendirme masrafı, yapının maliyetinin yaklaşık %10'u olarak hesaplanmıştır.

2 m uzunluğundaki tuğla duvar testlerinde, yatay yük kapasitesinde, boş duvar ile karşılaştırıldığında yaklaşık olarak 17 kat artış gözlemlenmiştir. Ayrıca enerji sönümlenme kapasitesi yaklaşık 30 kat artmıştır.

Bu testlerin sonucu göstermiştir ki, tuğla duvarlar üzerinde donatı demirleriyle yapılan ard germe işlemi, duvarların kendi düzlemleri içerisinde etkili ve ekonomik bir güçlendirme oluşturmuş ve bu sistemin depreme karşı savunmasız olan yığma binalar üzerinde ekonomik ve basit bir teknik olarak kullanılabilmesi görülmüştür. Yaylı demirler duvarın çatlama sonrası direncini yüksek tutarak çatlama sonrasında oluşan yüksek deformasyonlarda bile duvarın davranışını geliştirmiş ve duvarın enerji sönümlenme kapasitesini artırmıştır.

Anahtar Kelimeler: Deprem, Yığma bina, Düzlem içi, Donatı ard gemesi

To My Family

ACKNOWLEDGEMENTS

The author wishes to express his deepest gratitude to his supervisor Assist. Prof. Dr. Ahmet Türer for his guidance, advice, criticism, encouragement and insight throughout the project.

I would like to thank to technical staff of structural mechanics laboratory for their help and support in preparation of the tests.

I also would like to thank to my parents and all my family members for their encouragement and assistance throughout this long and difficult study.

This work is supported by Scientific Research and Technical Council of Turkey (TÜBİTAK). The funding provided by TÜBİTAK is gratefully acknowledged.

TABLE OF CONTENTS

ABSTRACT	iv
ÖZ.....	vi
ACKNOWLEDGEMENTS	ix
TABLE OF CONTENTS	x
LIST OF TABLES	xiii
LIST OF FIGURES.....	xiv
LIST OF SYMBOLS	xviii
CHAPTERS	
1. INTRODUCTION.....	1
1.1 The current percentage and distribution of masonry buildings in Turkey	2
1.2 Literature survey	4
1.3 Objectives and scope.....	13
2. VULNERABILITY EVALUATION STUDIES ON MASONRY BUILDINGS.....	15
2.1 Common collapse mechanisms of URM houses and analytical approaches to the problems	15
2.1.1 Overturning of the walls in out of plane direction	17
2.1.2 Blow-out of the wall.....	18
2.1.3 In-plane shear demand calculation and failure of URM walls.....	20
2.1.3.1 Example house	29
3. MATERIALS AND MATERIAL TESTS	33
3.1 Brick compression test	34
3.2 Mortar compression test.....	35
3.3 Masonry shear test (triplet test).....	36
4. HALF-SCALE BRICK MASONRY HOUSE TESTS	38
4.1 Evaluation of test setup	40
4.2 First test: Original unstrengthened specimen.....	42

4.3 Second test: Cracked specimen with 50 kN of weight over it	48
4.4 Third test: Cracked specimen with 10 ϕ 16mm vertical post-tensioning rebar (total vertical post-tensioning force of 200 kN and tightening bolt during testing)	51
4.5 Fourth test: New specimen with post-tensioning using spring boxes along with 10 ϕ 16mm vertical rebar (total vertical post-tensioning force of 200 kN).....	54
4.6 Fifth test: New specimen with post-tensioning using spring boxes along with 10 ϕ 16mm vertical rebar and 12 ϕ 16mm diagonal rebar (direct welding).....	57
4.7 Sixth test: New specimen with post-tensioning using spring boxes along with 10 ϕ 16mm vertical rebar and 12 ϕ 16mm diagonal rebar (heated to about 100 °C before welding into its place).....	60
5. REBAR POST-TENSIONED SINGLE BRICK MASONRY WALL TESTS ..	65
5.1 First test: Original unstrengthened wall	67
5.2 Second test: Cracked wall specimen strengthening using 4 ϕ 16mm vertical post-tensioning bars along with spring boxes (total vertical post-tensioning force of 4 \times 30kN =120 kN).....	71
5.3 Third test: Original unstrengthened wall.....	73
5.4 Fourth test: Cracked wall specimen strengthening using 4 ϕ 16mm vertical post-tensioning bars along without spring boxes (total vertical post-tensioning force of 4 \times 30kN =120 kN).....	74
5.5 Fifth test: Horizontally post-tensioned (third) specimen in addition to vertical post-tensioning using spring boxes along with 4 ϕ 16mm vertical rebar (total vertical post-tensioning force of 120 kN; total horizontal post-tensioning of 30 kN).....	77
5.6 Sixth test: New (4th) specimen with diagonal post-tensioning using spring boxes with 4 ϕ 16mm diagonal rebar (total vertical post-tensioning force of 85 kN).....	81

5.7 Seventh test: New (5th) specimen with diagonal post-tensioning using spring boxes with 4φ16mm diagonal rebars (total vertical post-tensioning force of 85 kN)	83
5.8 Eighth test: Horizontally post-tensioned (30 kN) new (6th) specimen with vertical post-tensioning using spring boxes along with 4φ16mm vertical rebars and diagonal post-tensioning using spring boxes along with 4φ16mm diagonal rebars (total vertical post-tensioning force of 205 kN) .	85
5.9 Ninth test: Similar to the eighth test without spring boxes; horizontally post-tensioned (30 kN) new (7th) specimen with vertical post-tensioning using 4φ16mm vertical rebars and diagonal post-tensioning using 4φ16mm diagonal rebars (total vertical post-tensioning force of 205 kN)	88
6. DISCUSSION OF RESULTS AND CONCLUSIONS	92
6.1 General discussion of results (overview)	92
6.1.1 Material Tests	93
6.1.2 Rebar Post-Tensioned Half-Scale Brick House Tests.....	95
6.1.3 Rebar Post-Tensioned Brick Masonry Wall Tests	99
6.1.4 Damage patterns and strengthening procedures for URM walls using post-tensioning rebars.....	102
6.1.4.1 Post-tensioning application using bolts.....	105
6.1.4.2 Example application using Antakya house and cost evaluation	106
6.2 Conclusions	111
6.3 Future studies	112
REFERENCES	113
APPENDICES	
A. STIFFNESS CURVES	116

LIST OF TABLES

Table 4.1 Data for wall segments of test house.....	43
Table 4.2 Smoke emitting temperatures for common oils (Derrick Riches)	62
Table 5.1 Analytically calculated and experimental strength values of unstrengthened wall.....	71
Table 5.2 Analytically calculated and experimental strength values of the second test	73
Table 5.3 Analytically calculated and experimental strength values of the fifth test	80
Table 6.1 Wall data of the example house in longitudinal direction.....	107
Table 6.2 Demands, strengths, and rating factors of the wall piers in longitudinal direction.....	108
Table 6.3 Required vertical force on the URM house.....	109
Table 6.4 Checking of the walls against diagonal shear failure due to applied vertical post-tensioning on the URM house.....	109
Table 6.5 Wall data of the example house in transverse direction.....	110
Table 6.6 Demands, strengths, and rating factors of the wall piers in transverse direction.....	110

LIST OF FIGURES

Figure 1.1 a) Out of plane failure, b) Corner opening, c) Vertical cracks, d) Roof falling	2
Figure 1.2 Distribution of ratio of masonry houses to total buildings in Turkey [19]	3
Figure 1.3 Population living in masonry houses in Turkey [19].....	3
Figure 1.4 Assumptions for rocking strength evaluation of a wall failing with crushing at the base corner	5
Figure 2.1 Out of plane collapse of URM wall	17
Figure 2.2 Assumed forces at the intersection for corner separation collapse.....	17
Figure 2.3 Assumed failure lines on the wall.....	19
Figure 2.4 Distribution of earthquake demand force through the walls.....	22
Figure 2.5 Shear stress distribution at central cross-section of the wall	25
Figure 2.6 λ vs. aspect ratio graph and developed formulation for λ value	25
Figure 2.7 a) Diagonal shear cracking, b) rocking of vertically loaded free to rotate wall.....	26
Figure 2.8 Mohr circle related to Figure 2.7 a)	27
Figure 2.9 a) Diagonal shear cracking, b) rocking of vertically loaded upper edge restrained wall	28
Figure 2.10 General view of example house.....	30
Figure 2.11 General appearance of the macro based excel program showing example house data	31
Figure 3.1 Percent distribution of common URM building materials	33
Figure 3.2 Dimensions of the brick used in tests, (in mm)	35
Figure 3.3 Force displacement graph of the brick test	35
Figure 3.4 Triplet Test setup	37
Figure 3.5 Shear stress vs. Lateral compressive stress graph (Average shear stresses)	37

Figure 4.1 Half-scale brick masonry house test specimen	39
Figure 4.2 Results of test house on macro based excel program	41
Figure 4.3 Original unstrengthened test specimen	42
Figure 4.4 Analytically fit capacity curve of unstrengthened test house	44
Figure 4.5 Force vs. Deflection graph of the first test.....	45
Figure 4.6 Cracks on the first specimen.....	46
Figure 4.7 Horizontal constant force developing at the corner of rocking walls ...	46
Figure 4.8 Analytically obtained load-deflection graphs of unstrengthened test house.....	47
Figure 4.9 Second test with 50 kN of weight above the house	49
Figure 4.10 Force vs. Deflection graph of the second test.....	50
Figure 4.11 Analytically obtained capacity curves of the first and second tests (cracked + 50kN DL)	50
Figure 4.12 Setup of the third test.....	52
Figure 4.13 Force vs. Deflection graph of the third test	52
Figure 4.14 Capacity increase on the test house against vertical load application	53
Figure 4.15 Linearized capacity increase against vertical load application.....	53
Figure 4.16 Diagonal shear cracks on vertically post-tensioned cracked house....	54
Figure 4.17 Setup of the fourth test.....	55
Figure 4.18 Force vs. Deflection graph of the fourth test	56
Figure 4.19 Unloaded springs due to wall crushing in the vertical direction.....	56
Figure 4.20 Cracks on the fourth test	57
Figure 4.21 Setup of the fifth test.....	58
Figure 4.22 Force vs. Deflection graph of the fifth test	59
Figure 4.23 Cracks on the fifth test	59
Figure 4.24 Force distribution on compression struts at the ultimate stage of the fifth house test	60
Figure 4.25 Strengthening of the slab	61
Figure 4.26 Rebar heating test.....	62
Figure 4.27 Pre-cracking regions of the fifth and sixth tests	63
Figure 4.28 Force vs. Deflection graph of the sixth test	64

Figure 4.29 Cracks on the sixth test	64
Figure 5.1 General test setup of the wall tests.....	66
Figure 5.2 Force distribution on the cracked wall.....	68
Figure 5.3 Schematic setup of the first test	68
Figure 5.4 Vertical loads on the first test wall	70
Figure 5.5 Force-Deflection graph of the first test.....	70
Figure 5.6 Schematic setup of the second test	71
Figure 5.7 Deformed wall in the second test.....	72
Figure 5.8 Force-Deflection graph of the second test	72
Figure 5.9 Force-Deflection graph of the third test.....	74
Figure 5.10 Schematic setup of the fourth test.....	75
Figure 5.11 Force-Deflection graph of the fourth test	76
Figure 5.12 Deformed wall in the fourth test	76
Figure 5.13 Comparison of force-deflection graphs of the 2 nd and 4 th tests	77
Figure 5.14 Schematic setup of the fifth test.....	78
Figure 5.15 Deformed wall in the fifth test	79
Figure 5.16 Force-Deflection graph of the fifth test	79
Figure 5.17 Schematic setup of the sixth test.....	81
Figure 5.18 Failure at the diagonal rebar during the sixth test.....	82
Figure 5.19 Force-Deflection graph of the sixth test	82
Figure 5.20 Bracing forces at the seventh test	83
Figure 5.21 Deformed wall in the seventh test.....	84
Figure 5.22 Force-Deflection graph of the seventh test.....	84
Figure 5.23 Schematic setup of the eighth test.....	85
Figure 5.24 Deformed wall in the eighth test.....	86
Figure 5.25 Force-Deflection graph of the eighth test	87
Figure 5.26 Force distribution on the eighth test wall at the ultimate stage	88
Figure 5.27 Schematic setup of the ninth test	88
Figure 5.28 Deformed wall in the ninth test.....	89
Figure 5.29 Force-Deflection graph of the ninth test.....	90
Figure 5.30 Comparison of force-deflection graphs of the 8 th and 9 th tests	90

Figure 5.31 Comparison of energy dissipation characteristic of the 8 th and 9 th tests	91
Figure 6.1 Force-Deflection Envelope Curves of Half-scale House Tests	97
Figure 6.2 Cycle Energy Dissipation Curves of Half-scale House Tests.....	98
Figure 6.3 Force-Deflection Envelope Curves of rebar post-tensioned brick masonry wall tests	99
Figure 6.4 Energy Dissipation versus Total Deformation Curves of rebar post-tensioned brick masonry wall tests.....	100
Figure 6.5 Ultimate Load Capacities of the wall tests	101
Figure 6.6 Capacity increment participation of test components.....	101
Figure 6.7 Strengthening procedure for single storey brick masonry houses	103
Figure 6.8 Possible crack patterns on a generic URM house.....	104
Figure 6.9 Schematic representation of post-tensioning mechanism using bolts	105
Figure a) Initial stiffness decrement of the brick wall tests.....	116
Figure b) Initial stiffness decrement of the half-scale brick house tests.....	116

LIST OF SYMBOLS

(I)	: importance factor
A	: area of mortar joint at horizontal cross-section of the wall
a_0	: horizontal ground acceleration
A_H	: area of mortar joint at vertical cross-section of the wall
B	: width of wall
b_r	: width of roof
D	: eccentricity between center of mass and center of rigidity of the house
d	: eccentricity between center of wall and center of rigidity of the house
F	: in-plane load capacity of the wall
F_a	: in-plane force on the wall due to direct lateral earthquake force
F_b	: in-plane force on the wall due to earthquake resultant torsion
F_d	: earthquake demand force on the wall
FRP	: fiber reinforced polymer
G	: shear modulus
g	: gravitational acceleration (9.81 m/s^2)
GFRP	: glass fiber reinforced polymer
h	: height of URM building
H	: height of wall
H^*	: distance between the bottom of wall pier and the ceiling
I	: moment of inertia
K	: total in-plane stiffness of the house
K_x	: x direction in-plane stiffness of the wall
K_y	: y direction in-plane stiffness of the wall
K_θ	: total torsion stiffness of the house
L	: length of URM building
l_r	: length of roof

m : mass at unit height of URM building
 M : unit moment at yielding lines on the wall
 m_t : total participating mass of the house in case of an earthquake
 n : total number of wall segments on layout of the house
 N : number of perpendicular supporting walls
NSM : near surface mounted
 P : vertical compressive force on the wall
 P_H : horizontal compressive force on the wall
 $R_a(T_1)$: structural behavior (reduction) factor
RC : reinforced concrete
 $S(T_1)$: spectrum coefficient
SB : spring box
 t : assumed mortar thickness between the bricks, ~ 100 mm
 T : total torsion on the house
 T_1 : first vibration period of the house
 t_r : thickness of roof
URM : unreinforced masonry
 w_{out} : seismic lateral inertial force acting on unit area of the wall
 x : x coordinate of center of wall
 X_m : x coordinate of center of mass of the house
 x_r : x coordinate of center of mass of roof
 X_r : x coordinate of center of rigidity of the house
 y : y coordinate of center of wall
 Y_m : y coordinate of center of mass of the house
 y_r : y coordinate of center of mass or roof
 Y_r : y coordinate of center of rigidity of the house
 δ : top deflection in the in-plane direction of the wall
 λ : shear stress distribution factor
 μ : coefficient of friction of masonry relative to mortar joint
 ρ_r : unit mass of roof
 ρ_w : unit mass of the walls

σ_{all} : allowable tensile strength of mortar joint
 σ_c : compression strength of URM wall
 σ_o : compressive stress on URM wall
 σ_t : tensile strength of URM wall
 τ_{ave} : average shear stress value
 τ_{max} : maximum shear stress value

CHAPTER 1

INTRODUCTION

Unreinforced Masonry (URM) walls manifest brittle behavior and are weak against lateral forces. Commonly heavy roof and wall material would generate large inertial forces during an earthquake. Brittle failure of walls leads to sudden collapse of the heavy roof which causes loss of life of residents. Main resistance of URM structures is in in-plane direction of the walls where they behave mainly as shear walls. As a result of the in-plane loading, diagonal cracks are formed due of principal tension caused by shear. The cracks usually follow the weaker path of the mortar layers between the bricks in a stair-like pattern. Less commonly, the walls may overturn as a rigid body if the height to width ratio is large. Out-of-plane failure, corner opening, vertical cracks at corners, roof falling off the wall support are other common failure mechanisms which might also govern the collapse (Figure 1.1). However, in this study, the main focus is kept on the in-plane shear behavior of the URM walls. Brick walls are tested under in-plane reversed cycling loading and forced to deform in in-plane direction which is the strongest direction of URM wall and most common load carrying system of URM houses during a seismic activity. The load carrying in-plane shear behavior of the brick walls are tried to be improved using steel rebars which is a very effective and low cost technique. The main purpose of this study is to improve the strength and the behavior of URM walls using low cost and yet simply applicable techniques.

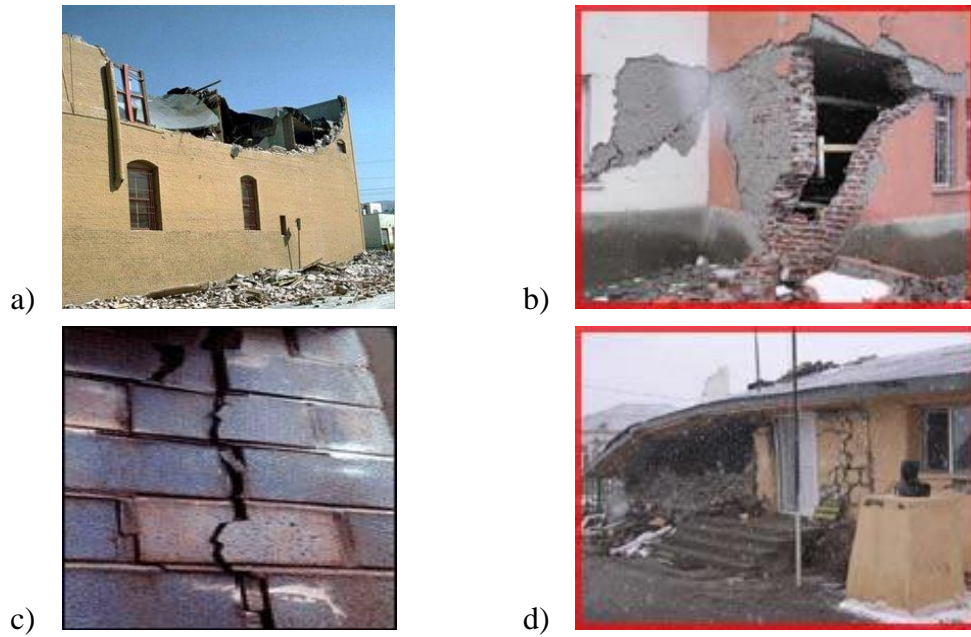


Figure 1.1 a) Out of plane failure, b) Corner opening, c) Vertical cracks, d) Roof falling

1.1 The current percentage and distribution of masonry buildings in Turkey

About half of the total building stock in Turkey (51% - 4.001.954 of 7.838.675 total buildings according to DİE 2000 [1]) is masonry type building. This data contains the information only with regions that have a municipality. If villages without a municipality are also considered, ratio of masonry houses in the total building stock is expected to increase. Distribution of the ratio, which is masonry houses with respect to total buildings, according to cities in Turkey are shown in Figure 1.2. It is seen that although the ratio is relatively higher in the east and middle regions of Turkey, metropolises of Turkey have also considerably high masonry ratios. (For example, İstanbul 22,6%, Ankara 68,6%, İzmir 37,3%, Adana 32,6%) [19] Total amount of people living in masonry houses throughout the cities in Turkey are also given in Figure 1.3 [19].

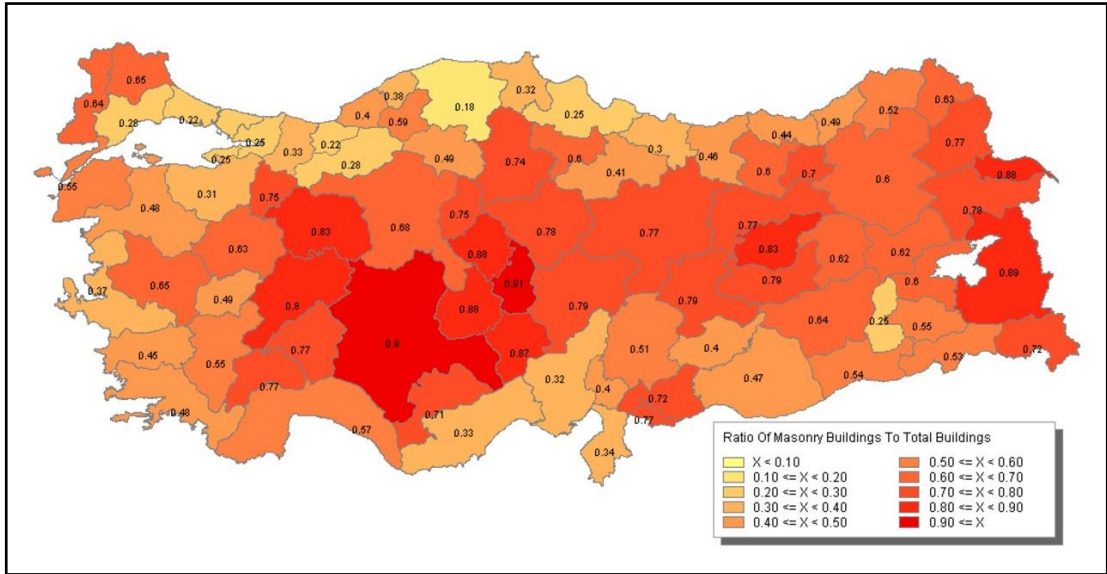


Figure 1.2 Distribution of ratio of masonry houses to total buildings in Turkey [19]

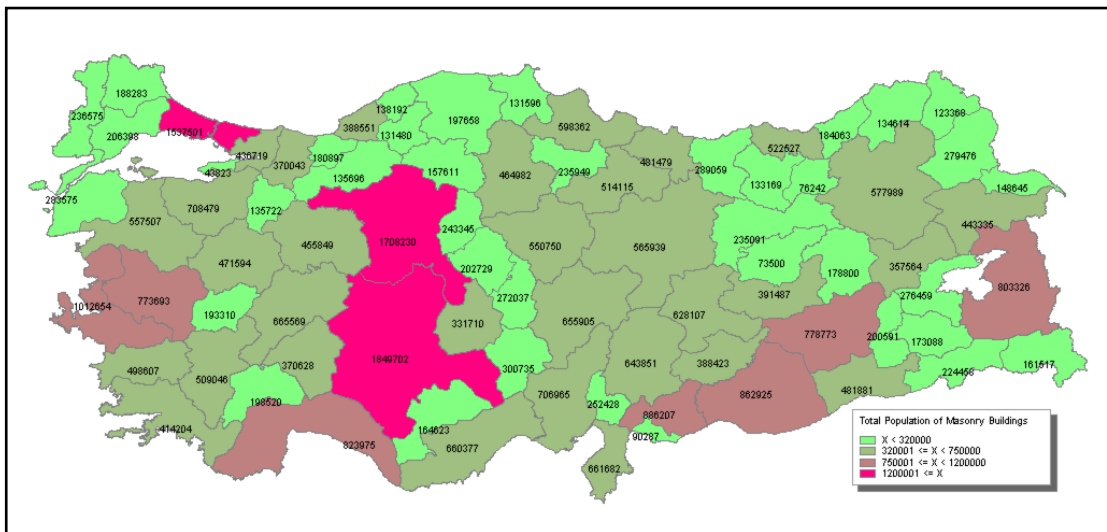


Figure 1.3 Population living in masonry houses in Turkey [19]

During seismic activities, masonry houses may quickly reach to their elastic limits which would quickly lead to brittle failure and collapse. Since masonry walls behave rigidly, they have a low deformation capacity and collapses occur suddenly without letting hosts to get out of the building. Considering the seismicity of Turkey, strengthening of masonry buildings deserves great attention.

1.2 Literature survey

Studies on masonry buildings have been performed till now by many researches to evaluate the resisting capacity of URM structures and to improve the behavior against destructive effects of earthquakes.

Moon et al. [2] conducted a full scale lateral load test of a two story unreinforced masonry structure. They studied modifications implied by FEMA 356 for the in-plane analysis of perforated URM walls. These modifications allow the model to address global issues such as flange participation, overturning effects, and global rocking. Following a description of each modification, the analysis results, obtained using the proposed model and FEMA 356, are compared with experimental results. In terms of base shear resistance, the proposed model displayed an average error of 13% compared with an average error of 21% from FEMA 356. The improved accuracy of the proposed model is primarily attributed to the consideration of global issues.

Magenes and Calvi [3] addressed the problems of evaluation of strength, deformability, and energy dissipation capacity of unreinforced brick masonry walls, within the context of seismic assessment of existing buildings. The role of the shear ratio in the shear failure mechanisms was put in evidence and shear strength formulae are proposed accordingly. Formulas were given under three different failure mechanisms as rocking, diagonal shear and base sliding. The maximum horizontal shear which can be resisted by a rocking pier failing under static in-plane loading was approximated introducing a proper stress distribution for the masonry in compression (Figure 1.4) and neglecting the tensile strength of bedjoints;

$$V_r = \frac{D^2 t p}{H_0} \frac{1}{2} \left(1 - \frac{p}{\kappa f_u}\right) = \frac{D t p}{\alpha_V} \frac{1}{2} \left(1 - \frac{p}{\kappa f_u}\right) \quad (1.1)$$

- D : Pier length
- H_0 : Effective pier height (distance from zero moment)
- t : Pier thickness
- p : P/Dt , mean vertical stress on the pier
- f_u : compressive strength
- κ : Equivalent rectangular stress block coefficient, 0.85

The effective height H_0 is determined by the boundary conditions of the wall and is related to the shear ratio α_v ;

$$\alpha_v = \frac{M}{VD} = \frac{H_0}{D} = \frac{\psi H}{D} \quad (1.2)$$

The value ψ assumes a value of 1 when the pier is fixed on one end and free to rotate on the other, and a value of 0.5 when the pier is fixed at both ends.

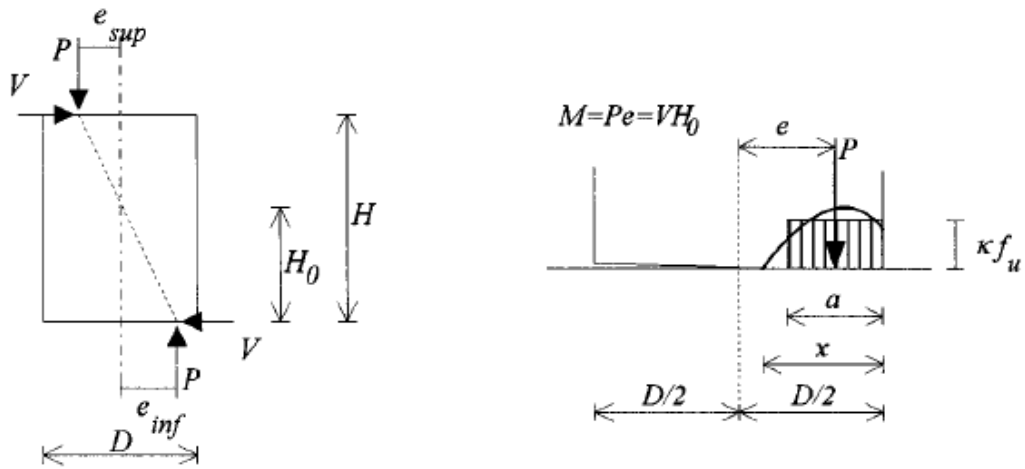


Figure 1.4 Assumptions for rocking strength evaluation of a wall failing with crushing at the base corner

Shear strength associated to diagonal cracking was predicted as;

$$V_d = Dt\tau_u \quad (1.3a)$$

$$\tau_{cs} = \frac{1.5c + \mu p}{1 + 3c\alpha_v/p} \text{ relevant to the cracked section} \quad (1.3b)$$

$$\tau_{ws} = \frac{c + \mu p}{1 + \alpha_v} \text{ relevant to the whole section} \quad (1.3c)$$

- τ_u : Mean shear strength
 c : Bedjoint cohesion
 μ : Coefficient of friction

The parameters c and μ should be corrected as $c' = \kappa c$, $\mu' = \kappa \mu$ where κ is;

$$\kappa = \frac{1}{1 + \mu 2\Delta_y/\Delta_x} \quad (1.4)$$

- Δ_x : Length of the brick
 Δ_y : Height of the brick

Shear strength associated to diagonal cracking may also be related to shear-tensile cracking of bricks and formula was predicted as;

$$V_{d,b} = Dt\tau_b = Dt \frac{f_{bt}}{2.3(1 + \alpha_v)} \sqrt{1 + \frac{p}{f_{bt}}} \quad (1.5)$$

- $V_{d,b}$: Shear strength related to shear-tensile cracking of bricks
 τ_b : Shear strength of a brick
 f_{bt} : Tensile strength of a brick

The shear strength of a wall was calculated as the lowest strength obtained from equations (1.3) and (1.5). Finally the strength of a pier undergoing sliding along a horizontal joint was expressed as;

$$V_s = \mu P \quad (1.6)$$

Where μ represents the sliding coefficient of friction of the masonry joint and cohesion is neglected invoking the fact that the joint is already cracked in tension due to flexure.

Tomazevic [4] introduced seismic resistance of masonry walls under three different failure patterns as rocking failure, diagonal shear failure and sliding shear failure as explained also by Magenes and Calvi [3]. He defined flexural resistance of a wall as ;

$$H_{f,w} = \frac{M_{Ru}}{\alpha h} \quad (1.7)$$

$$M_{Ru} = \frac{\sigma_0 t l^2}{2} \left(1 - \frac{\sigma_0}{f} \right) \quad (1.8)$$

$H_{f,w}$: Flexural resistance of the wall

M_{Ru} : Flexural capacity of the wall section

h : Height of the wall

α : Coefficient of effective wall height (0.5 for fixed-ended and 1.0 for cantilever wall)

σ_0 : Compression stress on the wall due to vertical loads

t : Thickness of the wall

l : Length of the wall

f : Compressive strength of the wall

The lateral resistance of a plain masonry wall panel failing in diagonal shear was evaluated by;

$$H_{s,w} = A_w \frac{f_t}{b} \sqrt{\frac{\sigma_0}{f_t} + 1} \quad (1.9)$$

A_w : horizontal cross-section area of the wall

f_t : tensile strength of masonry

b : shear stress distribution factor, depending on the geometry of the wall
($b = 1.0$ for $h/l \leq 1$, $b = h/l$ for $1 < h/l < 1.5$, $b = 1.5$ for $h/l \geq 1.5$)

The resistance of a masonry wall to sliding was expressed as;

$$H_{sl,w} = \mu_c N \quad (1.10)$$

μ_c : coefficient of friction of masonry relative to mortar joint

N : axial load

Cardoso, Lopes, and Bento [5] described a method developed to evaluate the seismic performance of old masonry buildings, which allowed identifying the expected structural collapse mechanism of the structure. The collapse mechanism was identified by the accumulation of several damaged structural elements in specific points of the structure. Their methodology allowed simulating the non-linear behavior of masonry buildings by making use of an iterative procedure, where the structure was changed at each step according to the cracking, yielding or collapse of structural elements at the previous steps. They discussed the advantages of the iterative procedure for the identification of the expected structural collapse mechanism of old masonry buildings.

Corradi, Borri, and Vignoli [6] presented the results of a research project carried out on masonry panels obtained from structures struck by the Umbria-Marchigiano earthquake of 1997–1998. Tests were performed in the laboratory and in situ in order to determine the correct parameters describing masonry behavior. As a result of the compression tests, diagonal compression tests, and shear-compression tests the shear strength, elastic modulus and shear modulus were measured. These results were compared with the values suggested by different standards. The experimental research allowed characterizing the mechanical properties of some typical masonry walls.

Elgawady, Lestuzzi, and Badoux [7] compared different models used to calculate the shear strength of URM walls that were retrofitted using fiber reinforced polymers (URM-FRP). The shear strengths of six tested URM-FRP walls were compared to shear strengths predicted by the models. Four of the specimens were tested under constant gravity load and incrementally increasing in-plane loading cycles. The other two specimens were tested on a uniaxial earthquake simulator. Each specimen was retrofitted on the entire surface of a single side using FRP with different axial rigidities. The model was explicitly developed to predict the shear strength of unreinforced masonry walls retrofitted using FRP. The model idealized masonry, epoxy, and FRP in a URM-FRP as different layers of isotropic homogeneous elastic materials. Then, using principles of the theory of elasticity, the governing differential equation of the system was formulated and linearly solved. They saw that with increasing FRP axial rigidity the differences between the models became more significant. They highlighted the advantages and disadvantages of each model.

Roca [8] presented a discussion on the possibility of using simple equilibrium models to estimate the ultimate capacity of masonry shear-walls. Their proposed models were based on load-path or strut-and-tie schemes representing the combination of the compression or tension stress fields which were mobilized at the ultimate condition. Tentative rules for the construction of the models and

specific solutions were presented for elementary solid walls subjected to different load conditions in their studies. The performance of the proposed models was analyzed by comparing their predictions with experimental results available for dry-joint and mortar-joint masonry subjected to different load or support conditions.

Paquette and Bruneau [9] tested a full-scale one-story unreinforced brick masonry specimen having a wood diaphragm subjected to earthquake excitations using pseudo-dynamic testing. The specimen was designed to better understand the flexible-floor/rigid-wall interaction, the impact of wall continuity at the building corners and the effect of a relatively weak diaphragm on the expected seismic behavior. The unreinforced masonry walls of this building were also repaired with fiberglass materials and re-tested. The overall building was found to be relatively resilient to earthquake excitation, even though cracking was extensive. The repair procedure was demonstrated to enhance this behavior. It was found that even though the diaphragm did not experience significant inelastic deformation, some of the existing seismic evaluation methodologies accurately captured the rocking/sliding behavior that developed in the shear walls under large displacement. In their studies, the responses of the wood diaphragm and its interaction with the shear walls have also been studied.

Benedetti, Carydis, and Pezzoli [10] presented the results of a large experimental program carried out on models, scaled 1: 2, of two-storey masonry buildings. After suffering damage, the models were repaired and strengthened and tested again. A total of 24 buildings were subjected to 119 shaking-table tests. With the help of horizontal ties and good quality of construction, no wall separation was observed during tests. The best results were achieved by using horizontal ties, vertical steel beams and curved steel blades placed at the intrados of the arches in the first or the second storey.

Shrive [11] suggested to use FRPs in order to gain advantage due to their lightweight. In this way, he claimed that they do not alter the mass of a structure and thus the inertial forces from seismic excitation. Their strength and, in the case of sprayed glass FRP, their toughness, indicate that they can alter the load deformation response considerably for the better. He concluded that FRPs open an exciting new line of possibilities for masonry.

Holberg and Hamilton [12] suggested using glass fiber reinforced polymer (GFRP) for strengthening of unreinforced or inadequately reinforced hollow concrete masonry structures. Quasi-static shear wall tests were conducted on unreinforced concrete masonry specimens that had been strengthened with unidirectional glass fiber strips applied to the surface of the masonry using a two-part epoxy to form a surface-bonded GFRP composite. The strips were strategically placed to improve both flexural and shear strength in the in plane direction. The GFRP composite system was combined with conventional structural steel and reinforcing steel connections that were designed to yield before the composite ruptured, resulting in a ductile failure mode under cyclic testing.

Tumialan and Nanni [13] recommended using externally bonded FRP laminates to increase flexural and shear capacity of masonry members. They also gave the use of near surface mounted (NSM) FRP bars as an alternative to the use of FRP laminates. They resulted in that strength and pseudo-ductility can be substantially increased by strengthening masonry walls with NSM FRP bars. They showed that masonry walls strengthened with NSM FRP bars exhibited similar performance to walls strengthened with FRP laminates. Also they investigated remarkable increases in shear capacity of masonry walls strengthened with FRP.

Kotorman and Ivanyi [14] performed numerical analyses on masonry-box buildings under horizontal loads with and without steel strengthening elements. They compared the results obtained by the numerical calculus program to one another in order to evaluate the suitability and effectiveness of a few steel

refurbishment methods applied to masonry buildings. They stated that according to the obtained results, from structural point of view the steel grid work fitted to the top of masonry walls seemed to be the most effective refurbishment method among the examined cases with regard to considerable reduction of both the stress state and horizontal displacements of masonry construction. They drew attention that using post-tensioned horizontal steel tie bars inside the masonry walls at floor and roof levels, by relatively slight amount of steel material a quite significant reinforcing effect can be easily achieved. They resulted in that, in case of a strong and severe earthquake, combination of those refurbishment methods would surely be more effective.

Rai and Goel [15] investigated that the system of wall piers and spandrels, created by openings, largely controls the in-plane lateral resistance of the wall. For the rocking-critical masonry wall piers, the overall hysteretic behavior can be significantly improved by installing a steel framing system consisting of vertical and horizontal elements around the wall - without any braces. Vertical elements provide the necessary hold-down forces to stabilize the rocking piers. The stabilized piers rocked through a number of cycles of large displacements (up to 2.5%) without crumbling or shattering, displaying a ductile response. The strengthened system has excellent strength, stiffness and ductility, despite the brittleness of the masonry because of considerable load sharing between the existing masonry and the added steel elements. Also they developed a simple mechanics based model to predict the load-deflection behavior of a stabilized rocking pier which can be used to design the strengthening system more rationally.

Altın et al. [16] performed a test on shaking table with a 3D one story masonry structure constructed with vertically hollow bricks. They repaired the damaged structure with four different arrangements of steel straps. Strengthened structure showed no significant crack propagation after successful tests. Although the diagonal steel strap arrangement was successful, the best results were achieved when diagonal and vertical straps were both used on the masonry walls.

Murtyl, Dutta, and Agrawal [17] tested a single-room, single-storey full-scale brick masonry building with precast RC roofing system three times under displacement controlled lateral cyclic loading, to assess the effectiveness of the basic repair and seismic strengthening techniques. Initially, the virgin building specimen was loaded laterally to failure. In the second stage, the damaged building was repaired by stitching across the cracks, and tested under the same lateral loading. In the third stage, the twice-damaged structure was repaired once more by stitching and strengthened by twin lintel belt in steel and vertical corner reinforcement, and re-tested. The building strengthened by twin lintel belt in steel showed about 28% higher strength under lateral loading than the virgin building.

1.3 Objectives and scope

The main objective of this study is to develop a low-cost and effective strengthening technique for URM brick walls by using steel rebars. The objectives of this study may be listed as follows:

- Strengthen URM brick walls by using rebars and simple connectors.
- Develop simple connectors between the rebars and the RC slabs.
- Develop a mechanism to apply post tensioning force on the rebars.
- Develop an equipment to prevent premature loss of post tensioning force during cyclic events of wall crushing and rebar yielding under seismic activity.
- Investigate the effect of rebar post-tensioning on brick walls in the in-plane shear direction using laboratory experiments.
- Investigate the most effective arrangement of rebars on brick masonry walls to achieve the best results.
- Achieve improvements on the ductility, ultimate strength, and energy dissipation capability of brick URM walls using rebars and springs.

- Obtain direct compression and mortar shear capacities for commonly used hollow bricks and cement mortar.

To achieve the objectives listed above; the scope of the study is summarized below;

- Conduct direct compression material tests on bricks and mortar to obtain material capacities.
- Conduct direct shear tests on mortar connecting bricks.
- Design connectors that are capable of transferring forces between the rebars and the slabs of the brick masonry walls.
- Conduct heat tests on rebars to achieve initial prestressing on the brick masonry walls.
- Conduct ½ scale 3D brick masonry building tests in the in-plane direction to experimentally obtain strength, ductility, energy dissipation, stiffness and damping changes between original and strengthened specimens.
- Conduct brick masonry wall tests to figure out the most suitable and effective rebar arrangement.
- Write an Excel based program for estimating the ratio between earthquake demand force and in-plane resisting capacity of masonry walls.

The details of the conducted studies and pertinent results are described in detail in the following chapters.

CHAPTER 2

VULNERABILITY EVALUATION STUDIES ON MASONRY BUILDINGS

Unreinforced masonry (URM) structures, built using hollow bricks and mortar, are the most commonly encountered masonry types in Turkey. Hollow brick and mortar together create a composite material. One of the most important parameters of brick masonry is the tension capacity of the mortar and bricks. Under the effect of seismic forces, the most common failure is due to low tensile capacity of the masonry building material. Even under pure shear, principal tension stresses are developed on the diagonal. Different failure mechanisms of URM structures exist, such as out-of-plane bending failure, in-plane shear failure, separation of orthogonal walls at the corners, etc. As those failure types can result in partial damage on the walls, they can lead to total collapse of the URM structure. Therefore, failure types of an URM structure should be well understood and analyzed in order to prevent the collapse of URM structures. Strengthening of the structure in its weakest failure pattern can help the structure to withstand in case of a seismic activity.

2.1 Common collapse mechanisms of URM houses and analytical approaches to the problems

Failure modes of masonry houses depends on numerous parameters; the most important ones being the number of storeys, existence and frequency of window and door openings, strength – quality of the building blocks (e.g., bricks, adobe,

stones) and mortar between building blocks, wall thickness, aspect ratio (length versus height) of the walls, existence and frequency of lintels, number and intervals of orthogonal walls supporting other walls in the out-of-plane direction, interlocking level of the walls that are orthogonal to each other (especially at the corners), slab and roof type, weight and mass of the house, footing and soil conditions, seismicity of the region, and closeness to the fault lines. The most common failure modes of masonry walls may be separated into two main categories as the “in-plane” and “out-of-plane” failure. The in-plane modes can be itemized as a) diagonal shear cracking, b) horizontal cracking at the top and bottom of the wall due to rigid-body rocking motions of the wall (rocking), and c) a single horizontal cracking that would cause shear failure (base sliding) [3], [4]. The out-of-plane failure is mostly dominated when walls are not supported at the ceiling level or not supported by orthogonal walls for long distances. Alternatively, the walls may fail in a bursting mode in the out-of-plane direction if the wall is supported at all sides but too thin to keep itself intact. The existence of a rigid diaphragm over walls by means of a concrete floor is very important to restrain the top edges of walls in the out-of-plane direction as well as distribute inertial forces to walls in their strong (in-plane) directions. Often times, the floors and roof are built using wooden logs or beams that are only supported by the two opposing and parallel walls. In that case, the inertial forces at the floor level are distributed to the two supporting walls in their weak and stronger directions; however, the governing failure mode is always the weak out-of-plane bending direction. Such a one-way slab floor would also do a poor job in restraining the other (non-supporting) walls at the floor level, leaving them vulnerable to the out-of-plane bending failure. Failure modes summarized above are discussed under each sub-heading below and simple assessment equations are provided for each relevant section.

2.1.1 Overturning of the walls in out of plane direction

Weaker connections of URM walls at intersections may fail in tension forming vertical cracks and lead to out-of-plane collapses. Separation of the wall at the orthogonal joints is followed by total collapse of the wall (Figure 2.1, Figure 2.2).

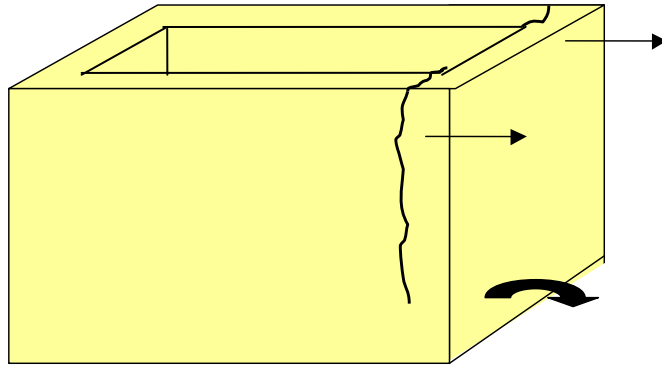


Figure 2.1 Out of plane collapse of URM wall

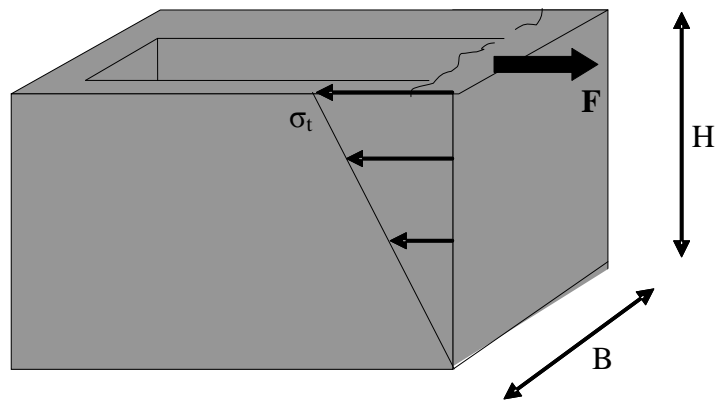


Figure 2.2 Assumed forces at the intersection for corner separation collapse

The main assumptions used for the evaluation of corner separation are:

- The roof is supported by two opposing walls and inertial roof forces directly act on the supporting walls in their out-of-plane directions.
- Roof slab does not exist and does not generate diaphragm action.

- Upper half of the failing wall is assumed to generate inertial forces while lower half is assumed to be fully supported by the ground and orthogonal walls.
- Spectrum Coefficient S(T) and Structural Behavior Factor (R) are assumed as 2.5 and 2.0, respectively in accordance with section 5.2.1 of Specification for Structures to be Built in Disaster Areas-2007, and Building Importance Factor (I) is accepted as 1.0.

Resisting moment with respect to the bottom of the wall,

$$\sigma_t \times \frac{H \times t \times N}{2} \times \frac{2 \times H}{3} \geq F \times H \quad (2.1)$$

$$F = \left(\frac{mass_{roof}}{2} + \frac{mass_{wall}}{2} \right) \times a_0 \times \frac{2.5}{2.0} \quad (2.2)$$

Therefore, no-collapse condition should satisfy;

$$\frac{\sigma_t \times H \times t \times N}{3} \geq \left(\frac{mass_{roof}}{2} + \frac{mass_{wall}}{2} \right) \times a_0 \times 1.25 \quad (2.3)$$

2.1.2 Blow-out of the wall

When the bond between slabs and the walls is strong enough then the wall is forced to blow out due to its own mass and inertia. As a result, wall behaves as if it is supported from the edges continuously. Using low quality mortar between the bricks or too small wall thickness may also cause this type of failure. Failure of the wall follows the pattern similar to the yield line theory (Figure 2.3).

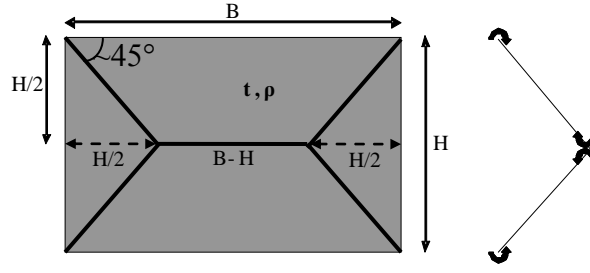


Figure 2.3 Assumed failure lines on the wall

Earthquake demand force on unit area of the wall;

$$w_{out} = 1m^2 \times t \times \rho_w \times a_o \quad (2.4)$$

Deflection of the wall is assumed as unit at the center. From the equilibrium of;

Force × deflection = unitmoment × lengthofyieldlines × deflectionangle

$$\begin{aligned} w_{out} \times (B - H) \times \frac{H}{2} \times \frac{1}{2} \times 2 + w_{out} \times \frac{H}{2} \times \frac{H}{4} \times \frac{1}{3} \times 8 \\ = M \times H \times \frac{1}{H/2} \times 4 + M \times B \times \frac{1}{H/2} \times 4 \end{aligned} \quad (2.5)$$

$$M = \frac{w_{out} \times H^2(3B - H)}{48(B + H)} \quad (2.6)$$

$$\sigma_t = \frac{M \times t/2}{I} \quad (2.7)$$

$$\sigma_t = \frac{w_{out} \times H^2(3B - H)}{8t^2 \times (B + H)} \leq \sigma_{all} \quad (2.8)$$

Therefore, no-collapse condition should satisfy;

$$\sigma_t = \frac{\rho_w \times a_o \times H^2 \times (3B - H)}{8 \times t \times (B + H)} \leq \sigma_{t_{all}} \quad (2.9)$$

2.1.3 In-plane shear demand calculation and failure of URM walls

When the slab or roof level forms a rigid diaphragm that connects the top of the walls, the inertial forces generated in the horizontal direction are distributed to the walls in accordance to their stiffnesses. The weaker walls take smaller share of the overall horizontal force while stronger walls resist a larger share. The walls that are perpendicular to the direction of loading are assumed to take zero share from the horizontal earthquake forces since the stiffness of the walls that are parallel to the forcing direction (in-plane loading) are dominant.

Simple, equation based checks are not quite possible for in-plane loading of the walls since loads in the in-plane direction are affected by relative stiffness of the walls as well as eccentricity between the mass and rigidity centers. Therefore, basic level of programming is needed to calculate the load demand acting on each wall. It is necessary to compute the rigidity and mass centers of the structure under consideration to compute eccentricity of inertial forces. The eccentricity would generate torsion on the structure creating additional shear forces on the walls. The in-plane stiffness of each wall is considered on a wall to wall basis, ignoring force transfer between the walls that are perpendicularly connected to each other. This assumption was based on the general corner separation commonly observed during earthquakes, which also made the analysis and related programming simpler.

A basic program to calculate the seismic force demand on each one of the walls was prepared using Excel's macros. The software requires the user to first draw a sketch of the structural walls using a general plan view of the house entering the

wall lengths and thicknesses. Window and door openings are considered as void spaces and generate discontinuities for the wall segments. The macro based program accepts the wall locations as starting and ending coordinates along with the thickness information. The input coordinates are automatically drawn in a graphical interface for visually checking the correctness of the input values. As the developed macro is executed, in-plane stiffness of each wall segment is calculated in the x and y coordinates. If there are any skewed walls, their stiffnesses are divided in the x and y directions in accordance with the $\cos(\alpha)$ and $\sin(\alpha)$, respectively; α being the skew angle. The mass and stiffness of the walls are calculated at their geometric centers. Similarly, structural mass and rigidity centers are automatically calculated using wall stiffness, wall and slab masses.

Earthquake demand on the structure is calculated by taking response spectrum coefficient $S(T_1)$ as 2.5 and structural behavior (reduction) factor 'R' as 2.0 as stated in section 5.2.1 of "Specification for Structures to be Built in Disaster Areas-2007". The importance factor '(I)' is assumed to be 1.0. The earthquake demand as a lateral force acting at the mass center is distributed to the wall segments assuming a rigid diaphragm as shown in Figure 2.4 and through the calculations listed below;

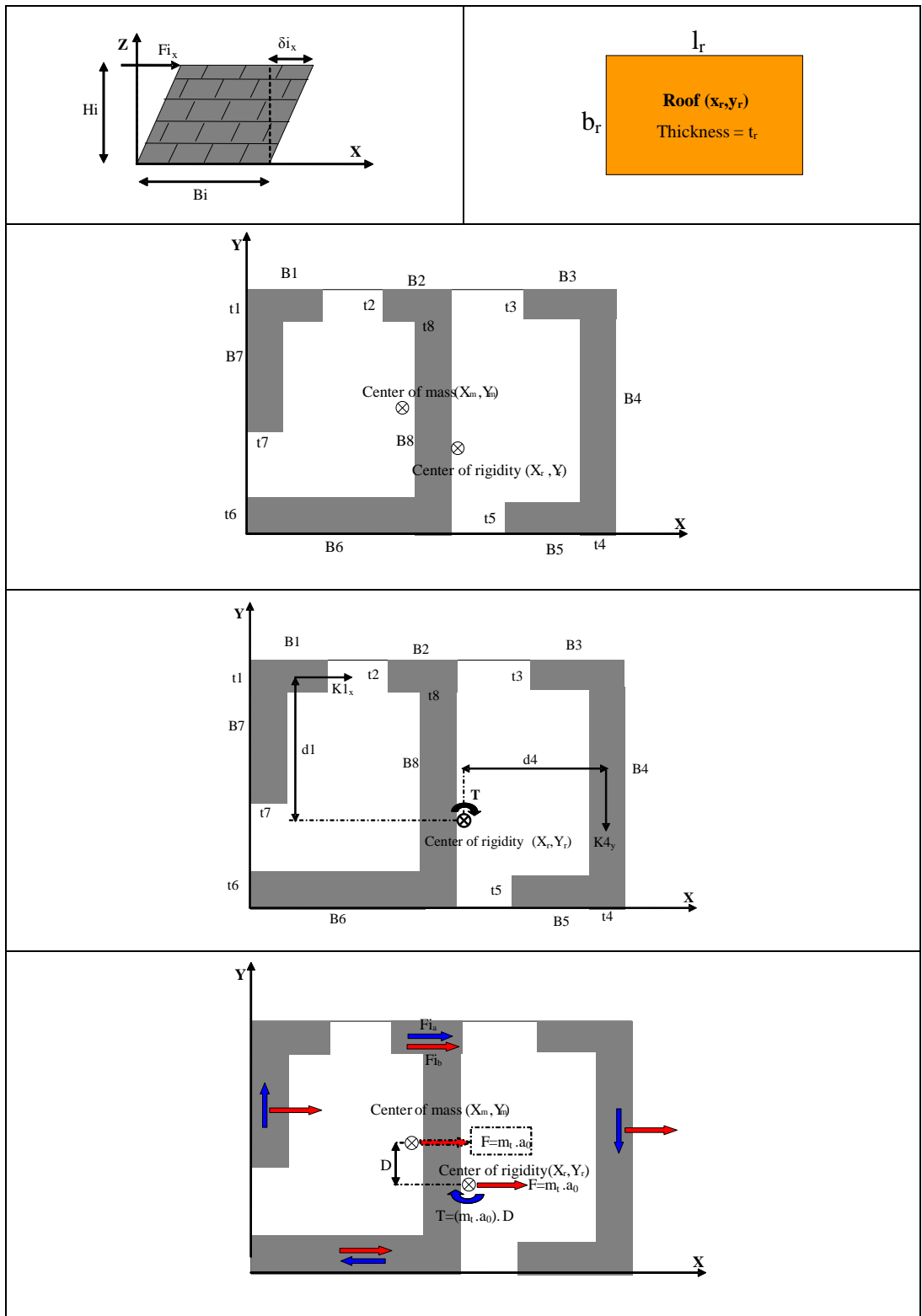


Figure 2.4 Distribution of earthquake demand force through the walls

In-plane stiffness of the wall for fixed end case as stated by Tomazevic [4],

$$K_{i(x,y)} = \frac{G \times A_i}{1.2H \left[1 + 0.83 \frac{G}{E} \left(\frac{H}{B} \right)^2 \right]} \quad (2.10)$$

By taking G is equal to E/2.5, stiffness of wall can be summarized as,

$$K_{i(x,y)} = \frac{E \times B^3 \times t}{H^3 + 3B^2 \times H} \quad (2.11)$$

Total participating mass of the structure in case of an earthquake,

$$m_t = \rho_r \times l_r \times b_r \times t_r + \rho_w \times \sum_{i=1}^n \left(\frac{H_i}{2} \times A_i \right) \quad (2.12)$$

Coordinates of center of mass,

$$X_m, Y_m = \frac{\rho_r \times l_r \times b_r \times t_r \times (x_r, y_r) + \rho_w \times \sum_{i=1}^n \left[\frac{H_i}{2} \times A_i \times (x_i, y_i) \right]}{m_t} \quad (2.13)$$

Total in-plane stiffness of the walls,

$$K_{(x,y)} = E \times \sum_{i=1}^n \frac{B_i^3 \times t_i}{H_i^3 + 3B_i^2 \times H_i} \quad (2.14)$$

Coordinates of center of rigidity,

$$X_r, Y_r = \frac{E \times \sum_{i=1}^n \left[\frac{B_i^3 \times t_i}{H_i^3 + 3B_i^2 \times H_i} \times (x_i, y_i) \right]}{K_{(x,y)}} \quad (2.15)$$

Total torsion stiffness of the walls,

$$K_{\theta} = \sum_{i=1}^n (K_{i(x,y)} \times d_i^2) \quad (2.16)$$

Total seismic force on the structure,

$$F_d = \frac{m_t \times a_0 \times S(T_1) \times (I)}{R_a(T_1)} \quad (2.17)$$

Total torsion on the house,

$$T = F \times D \quad (2.18)$$

In-plane force on a wall due to total seismic force,

$$F_{i_{a(x,y)}} = \frac{F}{K_{(x,y)}} \times K_{i(x,y)} \quad (2.19)$$

In-plane force on a wall due to total torsion,

$$F_{i_{b(x,y)}} = \frac{T}{K_{\theta}} \times d_i \times K_{i(x,y)} \quad (2.20)$$

Total in-plane earthquake demand force on a wall,

$$F_{d_{i(x,y)}} = F_{i_{a(x,y)}} + F_{i_{b(x,y)}} \quad (2.21)$$

Force acting on each wall develops shear and principal direction tensile stresses. At the central cross-section of the wall shear stresses that are developed due to in-

plane loading exhibit a parabolic distribution (Figure 2.5). The ratio of maximum shear stress τ_{\max} to average shear stress τ_{ave} is a function of the walls's aspect ratio. Calderini et al. [18] states that for an aspect ratio of 0.65, λ ($\tau_{\max} / \tau_{\text{ave}} =$ shear stress distribution factor) can be taken as 1.2. Also for aspect ratios of 1.35 and 2, λ values can be taken as 1.4 and 1.5, respectively. Using the suggested values of λ by Calderini et al. and taking maximum λ value as 1.5 from the shear stress distribution in beams and $\lambda=1.0$ for a very short (in height) but long (in length) wall, a curve can be fitted and λ value can be expressed as a bilinear curve (Figure 2.6).

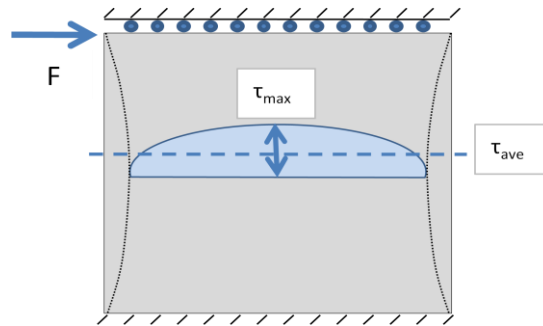


Figure 2.5 Shear stress distribution at central cross-section of the wall

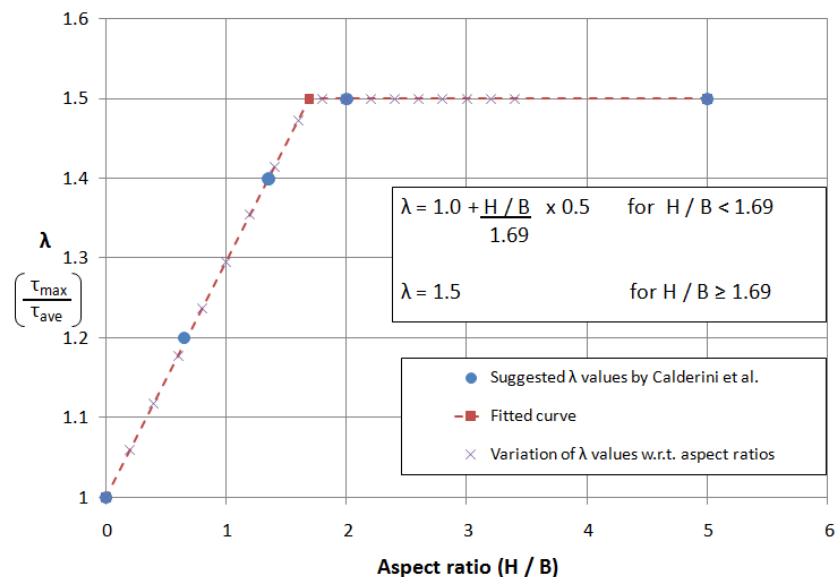


Figure 2.6 λ vs. aspect ratio graph and developed formulation for λ value

The in-plane failure mechanisms are affected by the boundary conditions and aspect ratio of the walls. If a small house with one or two wall segments in the same axis is considered, the top edges of the walls may be accepted as free to rotate, similar to a cantilever beam (Figure 2.7). On the other hand, if the slab is continuous over numerous wall segments, the top edges of the walls can be accepted as ‘restrained’ against rotation. In Figure 2.7 a), failure is assumed as diagonal shear cracking starting from the center of the wall which has the maximum shear stress due to narrowing of the effective shear area. Shear stress on infinitely small element at the center of the wall can be obtained by increasing the average shear stress value with shear stress distribution factor (λ) represented in Figure 2.6. Principal tensile stresses on that element can be obtained using Mohr circle as shown in Figure 2.8. Eqns. (2.22) and (2.23) were derived for diagonal shear failure of a one end fixed other end free-to-rotate masonry wall. Flexural failure (rocking motion) of the wall is represented in Figure 2.7 b) where rocking motion is assumed to be triggered by the tensional failure of base corner of the wall. It is also assumed that infinitely small element at the base and edge of the wall (wall corner) has only principal tensile stresses with zero shear stress for the shown orientation. The derivation of the assumed in-plane capacity of the wall towards rocking motion is given in eqns. (2.24) and (2.25). When eqns. (2.23) and (2.25) are compared for $P=0$, the critical ratio of H/B is found to be 0.175, which would determine the failure mechanism between diagonal shear and rocking. Usually, P is not zero and H/B ratio is well above 0.175. For the walls that have low level of P force and high H/B ratios, the failure is governed by the rocking motion.

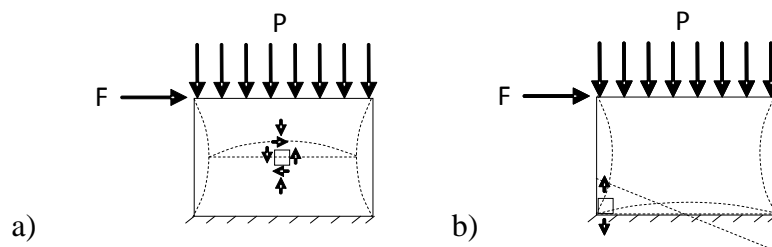


Figure 2.7 a) Diagonal shear cracking, b) rocking of vertically loaded free to rotate wall

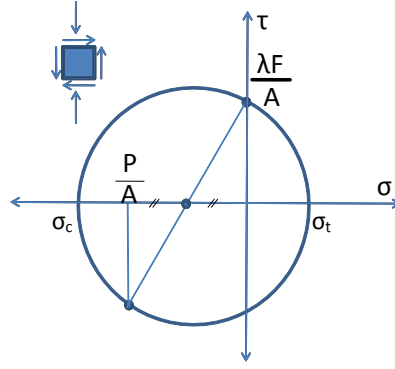


Figure 2.8 Mohr circle related to Figure 2.7 a)

$$\sigma_t = \left(\sqrt{\left(\frac{P}{2A}\right)^2 + \left(\frac{\lambda F}{A}\right)^2} - \frac{P}{2A} \right) \quad (\text{Figure 2.8}) \quad (2.22)$$

$$F = \frac{B \times t}{\lambda} \sqrt{\left(\sigma_t + \frac{P}{2B \times t}\right)^2 - \left(\frac{P}{2B \times t}\right)^2} \quad (2.23)$$

$$\sigma_t = \frac{F \times H \times \left(\frac{B}{2}\right)}{\left(\frac{B^3 \times t}{12}\right)} - \frac{P}{A} \quad (2.24)$$

$$F = \frac{B \times (B \times t \times \sigma_t + P)}{6H} \quad (2.25)$$

If there are multiple wall segments connected with a reinforced concrete ceiling on the same axis, the upper edges of the walls should be considered as restrained against rotation. The resulting stress distribution according to diagonal shear failure in Figure 2.9 a) on infinitely small element at the center of the wall is assumed to be the same as in Figure 2.7 a). For that reason, eqns. (2.22) and (2.23) can be used to evaluate the diagonal shear capacity of the wall. Two ends fixed

wall results in lower moments at the bottom of the wall, which causes lower principal tensile stresses on the infinitely small element at the base corner of the wall. Eqns. (2.26) and (2.27) represents the assumed rocking capacity of the wall.

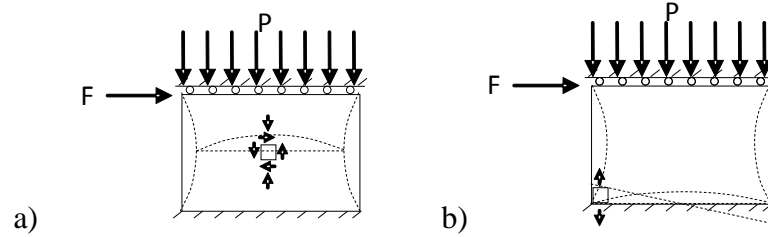


Figure 2.9 a) Diagonal shear cracking, b) rocking of vertically loaded upper edge restrained wall

$$\sigma_t = \frac{F \times \frac{H}{2} \times \left(\frac{B}{2}\right)}{\left(\frac{B^3 \times t}{12}\right)} - \frac{P}{A} \quad (2.26)$$

$$F = \left(\sigma_t + \frac{P}{B \times t}\right) \frac{B^2 \times t}{3H} \quad (2.27)$$

Apart from diagonal shear cracking and rocking failures, Tomazevic [4] stated that sliding shear failure can also be observed in case of an earthquake if walls are subjected to low vertical load but high seismic accelerations. The resisting capacity of the wall against sliding was proposed by Tomazevic [4] as;

$$F = \mu \times P \quad (2.28)$$

On the other hand, the base sliding failure mode can be triggered by the rocking motion. Following the crack formation at the base, the corner of the wall may slip if the earthquake force (F) is larger than the friction force transferred by the corner bricks ($\mu \times P$), which would yield the same eqn. (2.28).

The failure mode evaluation equations derived so far are also used by the evaluation program written in Excel. The seismic demand acting on each wall is computed by the program using Eqns. (2.10) through (2.21) and the earthquake force demand acting on each wall is automatically compared against the minimum resisting horizontal force capacity (F_{cr}) given in Eqns. (2.23), (2.25), and (2.27) regarding the boundary conditions and aspect ratio of the walls. The equation giving the minimum force (F_{cr}) also determines the governing failure mode. Regardless from the rocking or diagonal shear failure, subsequent failure modes of corner crushing and base sliding can be checked using eqns. (1.7) and (2.28), respectively.

2.1.3.1 Example House

A single storey URM house was selected as the case study for the evaluation part using macro based excel program. The house is placed in Antakya, Turkey (Figure 2.10) and has 7.5 m width, 17.5 m length, and 2.4 m wall height. To define the wall layout in the program, walls are defined as lines between wall corners and window–door openings (Figure 2.11).



Figure 2.10 General view of example house

In calculation of earthquake demand forces on the house and on the walls, Eqn. (2.21) was used. Evaluation of the house was performed using eqns. (2.23) and (2.27) since the reinforced concrete slab was assumed to restrain the rotation of the wall segments. The program has basic routines for drawing of layout of the walls, placing shear and mass centers graphically, calculating periods in x , y , and θ directions, and calculation of the most critical wall's rating factor and identify the governing failure pattern.

The user needs to manually remove the most critical wall from the definition table and rerun the analysis to see if remaining walls will successfully carry the earthquake forces. The wall removal would continue until the load is safely carried or structure will collapse. One of the weak walls defined in the house system may prematurely fail; however, the remaining walls may adequately carry the

earthquake forces. In that case, the house would not collapse but some of the walls would experience damage.

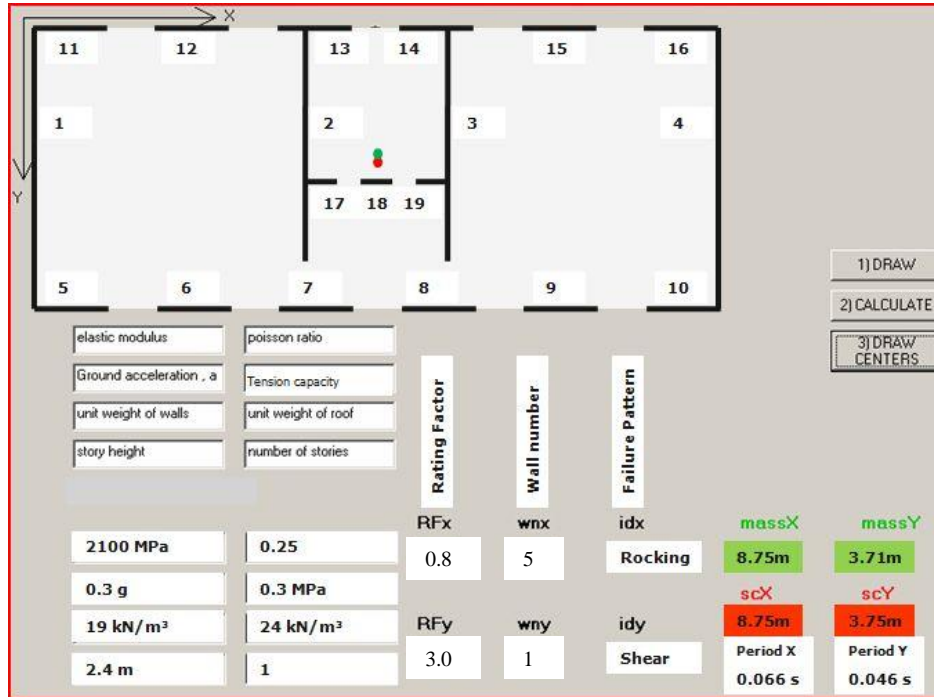


Figure 2.11 General appearance of the macro based excel program showing example house data

The necessary parameters to be used in the calculations are elastic modulus of the wall material, horizontal ground peak acceleration, unit weight of the walls and roof, storey height, tension capacity of the mortar, and number of stories. The general appearance of the program is given in Figure 2.11 along with the drawn data of the example URM house. For the demonstration house, a 0.3g horizontal earthquake acceleration was separately applied at the roof level both in X and Y directions. Half of the wall masses are also included for the translational and rotational masses. The wall heights for each segment were carefully defined considering the window and door openings effects on the wall height. “H*” were used in the place of “H” in the calculations (Section 6.1.4.2).

Number 17, 18, and 19 walls were extracted from the calculations since they were not assumed as load carrying walls. The results were obtained as a) number 5 and 11 walls have rating factors of 0.8 against rocking motion when the earthquake is in X direction, b) number 1, 2, 3, and 4 walls have rating factors of 3.0 against diagonal shear failure when the earthquake is in Y direction. Additional discussion is given in Section 6.1.4.2.

CHAPTER 3

MATERIALS AND MATERIAL TESTS

Several different materials are used for the construction of load bearing systems in URM structures. The common materials of masonry construction are brick, stone, adobe, and wood. According to census 2000, 41% of the masonry houses in Turkey are constructed using brick (Figure 3.2). Brick blocks are placed on top of each other using mortar layers in between them. The foundation and slab of the URM buildings are generally made from reinforced concrete. URM structures commonly have high vertical load carrying capacity; however, non-engineered URM structures may lack lateral load resisting capacity in the case of earthquakes. If heavy roofs are supported by URM, the increased mass results in development of larger lateral inertial forces.

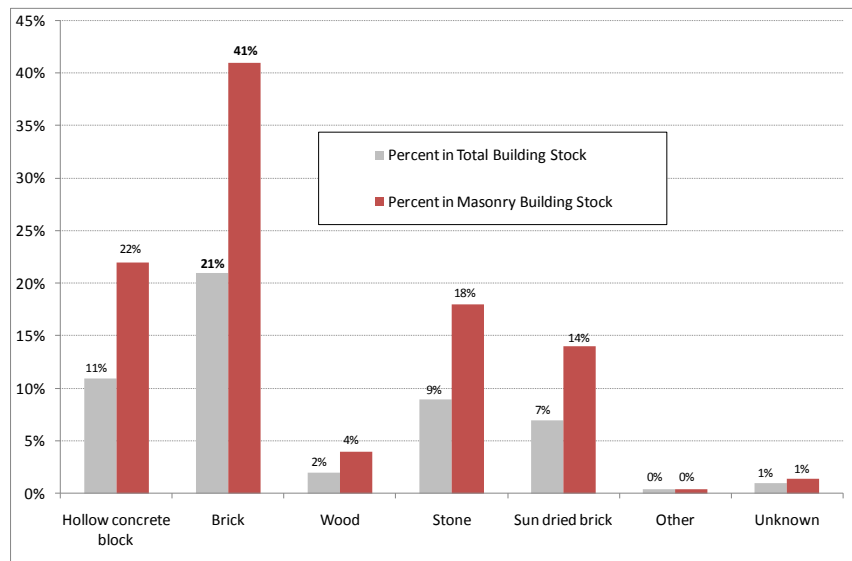


Figure 3.1 Percent distribution of common URM building materials

In addition to the layout of URM walls in the plan of a building and geometrical properties of the walls, there are different material parameters that affect the lateral load carrying capacity of a brick masonry house. Types of bricks used in the construction, mortar mix, quality and age of bricks, mortar brick interface and level of vertical force due to self-weight that is acting on the walls are some of the factors that determine the capacity of the walls.

A number of laboratory tests were conducted on the brick and mortar that were used for the wall test specimens. The mortar mix and workmanship used to construct the walls were tried to be replicated in the lab utilizing a skilled bricklayer. In order to obtain characteristic material capacity and behavior, some material tests were performed in the laboratory. These tests are;

- Brick compression tests
- Mortar compression tests
- Mortar shear tests (triplet test)

3.1 Brick compression test

Three 125 mm x 175 mm x 275 mm bricks were used with a void ratio of 60% (Figure 3.2). Brick was placed in the testing machine and loaded in the direction of the holes. For the displacement measurement, a Linear Variable Displacement Transducer (LVDT) was placed in the same direction. Average force displacement curve is obtained for the vertical compressive loading of the brick (Figure 3.3). Approximate vertical load carrying capacity of the bricks was found to be 330 kN as given in the graph. When the vertical load carrying capacity of a brick is divided by the total cross sectional area (including holes according to “Specification for Structures to be built in Disaster Areas-2007”), ultimate compressive stress is approximately found to be 6.86 MPa.

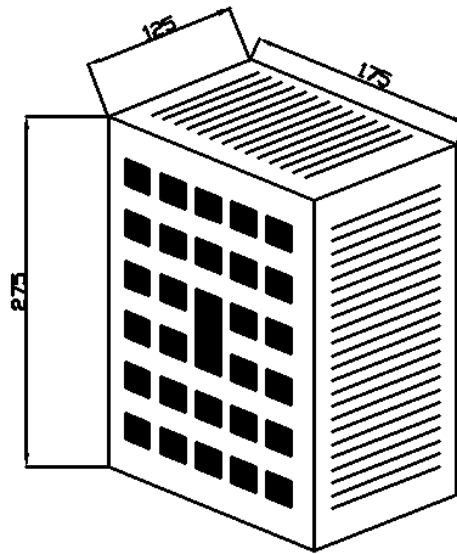


Figure 3.2 Dimensions of the brick used in tests, (in mm)

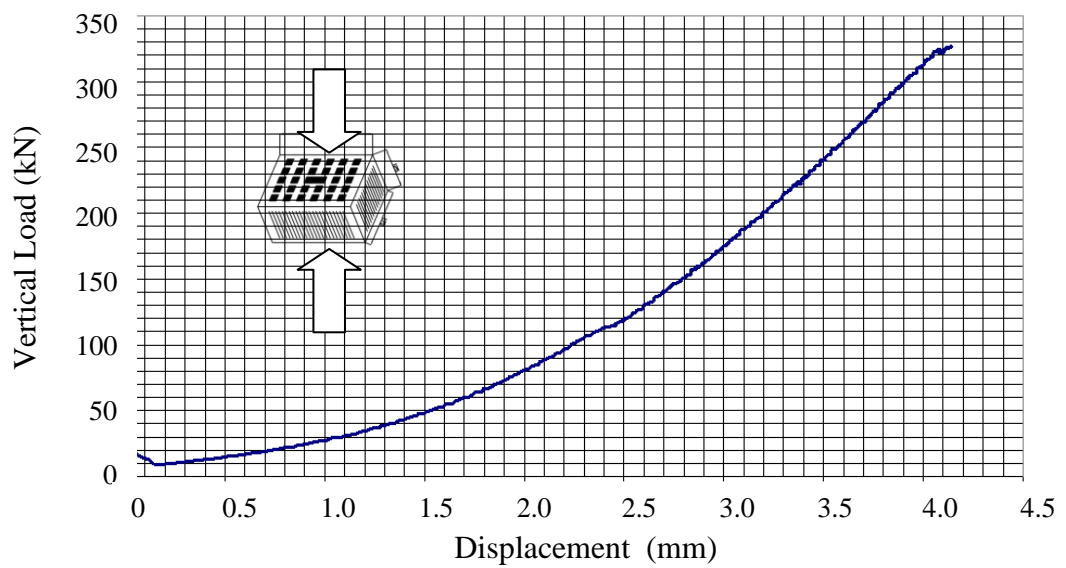


Figure 3.3 Force displacement graph of the brick test

3.2 Mortar compression test

Mortar was mixed on site using about 200 kg fine sand, 40 kg cement, 25 kg lime, and water is adjusted to maintain a workable paste and change as a function of the sand humidity (30-40 kg of water on average) to obtain about 300 kg of mortar.

Four cylindrical samples with 75 mm in diameter and 150 mm in height were tested in the direct compression machine. The ultimate strength for mortar tested on 8 and 28 days were obtained as 2 MPa and 3.85 MPa, respectively.

3.3 Masonry shear test (triplet test)

A testing mechanism called “triplet test” in accordance with EN 1052-3 standard was prepared in order to obtain average direct shear strength of the masonry and to observe the increase in shear strength through different levels of axial compressive load on the brick units. Three bricks were placed as shown in Figure 3.4 to ensure that only shear stresses develop in brick-mortar joints, which was also stated by Tomazevic [4]. Shear strength values of brick-mortar joints were obtained under zero compressive stress and by using compressive stress increments that are perpendicular to shear direction. Approximately 80% of brick area, which is 275x175 mm, was assumed as the mortar area at the intersection of brick with mortar, since the mortar is placed only at the edges of the bricks and the center is left for temperature insulation similar to the case used in the practice. Compressive force was applied in the perpendicular direction using steel plates compressed by tightening bolts (Figure 3.4).

The ultimate shear strength of the triple bricks was plotted against the perpendicularly applied compressive force in Figure 3.5 and a linear regression line was fit between the shear capacities and perpendicularly applied compressive forces.

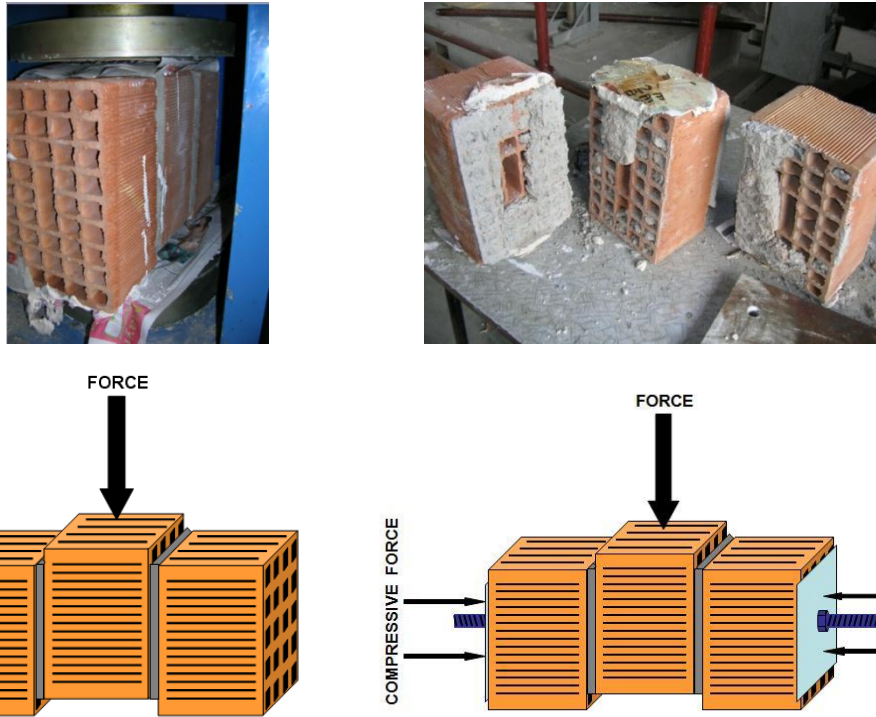


Figure 3.4 Triplet Test setup

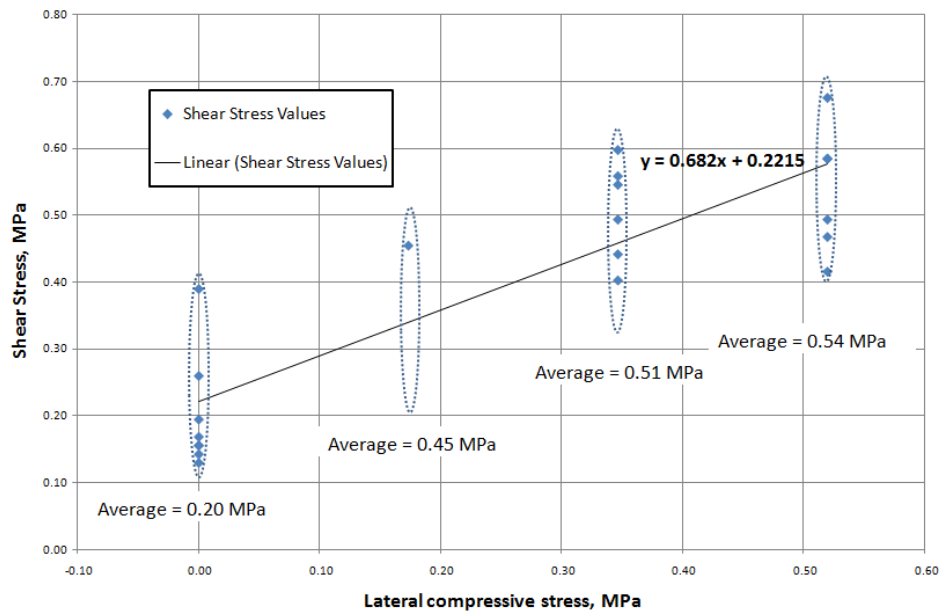


Figure 3.5 Shear stress vs. Lateral compressive stress graph (Average shear stresses)

CHAPTER 4

HALF-SCALE BRICK MASONRY HOUSE TESTS

Half-scale brick masonry houses were constructed in the laboratory in order to test performance of rebar post-tensioning based strengthening methods. The constructed URM lab specimen represented a single storey house with two rooms; a basic housing unit constructed using hollow clay bricks, which is one of the most frequently used masonry construction material in Turkey. The basic properties of the test model was to have multiple openings symmetrically placed on either sides and have a concrete slab that connects all of the walls from above. The purpose of the test was to test effectiveness of rebar based strengthening on the brick masonry house and document relevant performance improvement. Symmetrically constructed walls on two sides of the house were aimed to generate symmetry in deformation and damage, while walls placed in perpendicular direction were planned to use for lateral stability. The width of the test house was kept low at 1 meter to save from the material and laboratory space since the primary concern was testing the house walls in their in-plane direction. The ceiling slab was pushed and pulled using a hydraulic piston operated by an electric pump for reversed cyclic loading of the house. The load was initially force controlled up to the level of initial cracking and damage formation; then, the displacements were controlled to observe the post-cracking behavior of the test house.

The strengthening plan for the masonry house was to first demonstrate the use of vertical post-tensioning on the capacity increase of the walls and then demonstrate the strength improvement for diagonal rebar bracing on the test house. An

innovative approach using spring boxes were proposed to retain the post-tensioning force on the rebars, which can be easily lost due to cracking of the walls or yielding of the post-tensioning rebars. General behavior after strengthening was approximately predicted using simple relationships for design of strengthening on actual houses using the proposed technique. Dimensions of the wall parts and a general view from the test house are given in Figure 4.1.

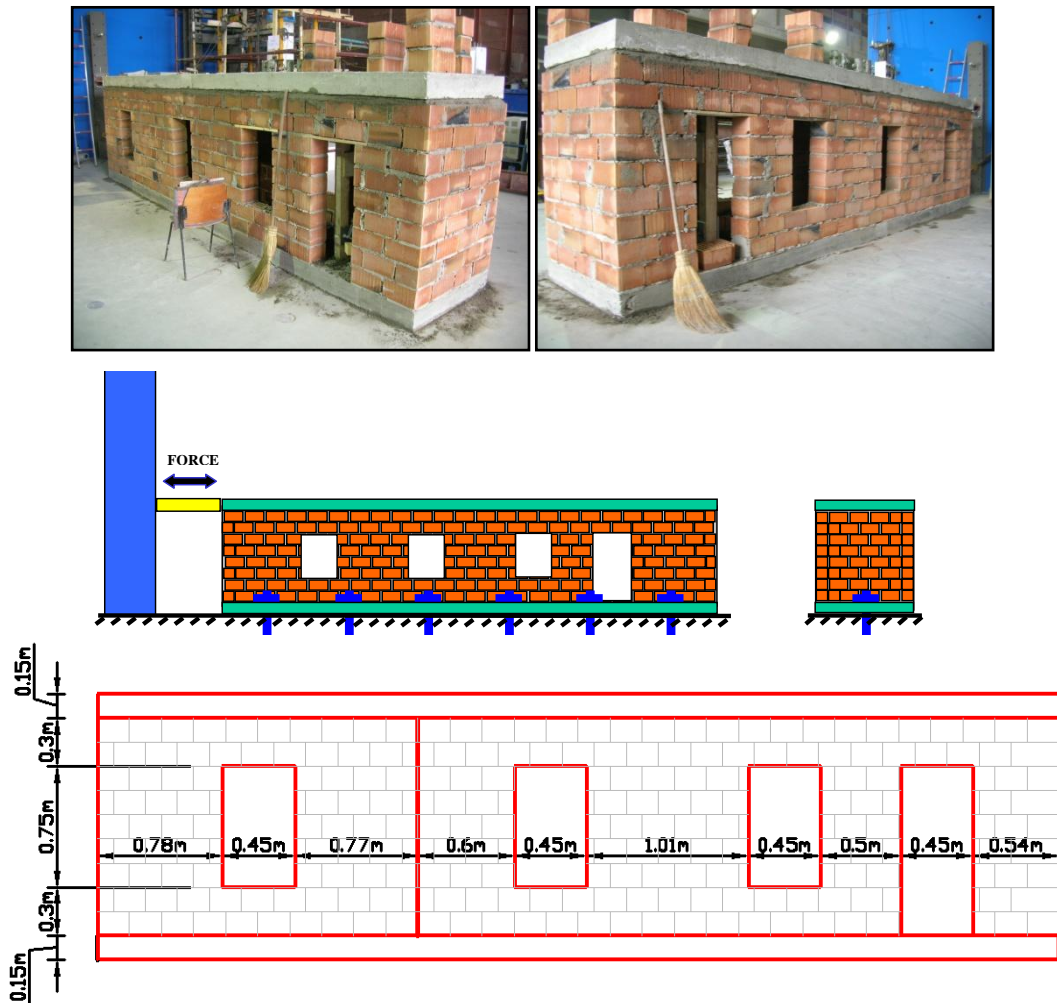


Figure 4.1 Half-scale brick masonry house test specimen

4.1 Evaluation of test setup

Before the experiments, the test specimen was evaluated analytically using the assumptions made in Chapter 2 and Eqns. (2.10) through (2.21) to calculate the load demand on the walls and house. Calculated load demands at each wall were compared with the smallest in-plane resisting capacity derived in Eqns. (2.23) and (2.27), which are the upper edge restrained cases since a rigid diaphragm was assumed for the roof (relocating H with H^*). Finally, rating factors of each wall were calculated by dividing the in-plane shear capacity of the wall to earthquake load demand on the wall. All of those computations were performed using the macro based excel program that is mentioned in Chapter 2.

Based on the results that are given in Figure 4.2, wall number 1 has the smallest resistance capacity relative to others. Nevertheless, the wall can resist 0.4 g earthquake acceleration demand with a rating factor of 5.7 in its in-plane direction. Although the lab house is constructed as 1 meter wide due to laboratory constraints, the actual house would be about 6 meters in width causing the earthquake demand to increase about 6 times. In that case, the rating factor would be reduced and become smaller than 1.0 with a rating factor of 0.96. The tested house may be assumed to be the first floor of a two-storey house. In that case, the total seismic demand would be doubled; however, wall capacities due to additional vertical force are not increased with the same proportion. So, the new rating factor for 6m wide test house with two storeys would be calculated as lower than 0.48.

Number 1 wall exhibits a rocking failure due to eqn. (2.27). Although number 1 wall fails in flexure it continues to carry vertical loads and horizontal force. Redistribution takes place between the other walls until all of the walls fail. Post-cracking strength of the wall was assumed to be zero; although, the cracked wall would continue to carry some amount of lateral force.

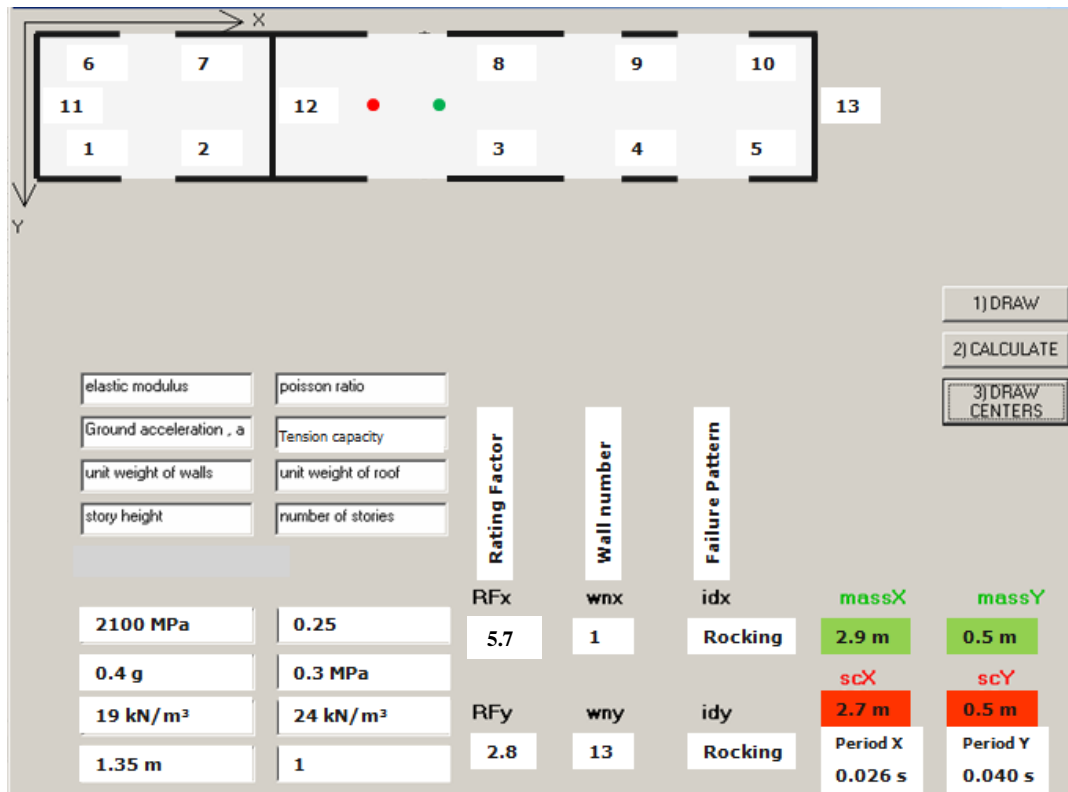


Figure 4.2 Results of test house on macro based excel program

Proposed strengthening techniques were tested on four different lab houses. The first house specimen was tested three times with minor damages at the second and third tests. Total of six half-scale house tests that were performed in the laboratory are summarized below. These are;

- First test: Original unstrengthened specimen
- Second test: Cracked specimen with 50 kN of weight over it
- Third test: Cracked specimen with 10 ϕ 16mm vertical post-tensioning rebars (total vertical post-tensioning force of 200 kN and tightening bolt during testing)
- Fourth test: New specimen with post-tensioning using spring boxes along with 10 ϕ 16mm vertical rebars (total vertical post-tensioning force of 200 kN)

- Fifth test: New specimen with post-tensioning using spring boxes along with 10 ϕ 16mm vertical rebars and 12 ϕ 16mm diagonal rebars (direct welding)
- Sixth test: New specimen with post-tensioning using spring boxes along with 10 ϕ 16mm vertical rebars and 12 ϕ 16mm diagonal rebars (heated to about 100 C° before welding into its place).

Each one of the performed tests was conducted to assess the improvement in strength of the original lab house. The increase in ultimate capacity for each test was compared against the original house as multiples of the original house ultimate capacity.

4.2 First test: Original unstrengthened specimen

Half-scale test house (Figure 4.3) was loaded to failure in its original condition without any strength improvement. Distribution of lateral load in accordance with the stiffness of each wall was considered before the test in order to analytically approximate an in-plane lateral load carrying capacity. The numbering of wall segments is given in Figure 4.2 and related data is presented in Table 4.1. Thickness of mortar joint was assumed as 120 mm and elastic modulus was taken as 2100 MPa.



Figure 4.3 Original unstrengthened test specimen

First of all, the initial stiffnesses of each wall were calculated using Eqn. (2.11) and total stiffness of test house was obtained by summing all of the stiffness values. Walls oriented in their out-of-plane direction were neglected in the stiffness calculations. Roof weight was distributed among the walls according to the length ratios of each wall segment. In-plane lateral load capacity of each wall was obtained by using the minimum of F values calculated from Eqns. (2.23) and (2.27). Lateral deformation capacity of each wall was found by dividing the obtained F values with stiffness values of each wall. Lateral load capacity of the house was obtained for each case by multiplying the lateral deformation of each wall with total stiffness of the house. Finally, the wall giving the minimum lateral load capacity of the house was assumed to be the governing condition for the initial damage and that wall was not included for the latter calculations. Although the wall has failed in the horizontal direction, it was assumed to carry vertical loads. After recalculating the load distribution ratios between the uncracked walls using the relative stiffness terms, demand versus capacity calculations and wall removal procedure was iterated until the failure of last wall. A capacity curve of the test house was obtained by plotting the load-deflection points before and after each wall's removal (Figure 4.4).

Table 4.1 Data for wall segments of test house

Wall	H (mm)	H* (mm)	B (mm)	t (mm)	λ
1	750	1050	780	120	1.28
2	750	1050	1370	120	1.16
3	750	1050	1010	120	1.22
4	900	1200	500	120	1.50
5	1050	1350	540	120	1.50
6	750	1050	780	120	1.28
7	750	1050	1370	120	1.16
8	750	1050	1010	120	1.22
9	900	1200	500	120	1.50
10	1050	1350	540	120	1.50

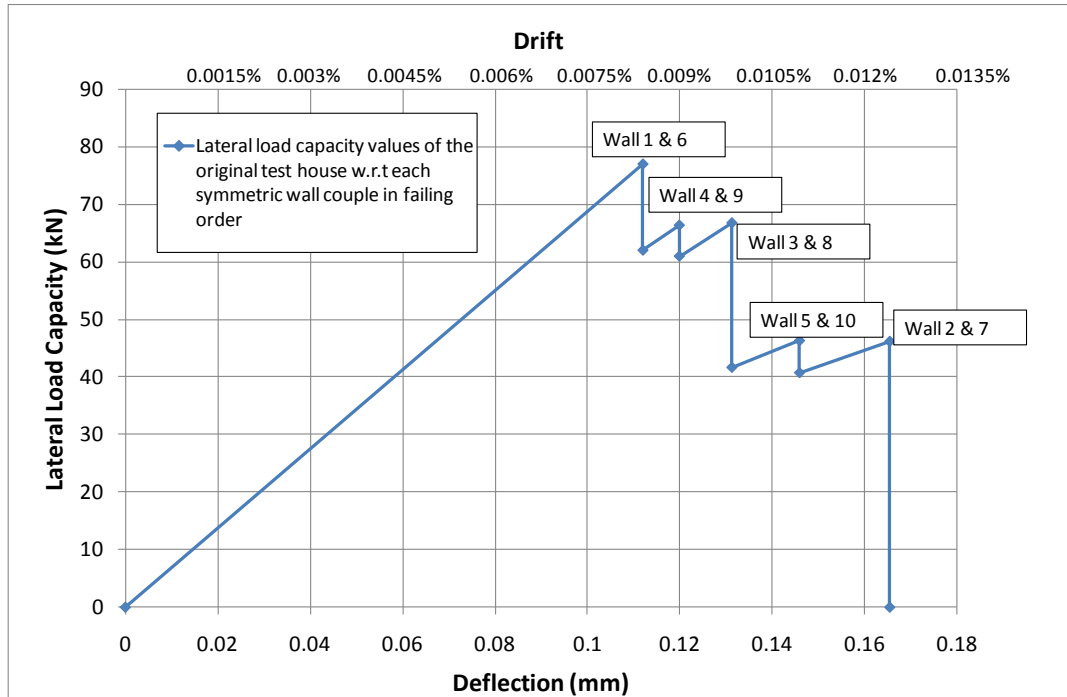


Figure 4.4 Analytically fit capacity curve of unstrengthened test house

Unstrengthened URM house specimen test was performed with increasing reversed cyclic loading until the first crack has formed. Initial loading step started from 10 kN and increased systematically with about 10 kN increments. Lateral force has reached to its ultimate value of 68 kN at around 0.42 mm (0.031%). The lateral force approached to about 50 kN plateau as the displacements are further increased (Figure 4.5). The forces approaching to a constant value is deemed to be due to a static equilibrium position as all of the walls were cracked in flexure (rocking mode) and the weight of the ceiling was supported by the lateral force. Assuming the diagonally formed compression struts are all inclined 45 degrees, the lateral force should have been equal to the weight of the ceiling, which is 32 kN. Since the test was stopped before excessive damage to the structure, the lateral force is expected to further decrease if the test was continued on until heavy damage.

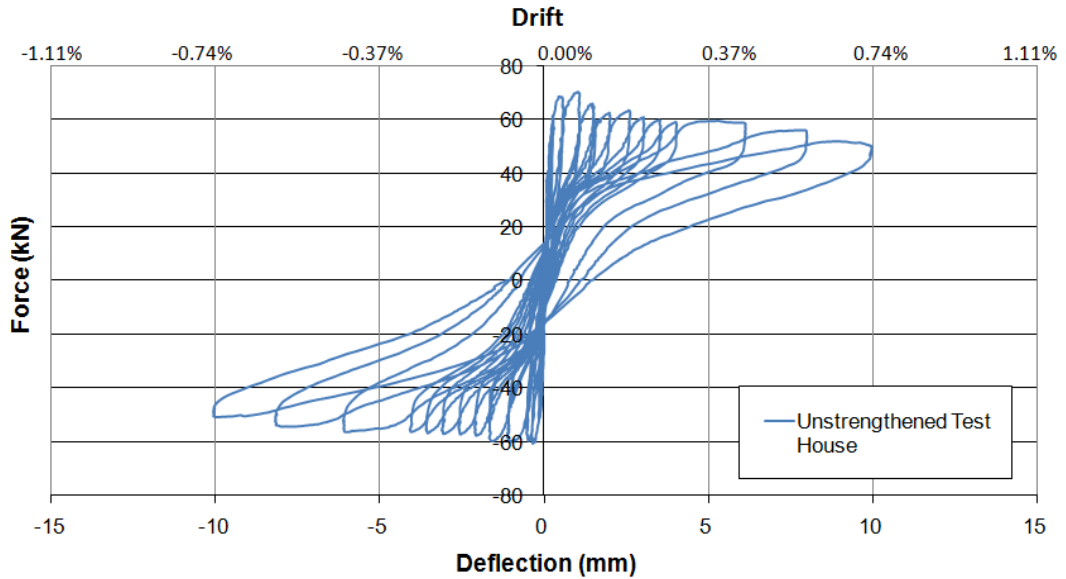


Figure 4.5 Force vs. Deflection graph of the first test

After the test house has reached at 68 kN at 0.42 mm (0.031% drift) the test was continued with deflection control until 9.9mm (0.73%). During the test, cracks were observed at the corners of window and door openings. Horizontal cracks on the walls followed a close to horizontal line that coincided with the edges of window and door openings (Figure 4.6). During the test, cracked wall segments rotated in their in-plane direction, which states that the rocking was the governing failure mode.

During the rocking motion, the ceiling is lifted upwards and a close to constant lateral force has been developed as a result of the diagonal compression struts. Therefore, the calculation steps used to obtain Figure 4.4 was modified to include the lateral force that was developing at the rocking corner of the walls. As the wall has passed beyond its flexural capacity in rocking failure mode, the stiffness of the wall was again assigned to be zero; however, a constant reaction force in the horizontal direction was kept in the calculations. Using equilibrium equations on the walls free body diagram (Eqn. (4.1)), the lateral force at the corner of the walls,

which has failed in the rocking mode, was calculated as a function of the vertical dead load acting on each wall as shown in Figure 4.7.



Figure 4.6 Cracks on the first specimen

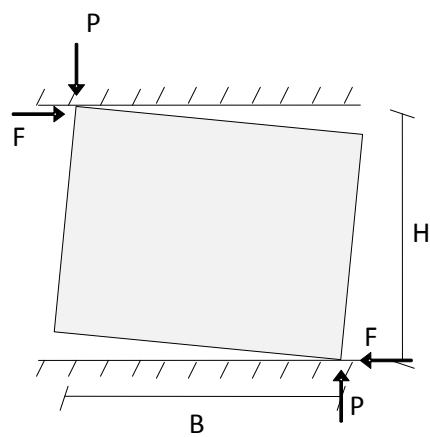


Figure 4.7 Horizontal constant force developing at the corner of rocking walls

$$F = P \times \frac{B}{H} \quad (4.1)$$

The comparison of the analytically obtained load-deflection graphs are compared in Figure 4.8. The curve obtained by considering static equilibrium of the walls that were cracked in rocking motion differs in the nonlinear range and has a constant remaining lateral force of about 40 kN as all of the walls have cracked and lost their stiffness.

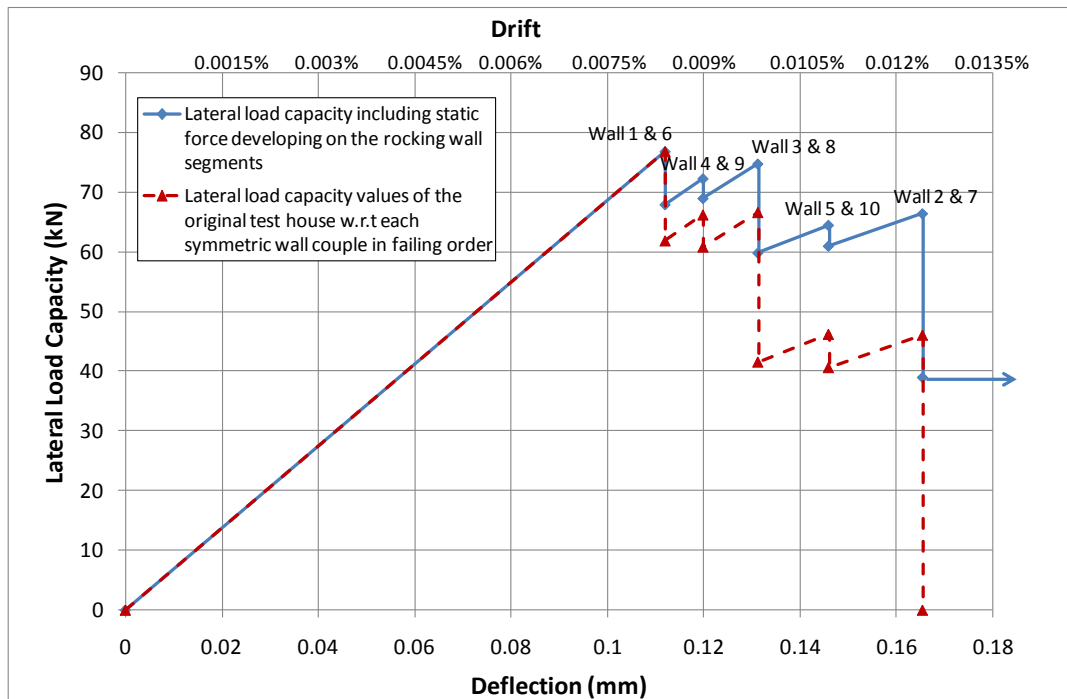


Figure 4.8 Analytically obtained load-deflection graphs of unstrengthened test house

It was observed that the test specimen had a remaining capacity in the range of 60 kN even after all of the walls were cracked (Figure 4.5). It is noteworthy to state that not all of the walls have the same aspect ratio. Walls with low aspect ratio (H/B) would experience a larger uplift for a unit lateral deflection, relative to the

other walls with higher aspect ratio. The outcome is that the ceiling would be lifted up the most by the walls that have the smallest aspect ratio. In that case, majority of the weight imposed by the ceiling on the walls is transferred to the walls that have the smallest aspect ratio, which would generate larger horizontal resisting forces. For example, wall number 2 in the test house has the lowest aspect ratio of 0.55 generating a horizontal force which is 1.82 times the vertical force acting on the wall. If majority of the ceiling weight acts on wall number 2, the horizontal reaction in the post-ultimate response can be calculated as $(32 \text{ kN dead load}) * 1.82 = 58 \text{ kN}$ which is quite close to the measured response of about 60 kN (Figure 4.5). On the other hand, the lifted ceilings orientation and interaction with the walls is very difficult to analyze considering bending deformations of the ceiling, uplift level over each wall, and walls that would mainly support the ceiling.

Performed mortar compression tests showed that the compressive capacity of the mortar was about 3 MPa and the tension capacity was assumed to be one tenth of the compressive capacity as 0.3 MPa. However, the hollow brick and mortar interface is quite complicated due to the void regions of the brick slightly submerged in to the mortar paste. Nevertheless, assuming 100% of the mortar surface being in contact with the brick is not possible. Hollow brick has 60% void ratio and mortar mix slightly moves into the voids and gets in contact with the side surfaces of the brick cells. Calibration of the tension capacity to achieve similar results have shown that accepting 0.25 MPa as tension capacity gives similar results obtained from the test as an ultimate capacity of about 68 kN.

4.3 Second test: Cracked specimen with 50 kN of weight over it

As the rotating (rocking) mechanism in the first test was evident, a simple restraining mechanism was thought to be the application of vertical compression force on the test house. The vertical compression on the walls can be applied using vertical post-tensioning or extra weight on the house. Although additional mass on the house would also increase the inertial forces generated during earthquakes, the

test setup is loaded with about 5000 kg mass above the roof in order to see the actual effect on the already damaged test house (Figure 4.9).

Although the test house was initially damaged before the second testing, the lateral load capacity was improved to about %147 of the original house, from 68 kN to about 100 kN (Figure 4.10). The walls still rocked following the existing cracks that were generated during the first test; however, the rocking was more difficult since the vertical force on the walls were larger and acting in the opposite direction to restrain the rotating walls. The added mass was about equal to the mass of the existing house, therefore representing a second storey above the existing one. On the other hand, existence of a second storey would at least double the earthquake demand (assuming very low period (T_1) for URM) and capacity increase in the order of 50% would not be adequate. Therefore, having a second storey would not be advantageous for earthquake loading as expected.

The displacement – load capacity curve was also obtained for the house with 50kN weight on the roof as shown in Figure 4.11. The initial stiffness degradation is shown with a dashed line since the walls were already cracked. The ultimate remaining capacity of the wall after all crack formations has obtained as about 100 kN as in Figure 4.10.



Figure 4.9 Second test with 50 kN of weight above the house

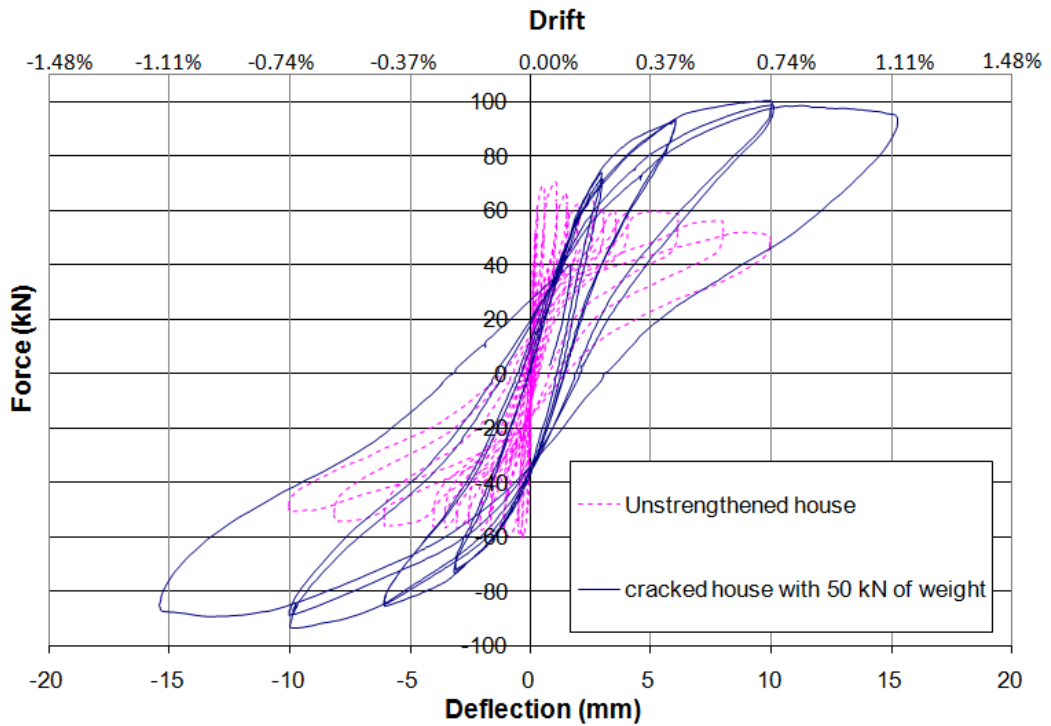


Figure 4.10 Force vs. Deflection graph of the second test

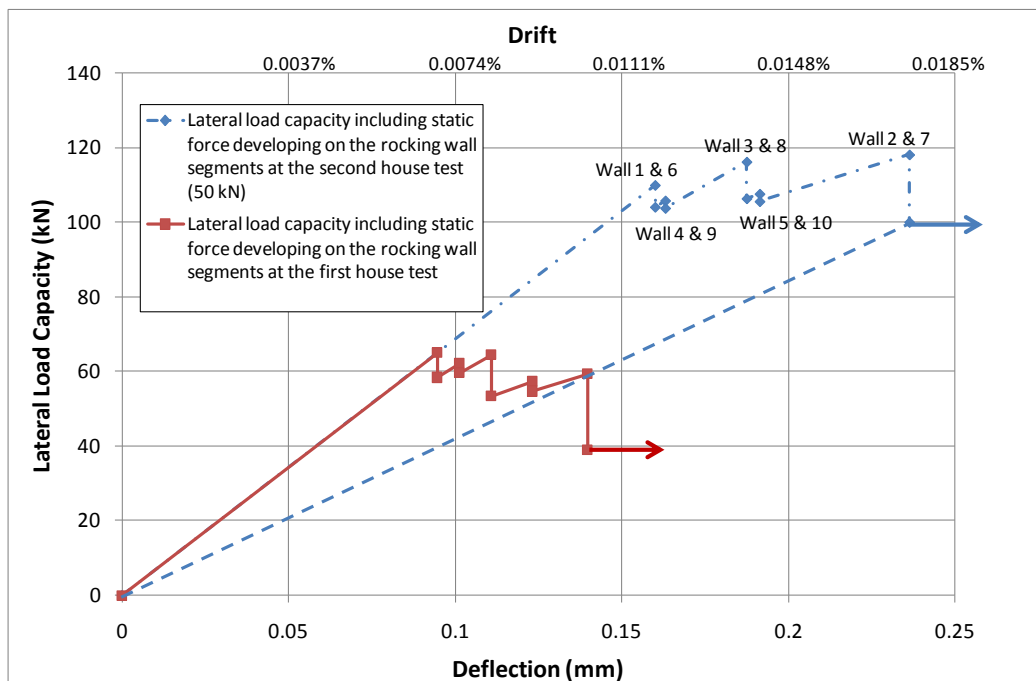


Figure 4.11 Analytically obtained capacity curves of the first and second tests (cracked + 50kN DL)

4.4 Third test: Cracked specimen with 10 ϕ 16mm vertical post-tensioning rebars (total vertical post-tensioning force of 200 kN and tightening bolt during testing)

The (damaged) original test house that has already been used in the first and second tests was also used in the third test where total of 10 vertical rebars with ϕ 16mm diameter were placed and stretched between the floor and ceiling slabs. The rebars were attached to the slabs using 10mm thick metal plates, which were anchored on the side surface of slabs using mechanical type steel anchor bolts. The mechanical bolts anchored in to the concrete can be found worldwide, which are first inserted into the drilled holes in the concrete and as the nut is tightened, a mechanism inside the drilled hole opens and locks the steel dowel inside the concrete. The locations of the vertical post-tensioning rebars are shown in Figure 4.12. Assuming the floor and ceiling slabs form a close-to-rigid connection between the upper and lower edges of the walls, the vertical rebars were arbitrarily placed, except for not blocking the window or door openings and leaving room for future cross-brace rebar placement.

Post-tensioning bars located in the vertical direction were used to apply vertical force of about 20 kN on each bar for a total of 200 kN. Considering the 5000kg of mass generated 50 kN in the vertical direction, the applied force was about 4 times the former test. The maximum capacity have reached to about 250 kN, which is about 4 times the original capacity of 68 kN and about 2.5 times the 100 kN capacity with 5000 kg mass on the ceiling (Figure 4.13).

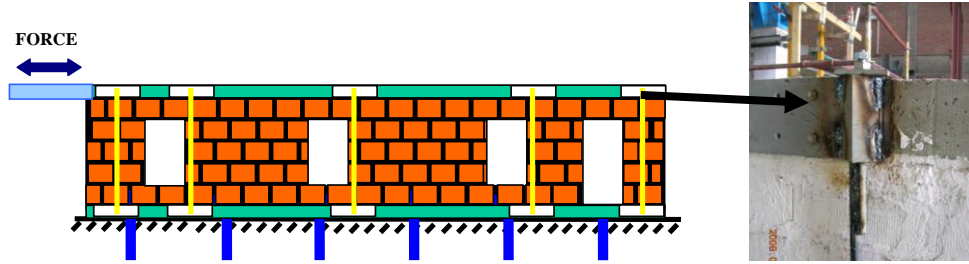


Figure 4.12 Setup of the third test

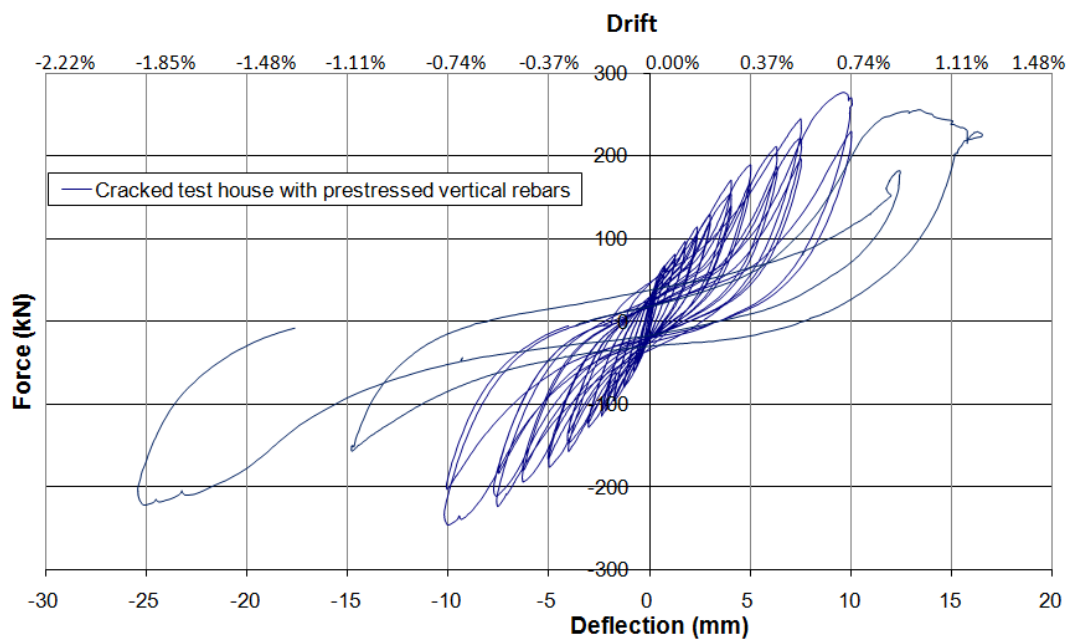


Figure 4.13 Force vs. Deflection graph of the third test

If the capacity increase is plotted against the level of vertical force application, a close to linear relationship is observed as given in Figure 4.14. The initial post-tensioning on the vertical rebars are likely to increase during the testing since vertical deflection demand on the vertical rebars would generate additional vertical force. Therefore, if a second graph is prepared using the initial slope of the curve for 32 kN and 82kN (32+50) vertical loads, the vertical force on the rebars are calculated as 284 kN (316-32) (Figure 4.15). Therefore, it may be concluded that significant amount of capacity increase can be achieved by using vertical post-

tensioning in the case of single or two-storey non-engineered brick masonry type buildings.

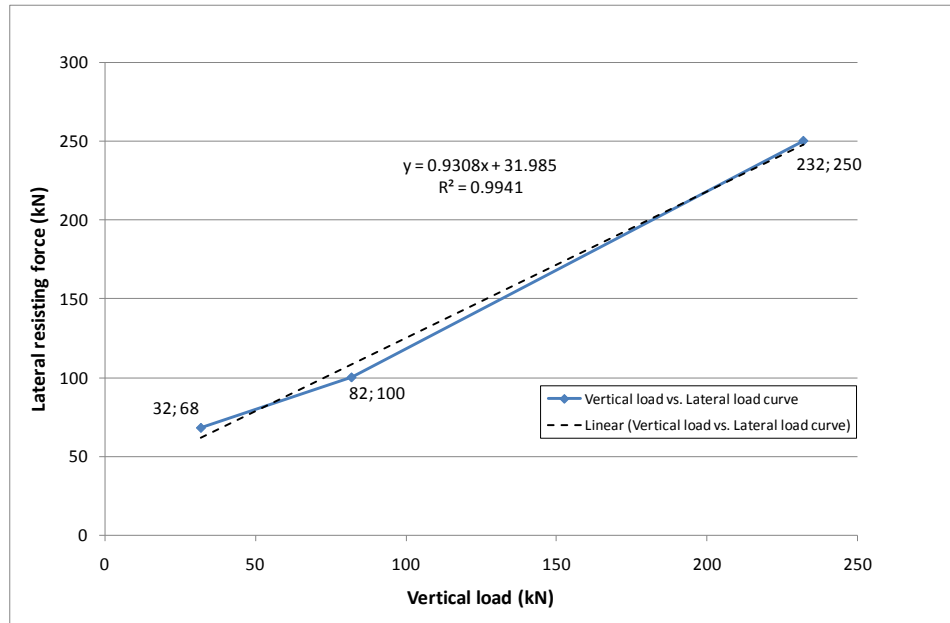


Figure 4.14 Capacity increase on the test house against vertical load application

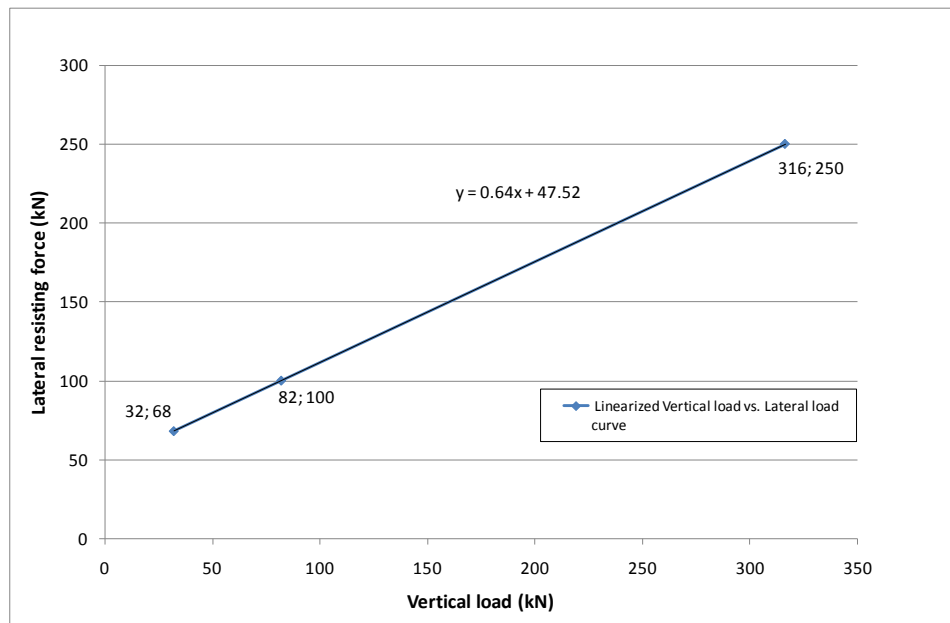


Figure 4.15 Linearized capacity increase against vertical load application

Crushing of the mortar joints due to larger compressive stresses during the test, has resulted in losing the initial post-tensioning of the vertical rebars which led to opening of the already existing flexural cracks. During the third test, re-application of post-tensioning force on the vertical rebars prevented the wall piers from rotating and caused them to crack diagonally as shown in Figure 4.16. As a result of loosening of the rebars during the test, bolts were tightened two times during the testing which indicated the need for a mechanism to tighten relaxing rebars during loading. A spring-box system was developed for the next rounds of tests to prevent premature loss of post-tensioning force. Details about the spring box based post-tensioning is given in the following sections.

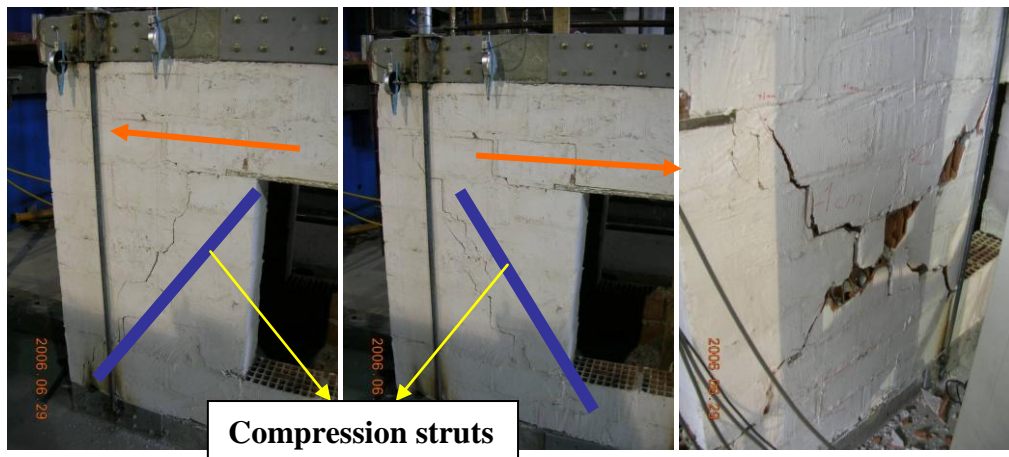


Figure 4.16 Diagonal shear cracks on vertically post-tensioned cracked house

4.5 Fourth test: New specimen with post-tensioning using spring boxes along with 10 ϕ 16mm vertical rebars (total vertical post-tensioning force of 200 kN)

During the third URM house test, it was noticed that the post-tensioning force in the rebars can easily be lost due to minor crushing of the URM walls. The height change in the order of 0.67mm would totally release all of the post tensioning force in the vertical rebars. A mechanism was needed to keep the post-tensioning force close to constant although the vertical height of the walls was decreased

during loading beyond the linear capacity (Figure 4.17). Spring boxes that include 18 disc type spring pieces with 37 kN/mm stiffness value connected serially were attached at the ends of the rebars and provided a spring stiffness of 2 kN/mm. Compression of the spring box for about 10mm would generate the desired post-tensioning force on the rebar. In this way, the force in the post-tensioning bar would only reduced by 6.7% if the same wall shortening of 0.67mm was experienced, which would release 100% of the post-tensioning force before utilizing spring boxes. Therefore, the post tensioning force in the rebars was kept close to constant for small changes of the wall height in the post-ultimate range.

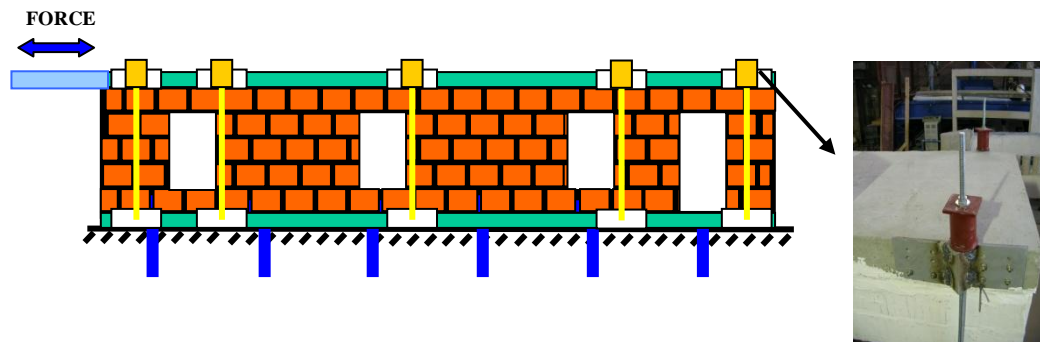


Figure 4.17 Setup of the fourth test

Figure 4.17 shows the setup of the vertically post-tensioned test house with springs at the connections of vertical rebars. Total of 200 kN force was applied vertically by compressing the spring boxes about 10 mm, similar to the third test with the exception of the spring boxes. Unlike the third test, the bolts were not re-tensioned during the fourth test. According to force deflection graph of the fourth test (Figure 4.18) it is seen that maximum load carrying capacity was slightly lower than the one obtained in the third test in which the pretension force was adjusted during the test. The slight reduction was deemed due to the minor loss of post-tensioning force. The vertical shortening of the walls was observed exceeding the compression capacity of the spring boxes as shown in Figure 4.19. Diagonal shear

cracks were observed at the walls numbered as 2, 3, 7 and 8 as in Figure 4.20. Remaining walls exhibited rocking failure due to higher aspect ratios.

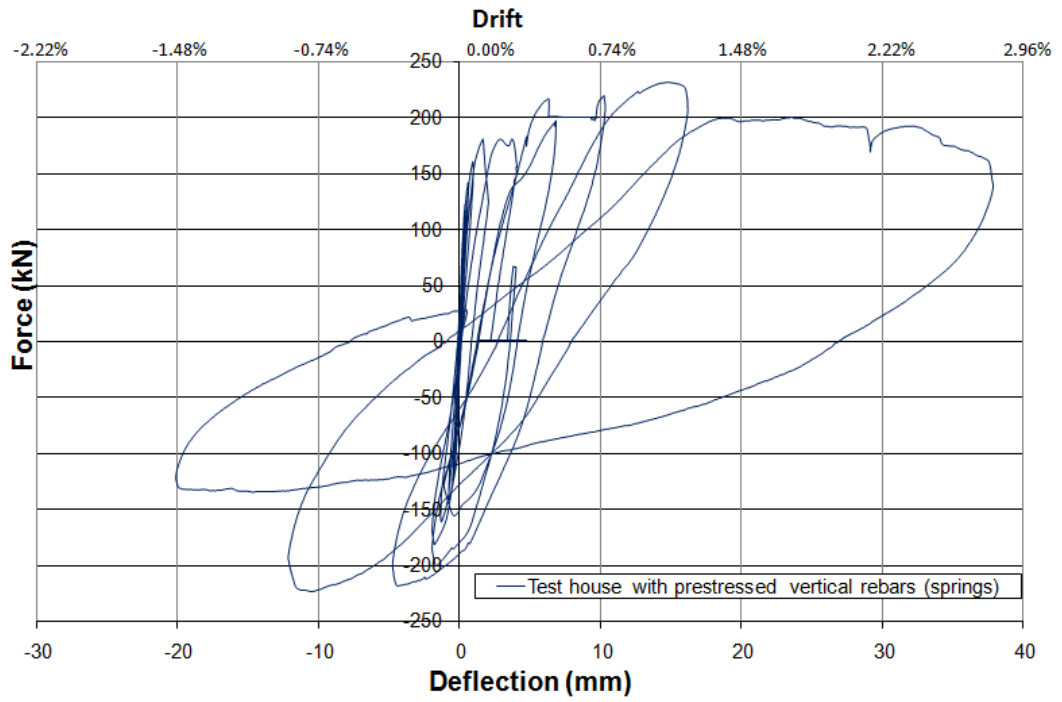


Figure 4.18 Force vs. Deflection graph of the fourth test



Figure 4.19 Unloaded springs due to wall crushing in the vertical direction



Figure 4.20 Cracks on the fourth test

4.6 Fifth test: New specimen with post-tensioning using spring boxes along with 10 ϕ 16mm vertical rebars and 12 ϕ 16mm diagonal rebars (direct welding)

The strength improvement achieved by vertical post-tensioning bars was successful in improving the capacity of the wall about four times, beyond the earthquake demand. However, placement of diagonal bars was also investigated in order to further improve the lateral load capacity of URM lab house.

Diagonally placed rebars with ϕ 16mm diameter were attached between the floor and ceiling slabs with changing inclinations in addition to the vertically oriented rebars (Figure 4.21). The vertical post-tensioning of about 200 kN was also applied using spring boxes. Diagonal rebars were connected to the test house by welding without any pre-tensioning force.

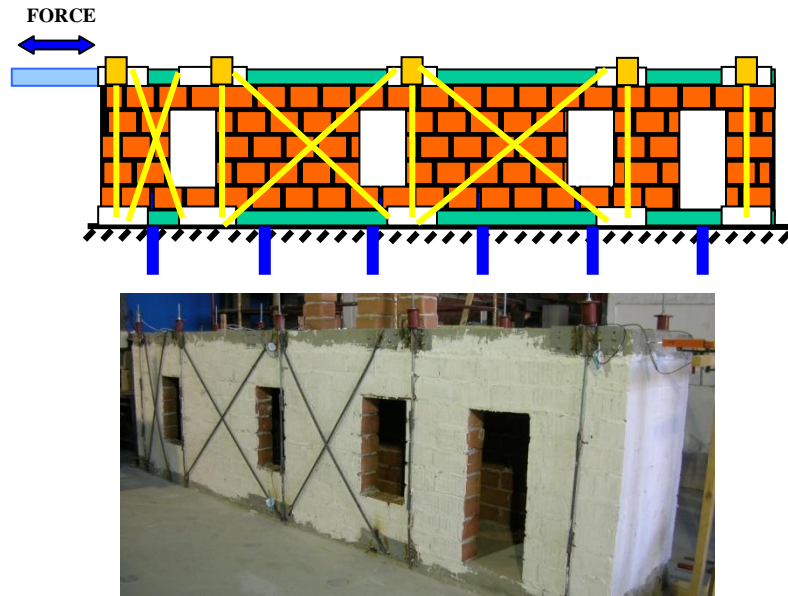


Figure 4.21 Setup of the fifth test

The test setup was prepared using a single hydraulic piston that would pull and push the slab level. The reinforcement placed inside the ceiling slab was welded to a horizontally placed loading beam which was connected to the hydraulic piston. The fifth test house, which had diagonal braces, could not be fully loaded in the pulling (tension) direction since the actuator – slab connection was separated due to excessive force. The house was loaded in pushing direction only beyond its ultimate capacity which has been recorded as 450 kN; a value that is about 6.6 times the original capacity (68 kN) (Figure 4.22). Diagonal braces were yielded while vertical braces remained in their elastic range.

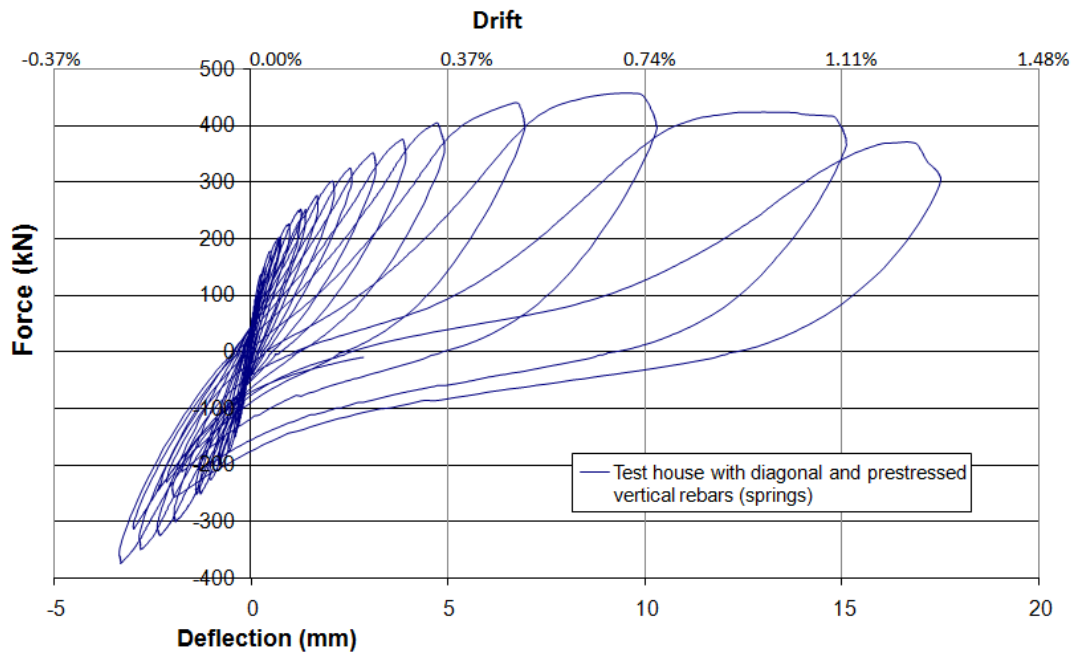


Figure 4.22 Force vs. Deflection graph of the fifth test

During the test, additional vertical forces were developed on the ceiling slab due to the vertical component of the forces in the diagonally placed rebar. Combined effect of the vertical post-tensioning and vertical component of the diagonal member forces, the rocking mode was suppressed and the walls have failed in diagonal shear cracking (Figure 4.23). Buckling of diagonal rebars during alternating loading directions verified the yielding – elongation of the diagonal rebars.



Figure 4.23 Cracks on the fifth test

The ultimate capacity of the third test house was measured as about 450 kN. The diagonal bars were placed with about 45° angle and ½ ratio for B/H in the first bay. The yielding stress was accepted as 450 MPa and $\phi 16$ mm bars yielded at 90 kN axial force. The horizontal component of all rebars on both sides of the house turns out to be 335 kN leaving about 115 kN for the load carried by the diagonal compression struts developing inside the wall segments. The failure was predominantly due to corner crushing; therefore, the crushing capacity of the corner bricks were calculated as 63.6 kN coming from the diagonal bar (vertical compression strut) and 31 kN generated by the diagonal compression strut (Figure 4.24). The vector combination of load in the range of 90 kN acting on a corner brick would be used for the future design applications of strengthening.

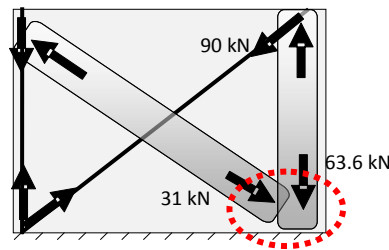


Figure 4.24 Force distribution on compression struts at the ultimate stage of the fifth house test

4.7 Sixth test: New specimen with post-tensioning using spring boxes along with 10 ϕ 16mm vertical rebars and 12 ϕ 16mm diagonal rebars (heated to about 100 °C before welding into its place)

Since the test setup in the fifth house test has failed in tension, the slab loading setup was modified to enable loading in the tension direction for higher demands (Figure 4.25). In the sixth and last test, the prestressing force on the diagonal rebars was applied by heating process. The diagonal bars which were post-tensioned by heating the bars to about 100 °C ($\sim 80^{\circ}\text{C} \times 12 \mu\epsilon / ^{\circ}\text{C} \cong 960\mu\epsilon$) prior

to welding two ends on the bolted plates have generated a post tensioning stress of about 190 MPa (~38 kN) considering losses due to support plate movement.



Figure 4.25 Strengthening of the slab

Experimental studies on heating of rebars (Figure 4.26) showed that significant axial force on rebars can be achieved. For example, if a post-tensioning force in the range of 50% of the yielding stress is needed, half of the yielding strain may be easily imposed by temperature increase of the bar. If the yielding strain is $2100 \mu\epsilon$, then (assuming that thermal expansion coefficient $\gamma = 12 \mu\epsilon/^\circ\text{C}$), a temperature increase of 83°C ($1000 \mu\epsilon / (\gamma \mu\epsilon/^\circ\text{C})$) in the rebar temperature would be enough to generate pretension about half of the yielding force on the rebar. Considering an ambient temperature of 20°C , the post-tensioning bar temperature must be increased by 83°C to 103°C . The overall temperature of a rebar can be measured by infrared based non-contact transducers; however, a primitive guess may be made by dripping water or oil on the heated post-tensioning bar surface. Boiling temperature of water can be taken as 100°C while a range of different oil types would start to emit smoke when they reach to a certain temperatures (Table 4.2).

Table 4.2 Smoke emitting temperatures for common oils (Derrick Riches)

Oil/Fat	Celsius	Fahrenheit
Canola Oil - Unrefined	107°C	225°F
Safflower Oil - Unrefined	107°C	225°F
Sunflower Oil - Unrefined	107°C	225°F
Corn Oil – Unrefined	160°C	320°F
Peanut Oil – Unrefined	160°C	320°F
Olive Oil - Extra Virgin	160°C	320°F
Safflower Oil - Semirefined	160°C	320°F
Butter	177°C	350°F
Olive Oil - High Quality, Extra Virgin	206°C	405°F
Olive Oil – Virgin	215°C	420°F
Corn Oil – Refined	232°C	450°F
Peanut Oil – Refined	232°C	450°F
Safflower Oil - Refined	232°C	450°F
Sunflower Oil - Refined	232°C	450°F
Canola Oil - Semirefined	240°C	465°F
Olive Oil - Extra Light	243°C	470°F
Canola Oil - Refined	243°C	470°F
Avocado Oil	270°C	520°F

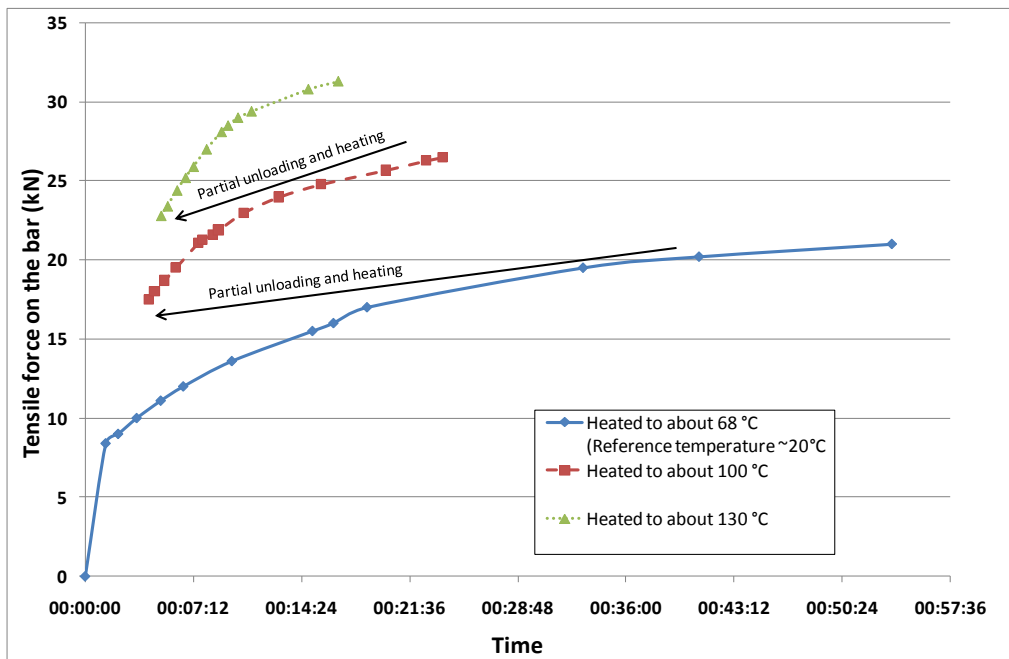


Figure 4.26 Rebar heating test

The load – deflection graph of the sixth house test house was obtained in tension and compression directions as shown in Figure 4.28. As expected, the ultimate load carrying capacity of the sixth test did not change in pushing direction and obtained as about 450 kN. Comparison of the initial load – deflection envelope curve of the 5th and 6th tests should show that the 6th test would perform better in the pre-cracking region. However, since the bar got extremely hot when welded to the steel plate, the overall temperature on the bars might be compatible, which has resulted in similar behaviors in the 5th and 6th tests (Figure 4.27). The response of the structure at higher deformations was similar since the diagonally placed rebars have yielded and lost their pre-tensioning force (Figure 4.29).

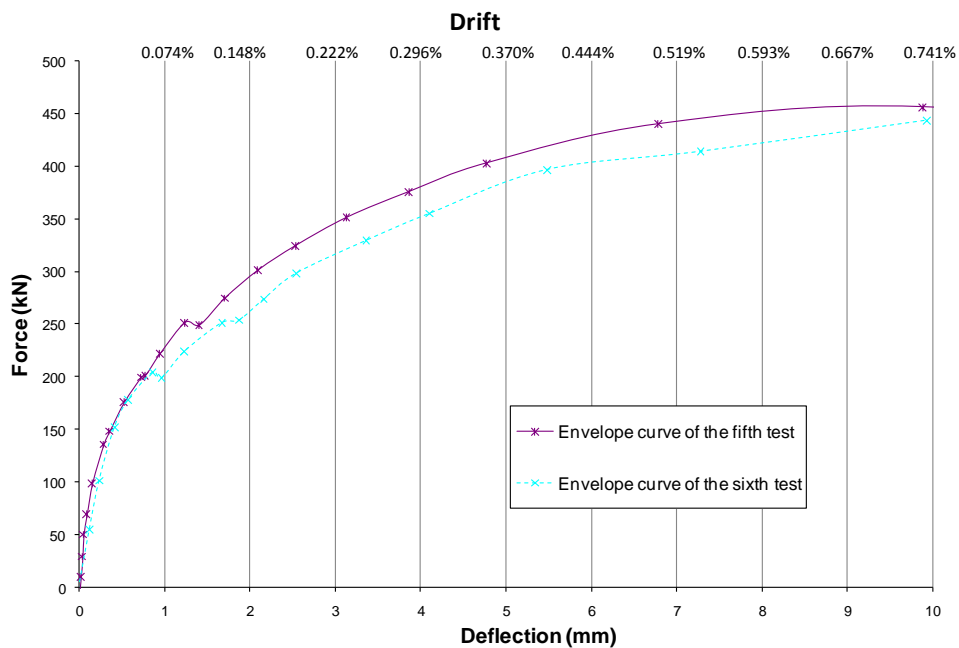


Figure 4.27 Pre-cracking regions of the fifth and sixth tests

The response of the 6th house in the tension side has reached to an ultimate of 600 kN. The reason for additional 150kN force could not be identified. However, recent tests conducted on some rebar specimens obtained from the laboratory rebar storage area have shown that some of the deformed bars have yielded at 250 MPa

while some other samples have yielded at 450 MPa. It may be possible that the yielding capacities of the rebars were not the same in the pulling and pushing directions.

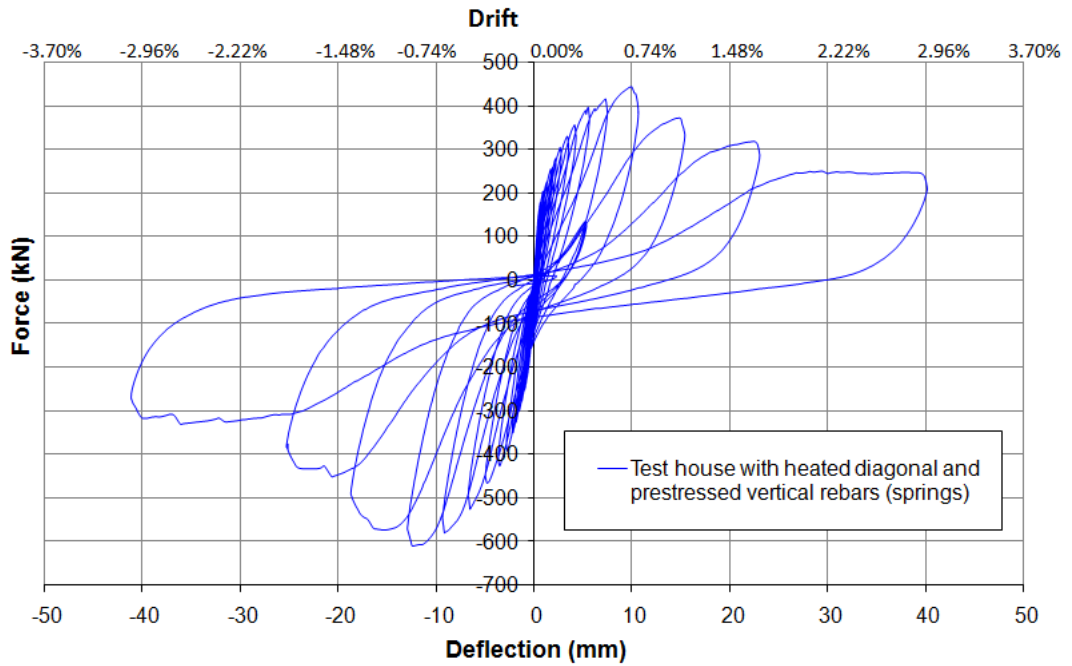


Figure 4.28 Force vs. Deflection graph of the sixth test



Figure 4.29 Cracks on the sixth test

CHAPTER 5

REBAR POST-TENSIONED SINGLE BRICK MASONRY WALL TESTS

Single brick masonry walls were constructed in the laboratory to better observe performance of rebar post-tensioning based strengthening methods. Test walls were 1300 mm in height and 2000 mm in length (Figure 5.1), which were constructed using hollow clay bricks. The mortar mix defined in Section 3.2 was used in single wall tests also. U220 steel beams were used both at the top and bottom of the test wall. Load was transferred to the wall through the top U220 steel beam using a hydraulic piston that was also used in the half-scale brick masonry house tests. Roller supports were placed at the sides of the specimen to hold the wall in the out-of-plane direction.

The strengthening studies included application of vertical post-tensioning of the wall using vertical rebars and strength improvement provided with diagonal rebars. Spring boxes were also used for the enhancement of the post-ultimate behavior of the test walls. General behavior and ultimate strengths of the test walls were predicted using the equations derived in Chapter 2 (Eqns. (2.23) and (2.25)) and they were compared with the ones expressed in literature by Tomazevic[4] and Magenes&Calvi[3].

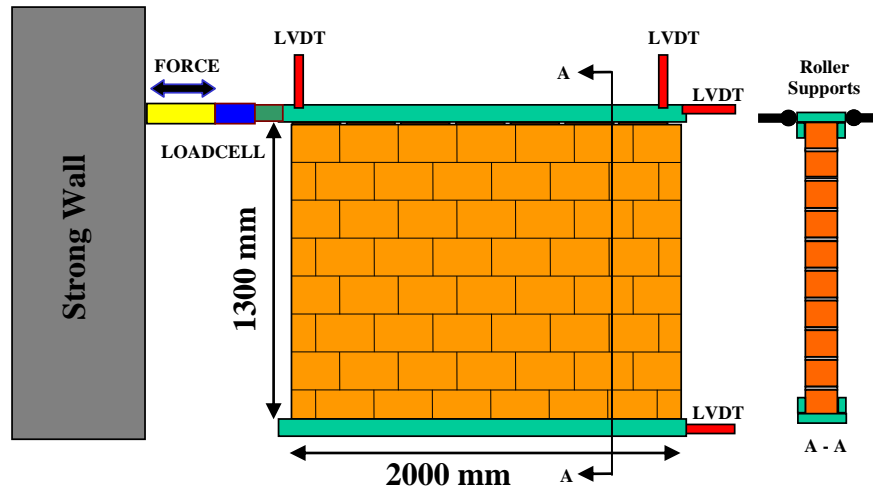


Figure 5.1 General test setup of the wall tests

Planned strengthening techniques were tested on seven different layouts for the test walls. Two of the test walls were first loaded to failure under nominal condition and then strengthened using some of the proposed techniques. Other seven wall tests were conducted on walls that were not loaded to failure under nominal conditions. Total of seven walls were tested under nine individual loading tests, which are further summarized below;

- First test: Original unstrengthened wall
- Second test: Cracked wall specimen strengthening using $4\phi 16\text{mm}$ vertical post-tensioning bars along with spring boxes (total vertical post-tensioning force of $4 \times 30\text{kN} = 120\text{ kN}$)
- Third test: Original unstrengthened wall
- Fourth test: Cracked wall specimen strengthening using $4\phi 16\text{mm}$ vertical post-tensioning bars along without spring boxes (total vertical post-tensioning force of $4 \times 30\text{kN} = 120\text{ kN}$)
- Fifth test: Horizontally post-tensioned (third) specimen in addition to vertical post-tensioning using spring boxes along with $4\phi 16\text{mm}$ vertical rebars (total vertical post-tensioning force of 120 kN ; total horizontal post-tensioning of 30 kN)

- Sixth test: New (4th) specimen with diagonal post-tensioning using spring boxes with 4 ϕ 16mm diagonal rebars (total vertical post-tensioning force of 85 kN). Note: diagonal rebar snapped during testing; therefore, deemed as unsuccessful and the test was repeated.
- Seventh test: New (5th) specimen with diagonal post-tensioning using spring boxes with 4 ϕ 16mm diagonal rebars (total vertical post-tensioning force of 85 kN)
- Eight test: Horizontally post-tensioned (30 kN) new (6th) specimen with vertical post-tensioning using spring boxes along with 4 ϕ 16mm vertical rebars and diagonal post-tensioning using spring boxes along with 4 ϕ 16mm diagonal rebars (total vertical post-tensioning force of 205 kN)
- Ninth test: Similar to the eighth test without spring boxes; horizontally post-tensioned (30 kN) new (7th) specimen with vertical post-tensioning using 4 ϕ 16mm vertical rebars and diagonal post-tensioning using 4 ϕ 16mm diagonal rebars (total vertical post-tensioning force of 205 kN)

Each one of the performed tests was conducted to assess the improvement in strength of the original nominal test wall. The ratio of the ultimate capacity of each performed test was calculated as multiples of the original wall capacity in order to quantify the ultimate strength improvement.

5.1 First test: Original unstrengthened wall

Initial analytical calculations were performed for the original unstrengthened wall (Figure 5.3) both for rocking and diagonal shear failure using Eqns. (2.25) and (2.23), respectively. The calculated results could not be compared with Eqns. (1.7) and (1.9) that were expressed by Tomazevic[4] and Eqn. (1.1) which was defined by Magenes&Calvi[3], since both equations are derived for walls that have constraints from the top and bottom. In the single wall tests that were conducted in the laboratory, however, the top edge of the walls was free to rotate and move in the vertical direction. The formulation given in Eqn. (1.3a) for diagonal shear

failure was also not used in comparison since it includes cohesion and friction coefficients that can be only found by performing special experiments on brick masonry walls. On the other hand, assuming vertical force is acting at the middle of the wall and top of the wall is free to rotate ($\alpha=1$), Eqn (1.7) expressed by Tomazevic[4] leads to a very similar relationship with the equation that was derived in Eqn. (5.1) for ultimate load capacity of the free end walls (Figure 5.2).

$$F = P \times \frac{B}{2H} \quad (5.1)$$

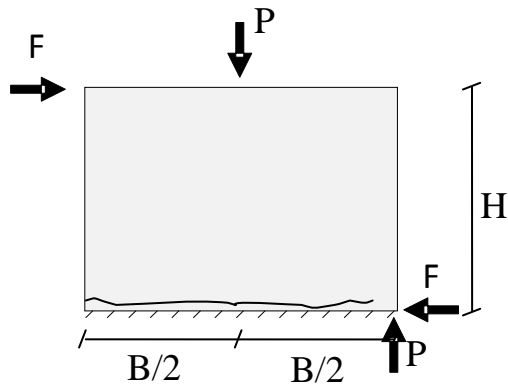


Figure 5.2 Force distribution on the cracked wall

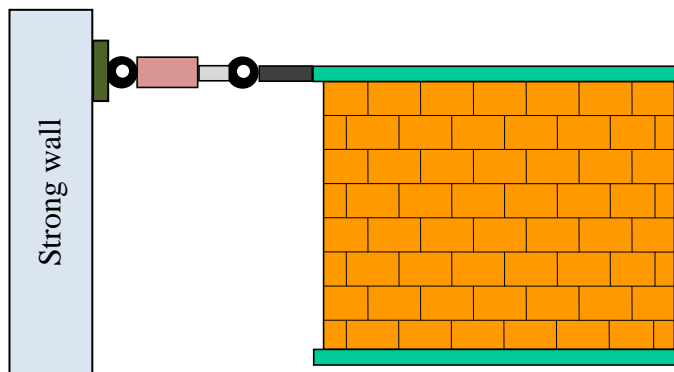


Figure 5.3 Schematic setup of the first test

The wall was loaded to failure in its original (nominal) condition without any strength improvement. Test was continued until the failure was initiated with the rocking motion as the formation of horizontal cracks at the bottom of the wall. The ultimate capacity has reached to 10 kN (Figure 5.5) and then gradually reduced to about 7 kN.

For the test walls, the assumed mortar thickness and tensile strength were 120 mm and 0.2 MPa, respectively. The analytically calculated lateral load capacity before cracking was found by using simple equilibrium equations (Eqn. (2.25)) and weight of the loading setup. It was noticed that the horizontal load capacities of the test wall were quite different in pulling and pushing directions. The reason was thought to be due to the eccentric vertical loads generated by the test setup (Figure 5.4). Therefore, the weight of the wall and additional vertical forces coming from the piston, extension beam, and mortar layer under the beam were taken as variables for calibration. Analytical calculations were repeated until similar capacities were obtained for the pulling and pushing directions and for both cracked and uncracked wall conditions.

The calibrated total weight of the wall, top loading beam, and mortar layer under the beam were taken as 5750 N. The expansion beam weight was taken as 700 N and the pistons vertical reaction at the tip of the expansion beam was taken as 700 N. The moment arms of the vertical forces acting on the wall were taken as 1000mm, 2250mm, and 2500mm from the far end of the wall, for the wall itself, extension beam, and pistons reaction, respectively (Figure 5.4). The eccentric forces caused by the piston and extension beam would resist the motion in pushing direction while reducing the capacity in the pulling direction.

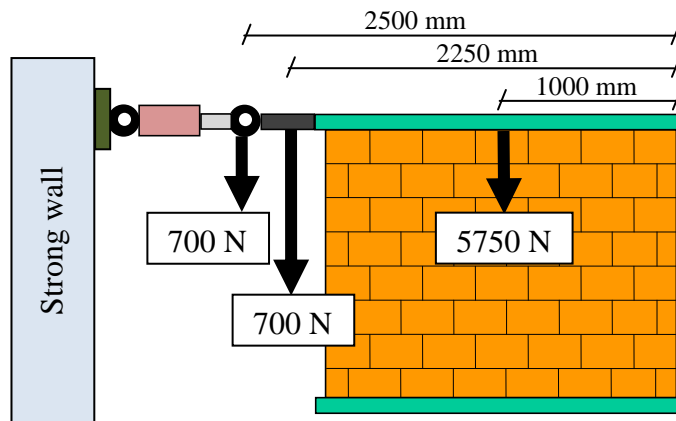


Figure 5.4 Vertical loads on the first test wall

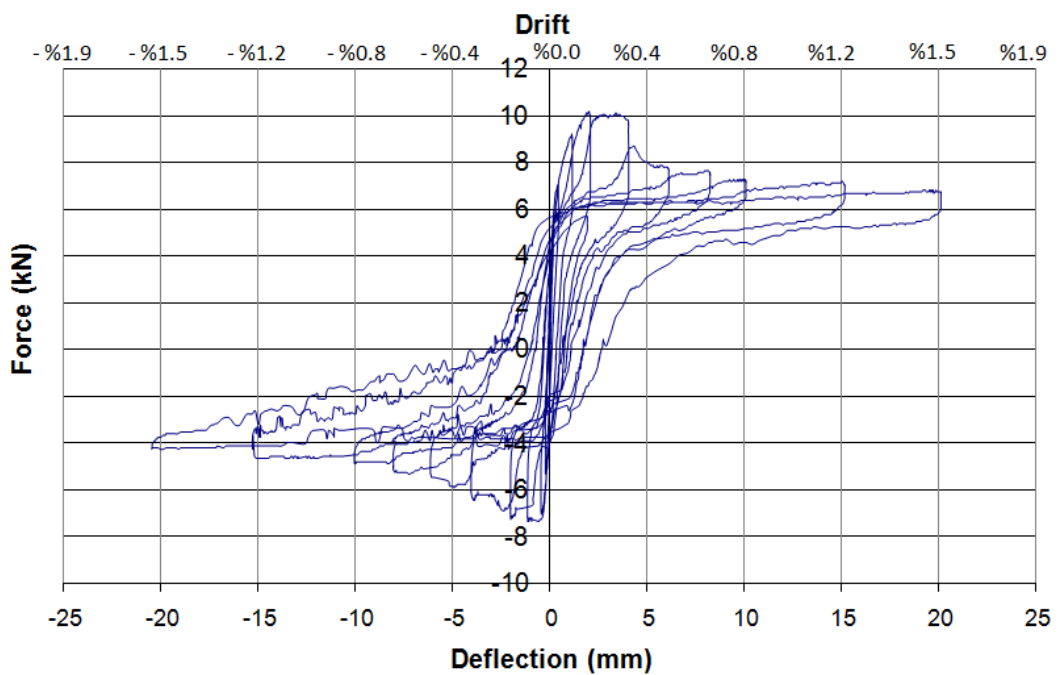


Figure 5.5 Force-Deflection graph of the first test

The experimentally obtained response (for the uncracked wall) was 10kN in pushing and 7kN in pulling directions, while cracked section mechanism responses were 7 kN and 4 kN in pulling and pushing directions, respectively. The analytical

calculations for the calibrated forces have totally matched the experimental values as shown in Table 5.1. The calibrated tensile capacity of the mortar was found to be 0.11 MPa. Alternatively, the accepted mortar width of the wall may be taken as a variable instead of assumed 120mm which would yield a tension capacity of 0.2 MPa.

Table 5.1 Analytically calculated and experimental strength values of unstrengthened wall

Strength Values (N)	Before Cracking		After Cracking	
Experimental	10000	7000	7000	4000
Analytical	9981	7019	6981	4019

5.2 Second test: Cracked wall specimen strengthening using 4 ϕ 16mm vertical post-tensioning bars along with spring boxes (total vertical post-tensioning force of 4 \times 30kN =120 kN)

The cracked test wall that has already been used in the first test was also used in the second test where total of 4 vertical rebars of ϕ 16mm diameter were placed and stretched between the bottom and top U220 steel beams. They were welded to the steel plate at the bottom and spring boxes with bolted connections were used at the top. (Figure 5.6)

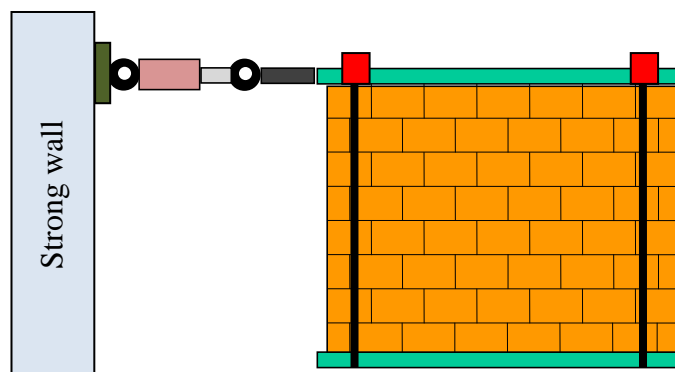


Figure 5.6 Schematic setup of the second test

Post-tensioning bars located in the vertical direction were used to apply vertical force of about 30 kN on each bar for a total of 120 kN. Diagonal shear cracks were observed at the end of the test (Figure 5.7). Test was ended with crushing of the bottom corner bricks. The maximum capacity has reached to about 65 kN, which is about 7 times the original capacity of 10 kN Figure 5.8.



Figure 5.7 Deformed wall in the second test

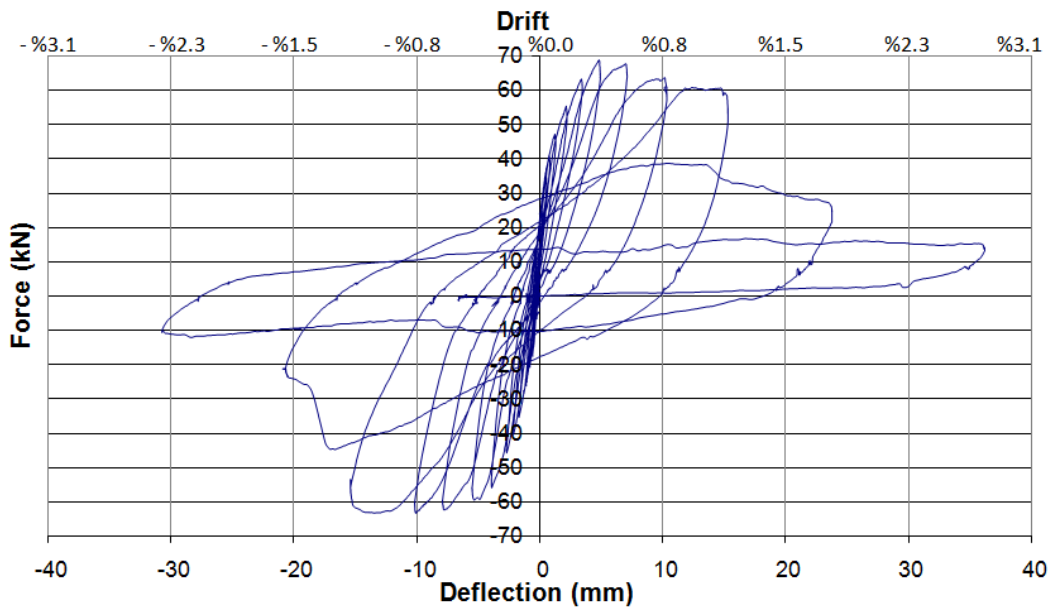


Figure 5.8 Force-Deflection graph of the second test

Maximum lateral strength values of the test wall are given in Table 5.2. Diagonal shear cracking strengths of the test wall were calculated since the wall was already cracked in flexure during the first test. Vertical post-tensioning on the wall was included in the calculations as 120 kN additional weight on the wall. Analytical results and experimental values showed slightly compatible results.

Table 5.2 Analytically calculated and experimental strength values of the second test

$\sigma_0 = 0.53 \text{ MPa}$	Strength (kN)	
	Rocking	Diagonal
Derived Formulas	-	54.0
Tomazevic	-	54.0
Experimental	-	65.0

5.3 Third test: Original unstrengthened wall

A new wall specimen in its unstrengthened original condition was tested to confirm the experimental results obtained in the first test. The wall has horizontally cracked at the bottom showing rocking failure and reached to a load carrying capacity of 8.5 kN which is slightly lower than the 10 kN capacity of the first original unstrengthened test wall (Figure 5.9).

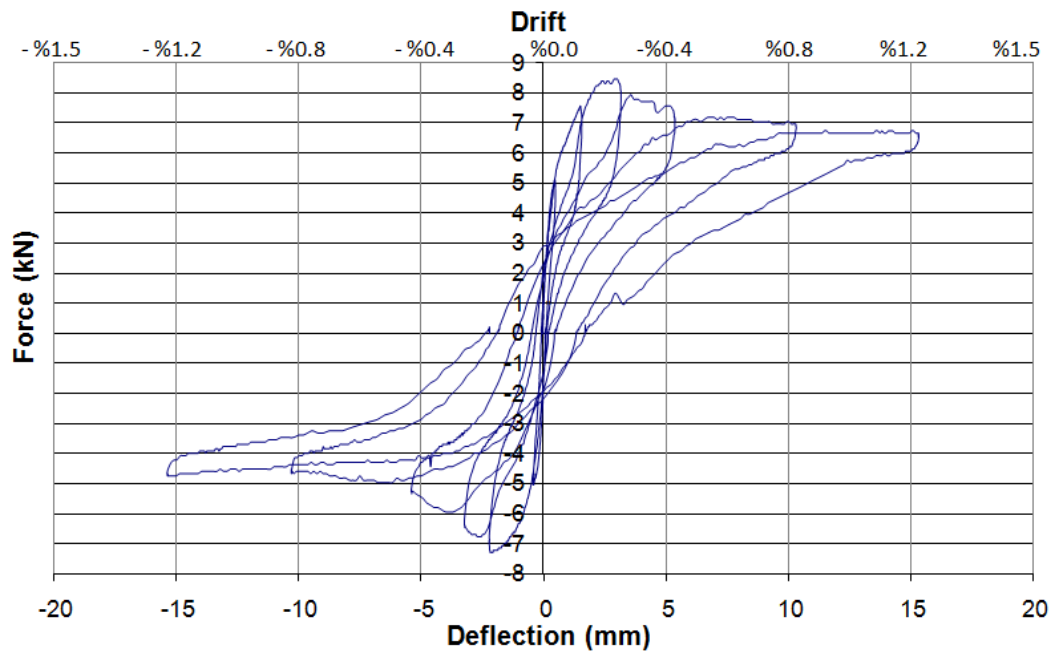


Figure 5.9 Force-Deflection graph of the third test

5.4 Fourth test: Cracked wall specimen strengthening using 4 ϕ 16mm vertical post-tensioning bars along without spring boxes (total vertical post-tensioning force of 4 \times 30kN =120 kN)

Cracked wall obtained from the third test was re-tested after vertically post-tensioned using 4 ϕ 16mm rebars (Figure 5.10). Rebars were placed without spring boxes and nearly 30 kN post-tensioning force was applied on each rebar. The aim of the test was to observe the effect of spring box usage.

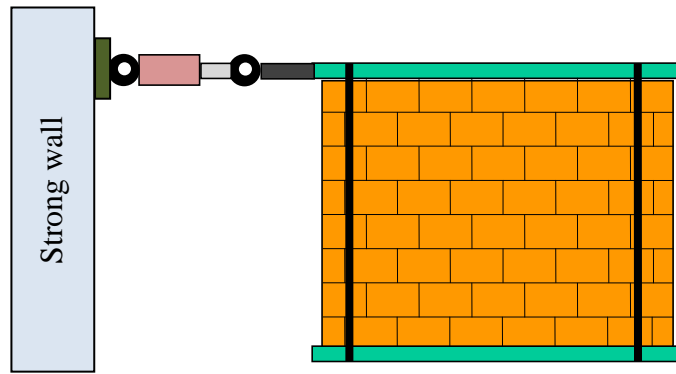


Figure 5.10 Schematic setup of the fourth test

The ultimate capacity of the test wall has reached to 55 kN (Figure 5.11) which is quite lower than the value of 65 kN obtained in the second test. The rocking capacity of the second wall (8.5 kN) was also lower than the rocking capacity of the first wall (10 kN). The relatively lower capacity observed in the second wall test can be related to the characteristics of the test wall. Although all of the test wall specimens were constructed at the same time and by the same bricklayer, small variations in the mortar or brick properties might have caused the difference. The rebars used for the two tests might have also different properties.

Diagonal shear cracks have opened relatively wider in the fourth test compared to the second test after the ultimate capacity was reached (Figure 5.12(a)). The poor post-ultimate behavior can be correlated with total loss of post-tensioning force on the wall due to the shortening of the wall height followed by crushing. The shortening of the wall height during testing (Figure 5.12(b)) can be better tolerated using rebar-spring box connection. Since the rebars retain most of their post-tensioning force after reaching the ultimate capacity, the post-ultimate behavior was greatly improved when spring boxes were used (Figure 5.13).

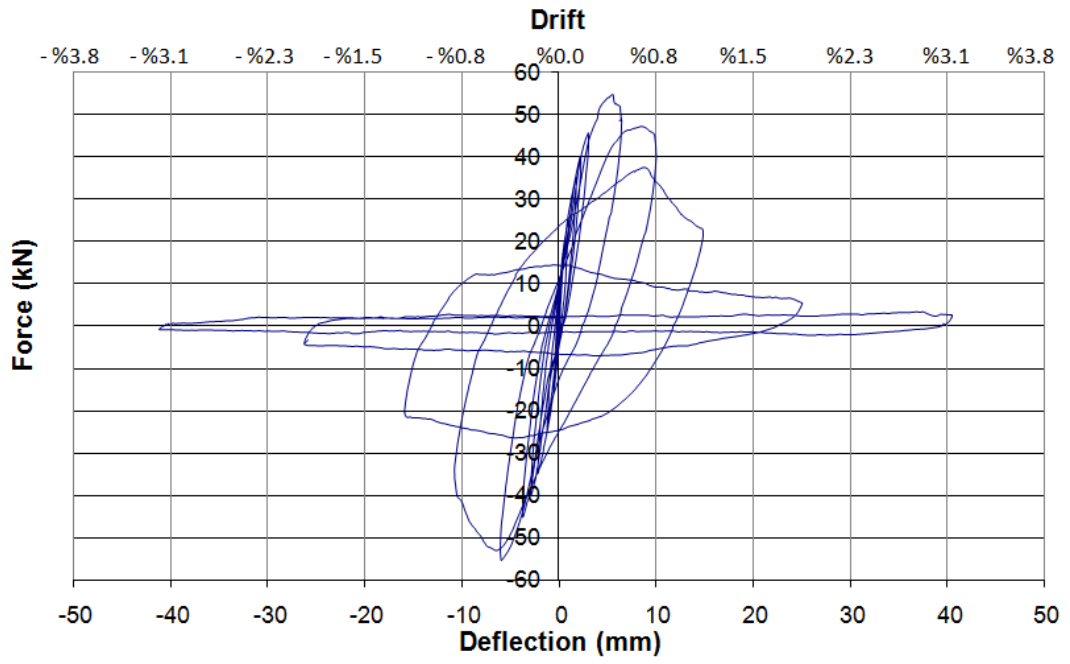


Figure 5.11 Force-Deflection graph of the fourth test

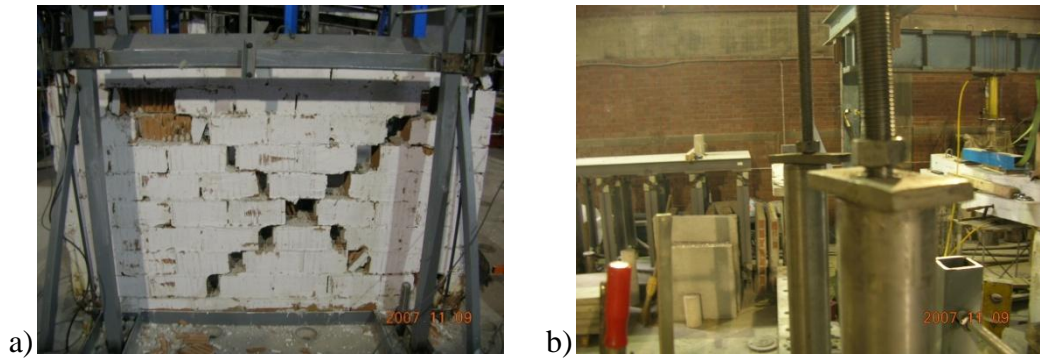


Figure 5.12 Deformed wall in the fourth test

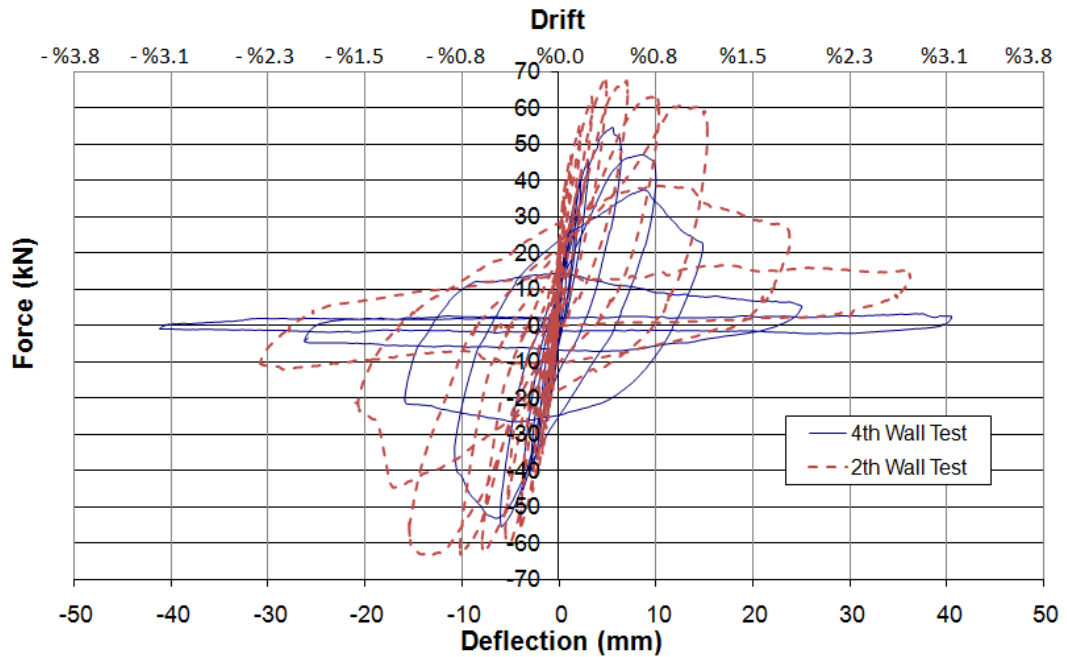


Figure 5.13 Comparison of force-deflection graphs of the 2nd and 4th tests

5.5 Fifth test: Horizontally post-tensioned (third) specimen in addition to vertical post-tensioning using spring boxes along with 4 ϕ 16mm vertical rebars (total vertical post-tensioning force of 120 kN; total horizontal post-tensioning of 30 kN)

Since the diagonal crack formation has left the triangular wall pieces at two edges of the wall in the fourth test, a horizontal direction post-tensioning was planned for the fifth test in order to prevent excessive crack opening in the horizontal direction and to better retain wall's stability. Fifth test wall specimen was post-tensioned in the vertical direction using 4 vertical ϕ 16mm rebars with spring boxes and post-tensioned in horizontal direction using 2 ϕ 12mm rebars, which are further connected to two wooden sections at the both edges of the wall. The effect of horizontal confinement (post-tensioning) was investigated in the fifth test (Figure 5.14). Vertical post-tensioning and horizontal compressing on the wall was about 120 kN and 30 kN, respectively.

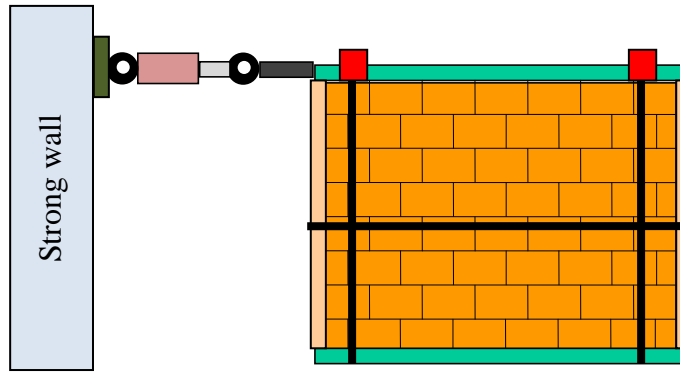


Figure 5.14 Schematic setup of the fifth test

Initially, diagonal shear cracks have been developed; however, base sliding have dominated the final collapse pattern at later stages of the test. The test wall exhibited sliding failure in post-ultimate range due to the effect of horizontal compressing of the wall (Figure 5.15). Calculation of the diagonal shear capacity of the wall was modified in Eqns. (5.2) and (5.3) by including the stresses developed by the horizontally post-tensioning. P_H denotes the horizontal compressive force and A_H is the the vertical wall area obtained by height (H) multiplied by wall thickness (t).

$$\sigma_t = \left(\sqrt{\left(\frac{P}{2A} - \frac{P_H}{2A_H}\right)^2 + \left(\frac{\lambda F}{A}\right)^2} - \left(\frac{P}{2A} + \frac{P_H}{2A_H}\right) \right) \quad (5.2)$$

$$F = \frac{A}{\lambda} \sqrt{\left(\sigma_t + \frac{P}{2A} + \frac{P_H}{2A_H}\right)^2 - \left(\frac{P}{2A} - \frac{P_H}{2A_H}\right)^2} \quad (5.3)$$



Figure 5.15 Deformed wall in the fifth test

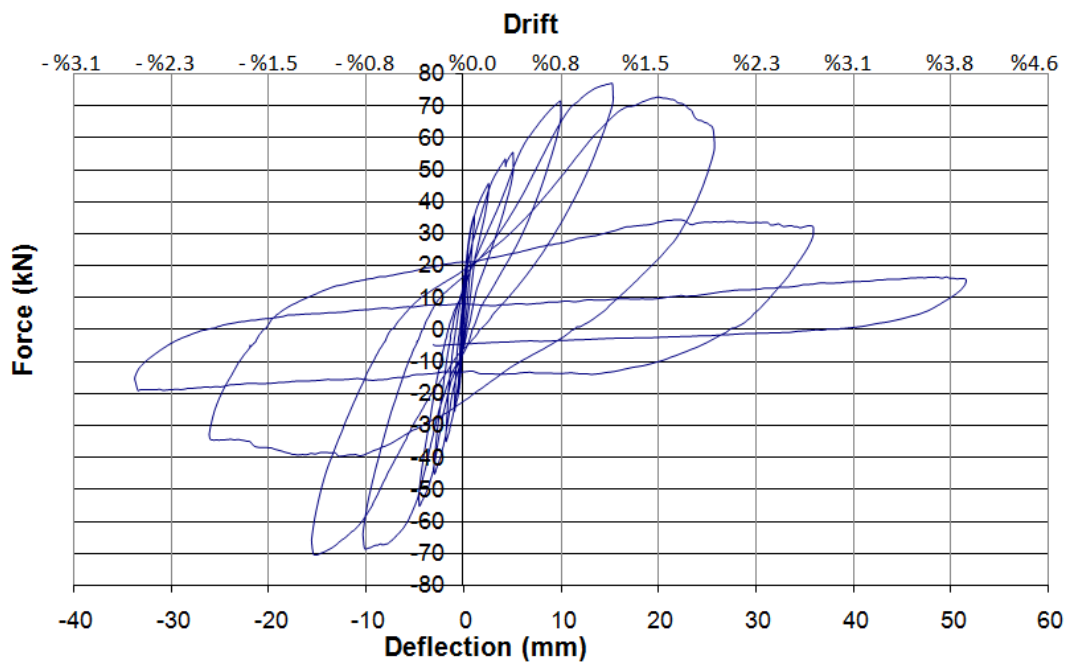


Figure 5.16 Force-Deflection graph of the fifth test

Careful investigation of the test videos has revealed that the test wall has experienced various damage stages. Analytical calculations of the capacity show

that the test wall has rocking failure capacity of 39.4 kN while diagonal shear capacity is relatively larger and calculated as 78.6 kN. Although not clearly seen from the videos and during testing, the test wall must have first horizontally cracked at the base in a rocking mode. There were two main failure mechanisms that would follow the rocking mode if the wall was vertically restrained: A) crushing of the corner bricks and B) forming a hinge at the corner and vertical rebar yielding. From the videos, it was observed that diagonal cracks have been formed and the corner brick has failed immediately after. Since the wall was also horizontally compressed by post-tensioning bars, the existing crack at the base has initiated a base sliding mode following the corner crushing.

The actual test measurements have shown that the wall has reached to a horizontal load capacity of 78 kN (Figure 5.16), which is in close agreement with the calculated diagonal shear capacity of 78.6 kN (Table 5.3). Diagonal capacity of the wall that is horizontally compressed is not defined by Tomazevic[4] equations; therefore, comparison with the literature formulations was not possible.

Hypothetically, if the corner crushing were prevented and the vertical bar yielding would have governed the failure, then the ultimate load capacity of the wall would have been calculated as 92.4 kN and 91.4 kN for Tomazevic[4] and Magenes&Calvi[3], respectively. Similar result of 97 kN could also be obtained using developed Eqn. (5.1).

Table 5.3 Analytically calculated and experimental strength values of the fifth test

$\sigma_0 = 0.53 \text{ MPa}$	Strength (kN)	
	Rocking	Diagonal
Derived Formulas	39.4	78.6
Tomazevic	92.4	
Magenes&Calvi	91.4	-
Experimental	-	78.0

5.6 Sixth test: New (4th) specimen with diagonal post-tensioning using spring boxes with $4\phi 16\text{mm}$ diagonal rebars (total vertical post-tensioning force of 85 kN)

The strength improvement achieved by vertical rebars was about 8 times the original capacity of 10 kN. In order to investigate the behavior and strength improvement of test walls, specimens were strengthened using diagonally placed rebars ($4\phi 16\text{mm}$) (Figure 5.17). Each rebar accompanied with a spring box which would retain most of the post-tensioning force for small shortening of wall height as well as slowly release the tension if the bar experiences compressive deformations. Ultimately, the spring box would release all of the tensile force but would not allow development of compressive forces by its free end. In this way, buckling of the rebars was prevented.

Each one of the $4\phi 16\text{mm}$ rebars were post-tensioned to 30 kN, which generated a total of 85 kN vertical post-tensioning force on the wall. The horizontal component of the diagonal rebars would resist the lateral force at the ultimate state of the test while vertical compression strut formation would develop a stable resisting structure. The ultimate load carrying capacity of the wall was expected to be determined either by the crushing strength of the corner wall or yielding of the diagonal rebars.

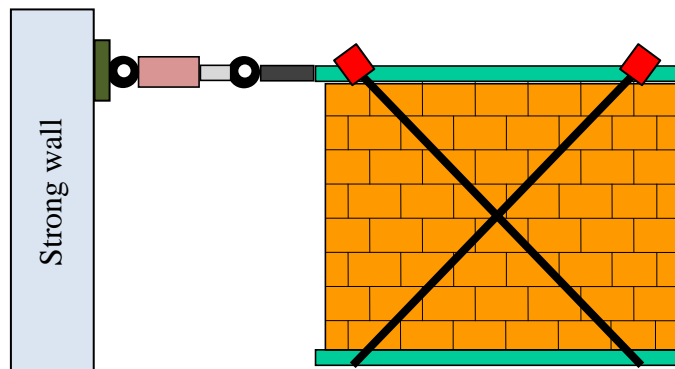


Figure 5.17 Schematic setup of the sixth test

One of the diagonal rebars has ruptured due to a deficiency at the welding between the treaded bolt and diagonal rebar during the test (Figure 5.18). For that reason, the test was ended prematurely at a maximum horizontal load of 120 kN (Figure 5.19). The same test was repeated using a new test wall.



Figure 5.18 Failure at the diagonal rebar during the sixth test

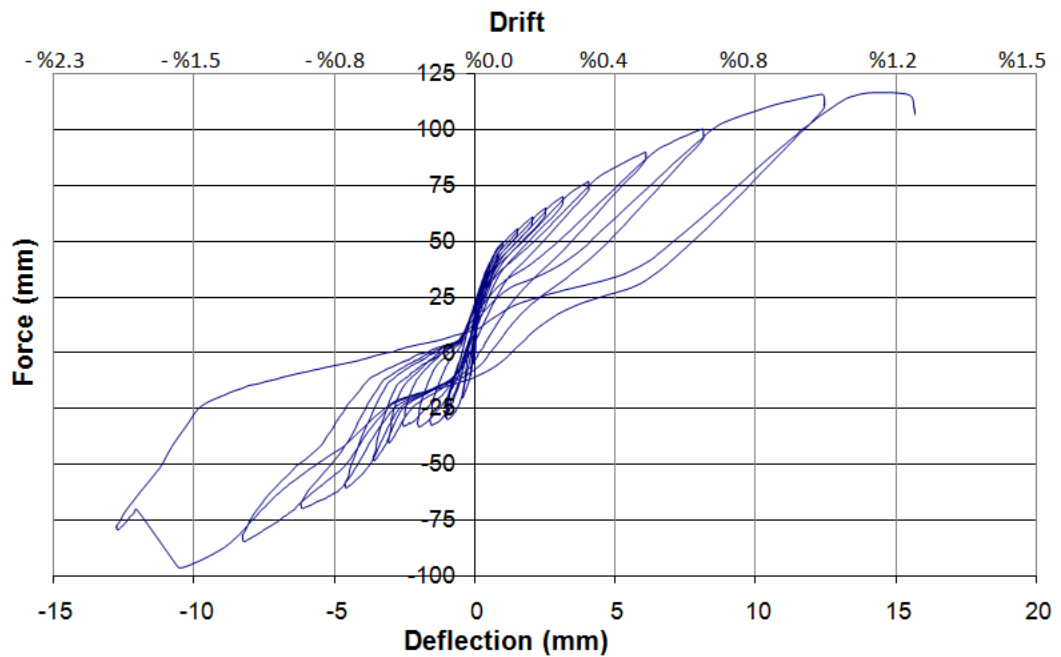


Figure 5.19 Force-Deflection graph of the sixth test

5.7 Seventh test: New (5th) specimen with diagonal post-tensioning using spring boxes with 4 ϕ 16mm diagonal rebars (total vertical post-tensioning force of 85 kN)

Due to the rebar failure in the sixth test, seventh test was performed identical to the sixth test. Due to the absence of vertical rebars, diagonal compression struts would not develop. Instead, the force on the diagonal rebar would be horizontally balanced by the laterally applied external load “F” and vertically balanced by the vertical compression strut force (Figure 5.20).

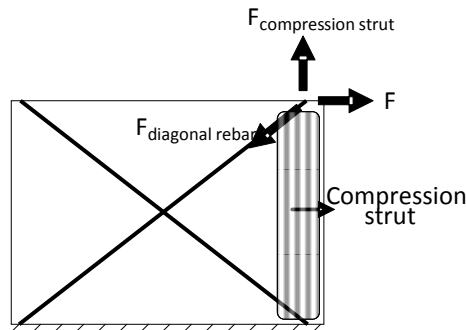


Figure 5.20 Bracing forces at the seventh test

Absence of horizontal post-tensioning rebars would also result in a considerable amount of loss of the vertical compression. As a result, the rocking mode would be more critical. Furthermore, loss of diagonal compression strut would generate larger forces on the vertical compression strut causing split cracks. Cyclic loading combined with vertical split cracks and rocking motion left sides of the walls without any support and susceptible to failure (Figure 5.21). The stability of the wall was considerably lost after the failure of the compression strut. The ultimate load capacity of the wall was observed as 110 kN until the loss of wall stability (Figure 5.22).

The vertical load carrying capacity of the vertical compression strut was deemed to determine the ultimate capacity as the diagonal rebars did not show any signs of

yielding. The vertical compression capacity of the strut is found to be in the range of 110 kN assuming the rebars are about 45° inclined.



Figure 5.21 Deformed wall in the seventh test

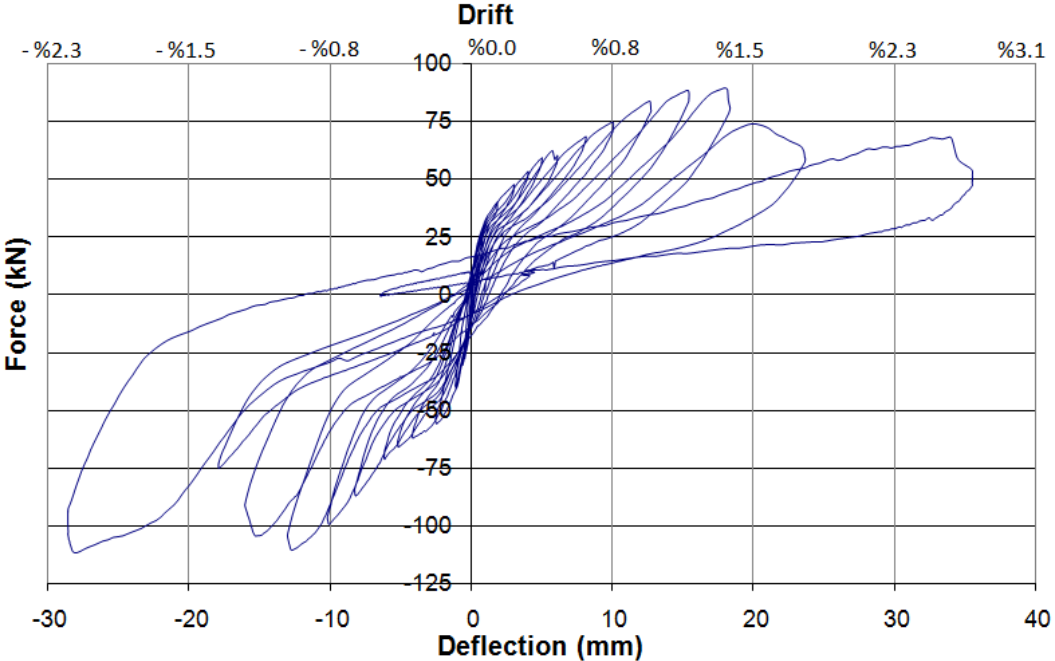


Figure 5.22 Force-Deflection graph of the seventh test

5.8 Eighth test: Horizontally post-tensioned (30 kN) new (6th) specimen with vertical post-tensioning using spring boxes along with 4 ϕ 16mm vertical rebars and diagonal post-tensioning using spring boxes along with 4 ϕ 16mm diagonal rebars (total vertical post-tensioning force of 205 kN)

The loss of the compression strut in the seventh test has showed the need for a horizontal holder at the ultimate stages of the tests to prevent the separation and stability loss of the test wall (Figure 5.23). The test wall in the 8th test was horizontally compressed to about 30 kN by using two ϕ 12mm rebars as in the 5th test. Vertical post-tensioning rebars were also used in addition to the diagonal bars. Therefore, total vertical post-tensioning force was applied in the range of 205 kN, stretching each rebars about 30 kN. Spring boxes were used at all of the rebar connections to improve the post-ultimate performance of the wall.

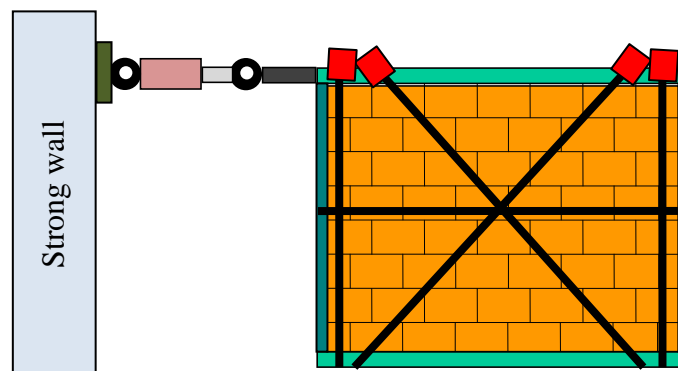


Figure 5.23 Schematic setup of the eighth test

The governing failure pattern of the wall was observed to be the crushing of the corner bricks however extending towards the center this time (Figure 5.24). The extensive crushing of the base bricks have resulted in reduction of the wall height, which has resulted in a partial loss of post-tension force on the rebars. The reason of having a longer crushing failure at the base of the wall towards the corners was thought to be due to the combination of two compression struts, one developing in the diagonal due to vertical rebars and one developing in the vertical direction due

to the diagonal rebars. Both struts approaching to the same corner has resulted in a wider crushing area.



Figure 5.24 Deformed wall in the eighth test

The ultimate load capacity of the 8th wall test was obtained as 170 kN, about 17 times the original capacity (Figure 5.25). The analytical load capacity of the wall can be obtained using the force distribution at the ultimate stage (Figure 5.26). Diagonal rebar was observed to yield at the ultimate stage and the force on the diagonal rebars was taken as 90 kN ($450 \text{ MPa} \times 200 \text{ mm}^2$) for a total of 180 kN. The force on the vertical rebars is not clearly known although the initial post-tensioning was $2 \times 30 \text{ kN}$. During testing, the vertical rebars may take forces up to a total of 180 kN at yielding, or may even get smaller than 60 kN due to height change by crushing of the brick wall. Assuming 180 kN force on the diagonal rebars and 60 kN force on the vertical rebars, the load capacity of the wall is analytically calculated as 243 kN by using moment equality at the point “a” (Figure 5.26) using Eqn. (5.4). Calculated capacity value of 243 kN is higher than the experimental result of 170 kN, which can be replicated by taking vertical force on the rebars as 12.4 kN with a vertical post tensioning loss of 79%. In this way, the axial force in the diagonal and vertical compression struts were calculated as

23 kN and 98 kN, respectively. The existence of horizontal tie should have some effect on the walls response by transferring some forces across the diagonal crack; however, the behavior is very complicated considering the nonlinear behavior of the wall along with the spring boxes.

$$F \times H = 2 \times F_{verticalrebar} \times B + 2 \times F_{diagonalrebar} \times \frac{B \times H}{\sqrt{B^2 + H^2}} \quad (5.4)$$

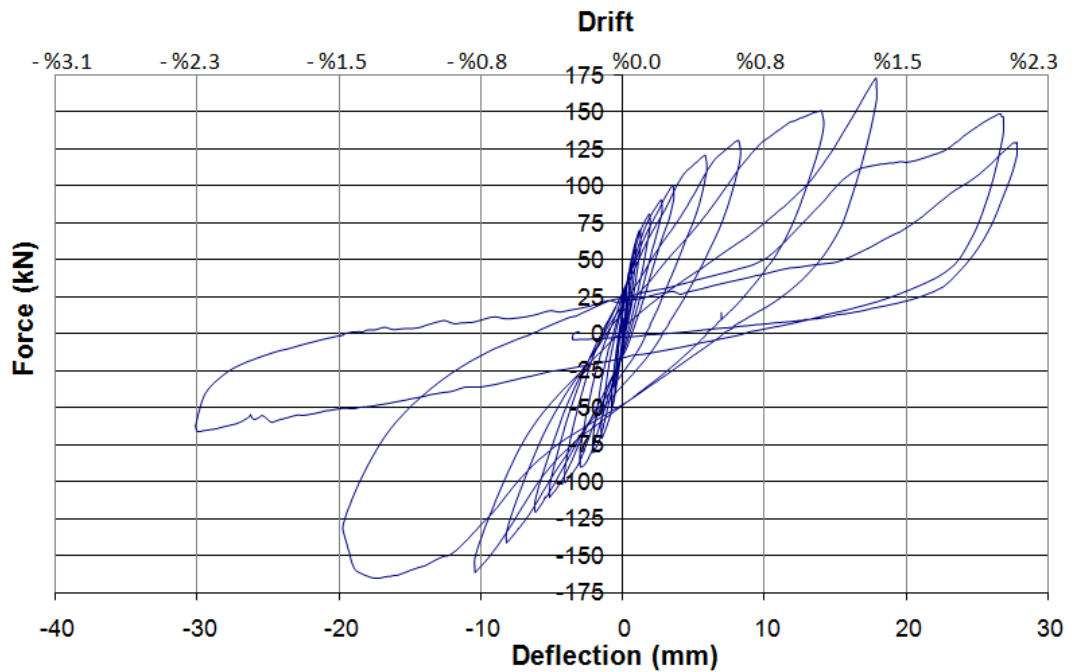


Figure 5.25 Force-Deflection graph of the eighth test

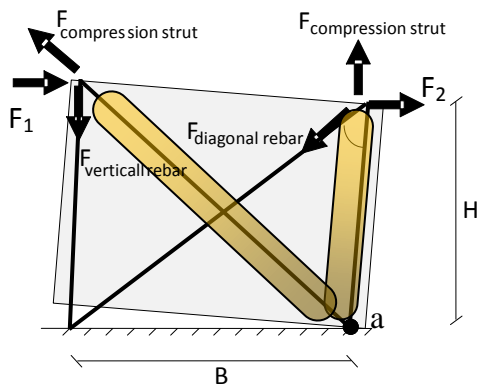


Figure 5.26 Force distribution on the eighth test wall at the ultimate stage

5.9 Ninth test: Similar to the eighth test without spring boxes; horizontally post-tensioned (30 kN) new (7th) specimen with vertical post-tensioning using 4 ϕ 16mm vertical rebars and diagonal post-tensioning using 4 ϕ 16mm diagonal rebars (total vertical post-tensioning force of 205 kN)

The 9th test was conducted using same test setup and rebar layout of the 8th test except for the spring boxes, which were omitted in order to observe the effect of spring boxes on the rebar arrangement of the 8th test (Figure 5.27).

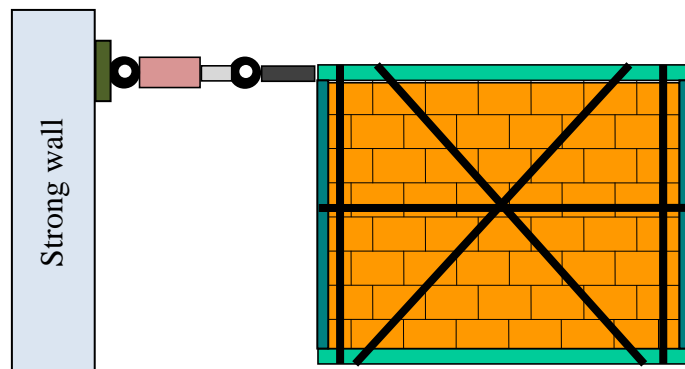


Figure 5.27 Schematic setup of the ninth test

Crack pattern and failure type was the same as in the previous test (Figure 5.28). However, the shortening of the wall due to bottom brick crushing could not be tolerated as much as in the case in the 8th test and the ultimate load capacity of the wall has reached to about 150 kN (Figure 5.29), which is 13% lower than the ultimate capacity of the 8th test wall (Figure 5.30). Experimentally obtained load capacity of 150 kN can be calculated using Eqn. (5.4) by assuming zero post tensioning force on the vertical rebars and taking 180 kN on the diagonal rebars (yielding). Also, the energy dissipation of the wall at the post-ultimate range is lower than the one at the 8th test (Figure 5.31).



Figure 5.28 Deformed wall in the ninth test

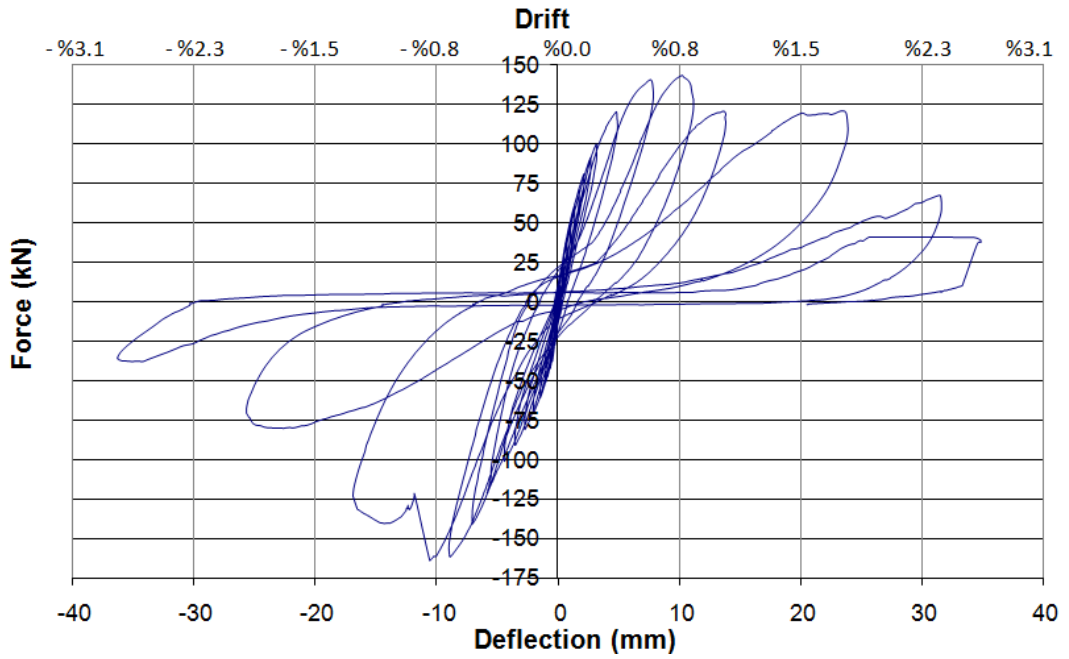


Figure 5.29 Force-Deflection graph of the ninth test

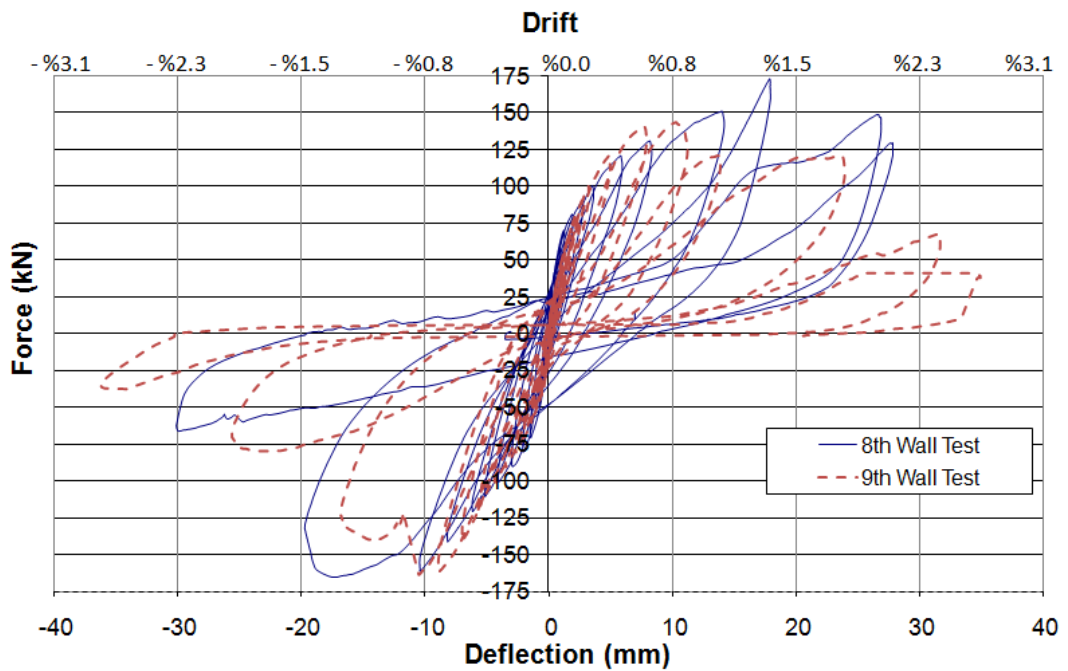


Figure 5.30 Comparison of force-deflection graphs of the 8th and 9th tests

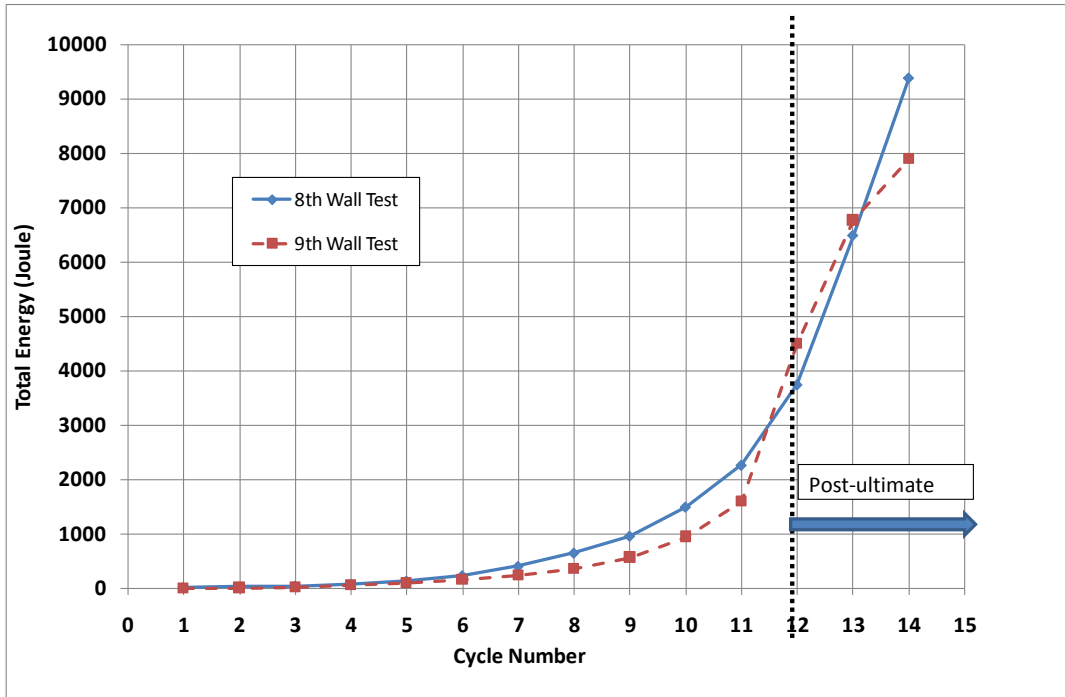


Figure 5.31 Comparison of energy dissipation characteristic of the 8th and 9th tests

CHAPTER 6

DISCUSSION OF RESULTS AND CONCLUSIONS

6.1 General discussion of results (overview)

In this study, individual brick URM walls and combination of wall segments in the form of a house were tested. A total of 4 brick URM 6m long house half scale specimens were tested under 6 different test arrangements of post-tensioning using rebars. Additional 9 tests were conducted on 7 individual brick URM walls with 1.3m in height and 2m in length. Simplistic analytical equations were derived to calculate the cracking and ultimate capacities of URM walls and predict capacities after strengthening. An MS-Excel based macro program was developed to calculate the earthquake demands and evaluate the capacity of URM houses. A general design procedure was developed to strengthen URM houses using vertical and diagonal rebars, which are post-tensioned using threaded bolts and nuts. An innovative spring box system was developed to minimize the post-tensioning losses due to minor crushing-shortening of the URM walls during a seismic activity. The strength improvement of walls due to different rebar placement was investigated for the experimental tests conducted in the laboratory.

In the conducted laboratory tests, in-plane strength and ductility improvement was targeted. Different layouts of rebars in vertical and cross-brace directions were tested. The walls were post-tensioned with rebars using bolted connections. The dominant brittle failure mode of walls in rocking and diagonal cracking were tried to be improved using vertical and diagonal rebar placement. The stability of the

walls is lost as diagonal cracks form in both directions. The diagonal crack formation was delayed and unstable triangular wall segments that form after diagonal cracking were kept together in the horizontal direction using horizontal post-tensioning ties.

The lateral strength of the original 6m brick URM house specimen (without strengthening) was about 68 kN. Placement of the vertical rebars and post-tensioning to a force of 200 kN (about 4 times the weight of the house) has increased lateral capacity to about 250 kN and altered rocking mode of failure to diagonal cracking mode. About 3.5 times strength improvement achieved by the vertical post-tensioning have been further improved to about 6.5 times when diagonal rebars were used in addition to the vertical rebars, as the capacity has reached to about 450 kN.

In the case of the 2m long brick URM wall strengthening tests, the nominal capacity of the walls were in the range of 10 kN, which was also improved significantly using vertical, horizontal, and diagonal rebar post-tensioning up to 170 kN range with an improvement of about 17 times.

Further details, discussions and comparisons of measured data are provided in the following sections.

6.1.1 Material Tests

Brick compression tests showed that bricks are quite strong building blocks under direct compression in the direction of the holes; a brick can stand up to about 330 to 500 kN in the vertical direction. When the shear and bending forces are combined together though, load bearing capacity of bricks considerably decrease. Decrease in load capacity of the brick depends on many parameters, such as, wall dimensions, construction technique, wall position on the plan of the structure,

loading angle and loading rate, strengthening rebar arrangement, cracking in the vicinity of a brick, mortar properties, stress concentrations, etc.

Compressive tests on mortar cylinders showed a compressive strength of approximately 2 MPa at the 8th day and 3.85 MPa at the 28th day. Effective cure of specimens also played an important role in the strength increase.

Interaction of mortar with bricks was tested using three-brick direct shear tests. Confinement of the bricks was investigated to see if it would play a role on the maximum shear capacity of the mortar layer. The comparison of vertically post-tensioned and original three-brick shear test have shown that the original capacity of about 15 kN increased to 35 kN when the bricks are compressed across by 10 kN in perpendicular direction to the shear loading direction. Further compression of bricks by 30 kN have resulted shear capacity to increase up to 40 kN. Therefore, the three-brick direct shear tests have shown that under 10 to 30 kN per brick, the direct shear capacity increases by about two times. In 2m wall tests, the bricks were post-tensioned in the vertical direction by 4 rebars with 30 kN of post-tensioning in each, for a total of 120 kN. In the 2m length of the wall, there were about 6.5 bricks with about 20 kN of vertical compression on each brick. 20 kN of compression was insignificant when compared with the 300 kN of axial load capacity; however, shear strength increase of the mortar layer was significant in the order of two times.

When the 2m wall was not post-tensioned in its nominal state, the horizontally applied force causing failure was about 10 kN, although for 6.5 bricks and 15 kN/brick shear capacity would yield 98 kN of shear capacity. The significant difference between the direct shear test results of three-brick tests and actual wall tests was due to the wall height parameter. If the wall specimen had only two layers of brick, then the capacity would be expected to be in the range of 98 kN. If no diagonal strengthening bars were used, the calculated capacity of the brick wall (i.e., 98 kN) using three-brick direct shear test results would set an upper limit.

6.1.2 Rebar Post-Tensioned Half-Scale Brick House Tests

Six tests on four half-scale brick masonry houses have been conducted to understand the geometric effect (e.g. existence of doors and windows, as well as a number of walls in the same direction) and wall boundary conditions on the behavior and capacity of the wall system. The rebar based strengthening techniques were investigated in the 6m wall tests in an attempt to increase the overall strength as well as ductility and energy dissipation capacity of the test house. The tests have shown that vertical and diagonal post-tensioning of the walls using rebars have increased both load and energy dissipation capacities of the house specimens. Application of only vertical bars increased the strength of house in the range of 3.5 times the nominal strength while usage of both diagonal and vertical bars gave better results in the range of 6.5 times the original house strength. Load-deflection envelope curves of the six tests are provided in Figure 6.1. Total energies dissipated during the tests were calculated using the areas under the force-deflection curves of the tests and shown in Figure 6.2. The main observations obtained from the six tests are given below;

- Original house test (1st Test) has the smallest load carrying (68 kN) and energy dissipation capacities (Figure 6.1, Figure 6.2).
- Placing about 50 kN of weight above the first specimen (2nd Test) which was already cracked in the first test has increased load carrying capacity from 68 kN to 100 kN and also the energy dissipation capacity (Figure 6.2).
- About total of 200 kN of post-tensioning force applied with 10 vertical rebars (3rd Test) on the already cracked and two times tested house specimen increased load carrying capacity nearly 3 times as compared with the initial test. Loosening of rebars was observed and bolts were tightened two times during the testing which indicated the need for a mechanism to tighten relaxing rebars during loading.

- The same 200 kN of post-tensioning force applied with vertical rebars that were connected using spring boxes (4th Test) did not provide extra load carrying capacity increase. However, the spring boxes prevented early loss of post-tensioning force due to wall crushing and rebar yielding; therefore, ductility and energy dissipation capacities have increased.
- When diagonal steel rebars were used together with the vertical rebars (5th Test), load carrying capacity has increased up to about 1.7 times the vertically post-tensioned specimens test and about 6 times the original specimen's test. Because of connection problems at lateral load transferring point of the upper slab and hydraulic piston connection, specimen could only be loaded in the pushing direction.
- The test setup was improved before the 6th test, which would enable application of larger tensile forces on the upper slab level. The diagonal bars in the 5th test were welded in place without post-tensioning. However in the 6th test, the diagonal bars were first heated up before both ends were welded to the connection plates. Therefore, an initial post-tensioning was applied on the diagonal bars as well. The bars were heated up to about 100 C° generating about 900µε tension, causing 190MPa initial tensioning stress (38 kN force, close to half of the yielding) in the rebars. The maximum capacity in pushing direction was obtained similar to the 5th test result as 450 kN. Slight reduction on the ultimate strength and pre-ultimate behavior of 6th test was observed in comparison with the 5th test in pushing direction (Figure 4.27). On the other hand, pulling direction ultimate capacity have reached to 600 kN in the 6th test, which is about 33% larger than the maximum capacity achieved in both 5th and 6th tests in the pushing direction.
- Slight differences in the pushing direction and ambiguously large capacity obtained in the pulling direction as well as initial stiffness and ultimate strength comparisons indicate that:

- a) variations may be due to small differences between the quality of bricks and mortar, connection, welding, and yielding capacities of the rebars used in the 5th and 6th test house specimens. Direct tension tests conducted on three identical looking deformed bar specimens taken from the laboratory steel storage bin have reached their ultimate tensile capacities at 250 MPa, 450 MPa, and 450 MPa. It was assumed that all deformed bars in the lab are StIII and have the same yielding stress of 420 MPa.
- b) when one of the sides of cross-braces is welded to the plates, the bar gets extremely hot. Steel being a good heat conductor, the overall bar temperature in both 5th and 6th tests might be compatible.

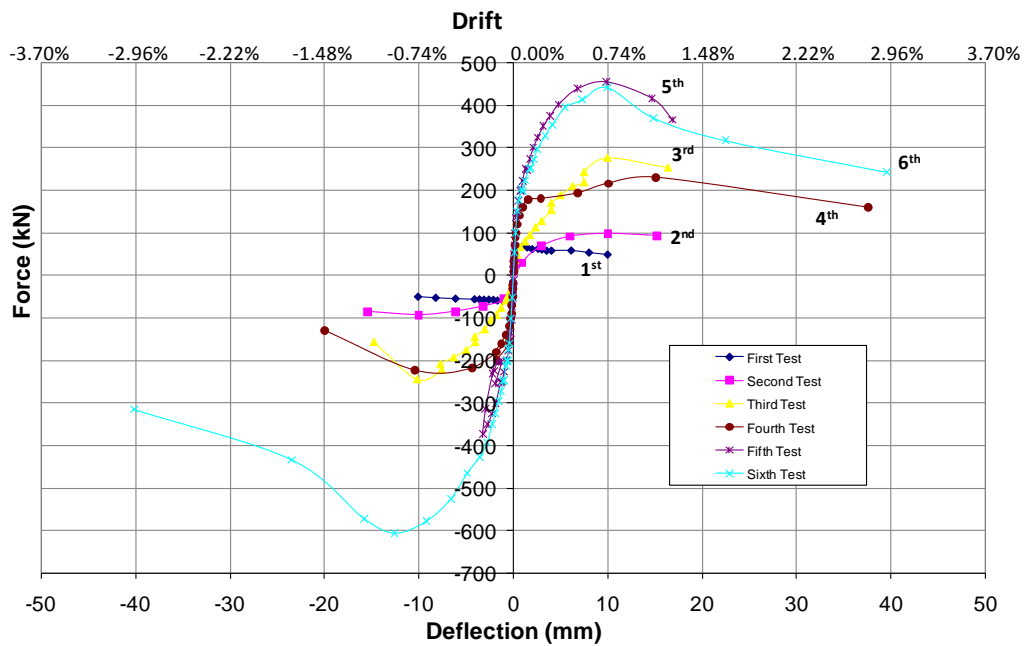


Figure 6.1 Force-Deflection Envelope Curves of Half-scale House Tests

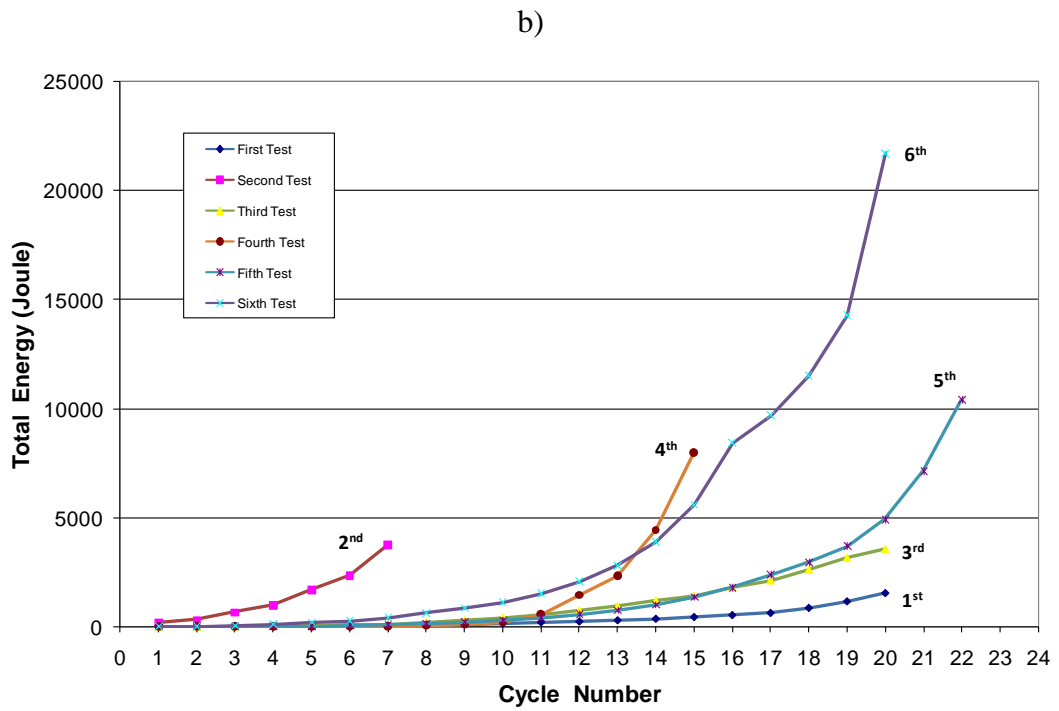
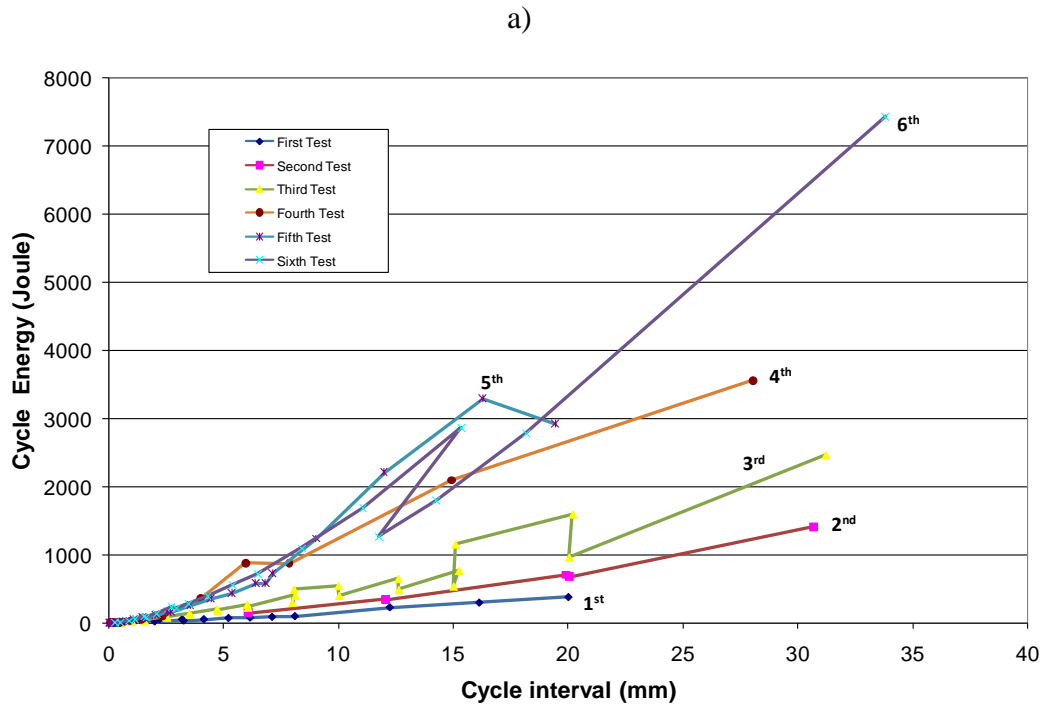


Figure 6.2 Cycle Energy Dissipation Curves of Half-scale House Tests

6.1.3 Rebar Post-Tensioned Brick Masonry Wall Tests

Rebar post-tensioned single brick masonry wall tests gave better results in understanding the behavior of wall under different post-tensioning rebar layout configurations. The results that can be drawn from these tests are listed below;

- Original wall test (1st Test) has the smallest load carrying capacity of 10 kN (Figure 6.3) and energy dissipation capacity (Figure 6.4).
- Using only vertical rebars has significantly improved the load carrying capacity from 10 kN to 65 kN as well as energy dissipation capacities.
- Applying spring box connections on vertical rebars and utilizing additional horizontal tie has slightly increased the ultimate load capacity to 78 kN, however, energy dissipation of the system has improved about 4 times as compared with the vertically post-tensioned test wall (Figure 6.4).
- Placing only diagonal rebars, resulted in another leap of increase in the ultimate load carrying capacity to 110 kN when compared with the vertically post-tensioned wall test (65 kN) and original wall test (10 kN).
- Finally, using vertical and diagonal rebars together with horizontal tie let the wall to achieve the largest lateral load capacity among the 2m wall tests with 170 kN, which is 17 times the original capacity.

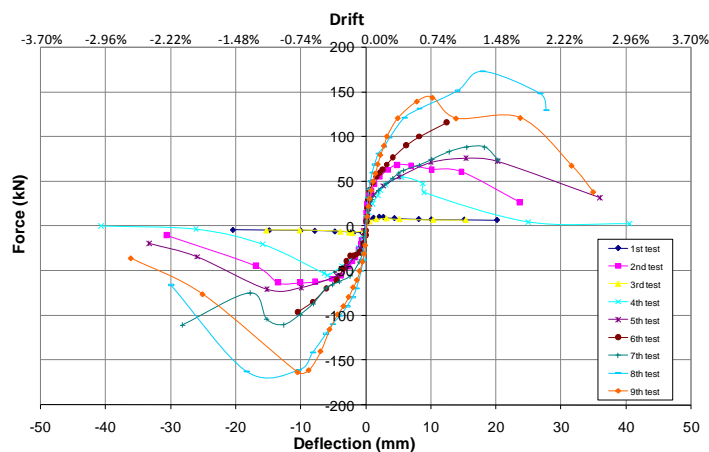


Figure 6.3 Force-Deflection Envelope Curves of rebar post-tensioned brick masonry wall tests

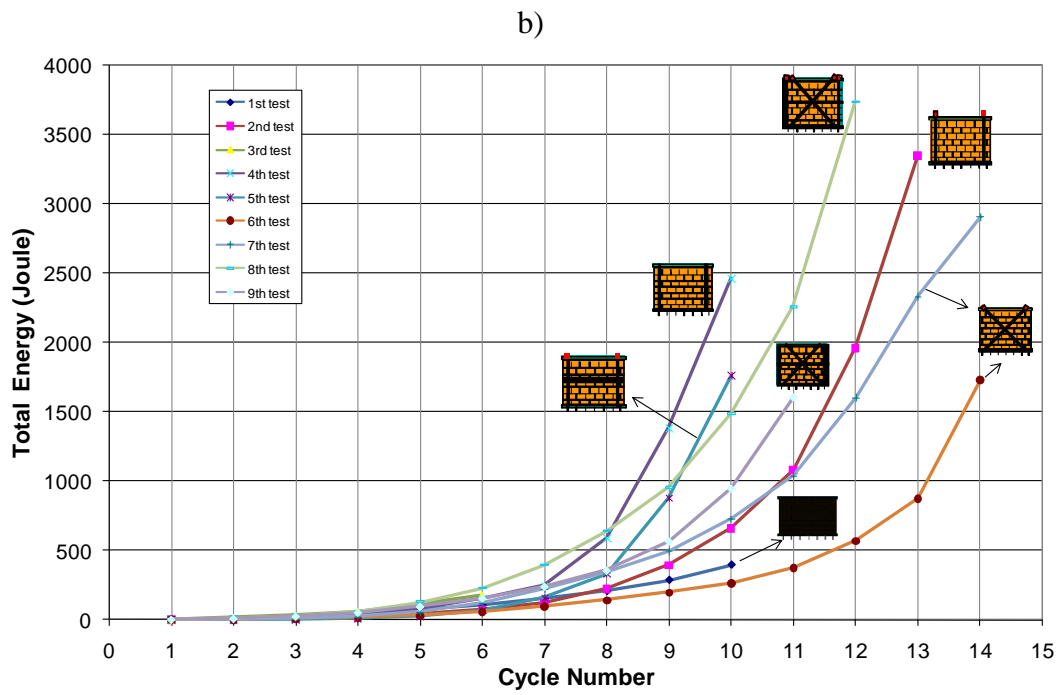
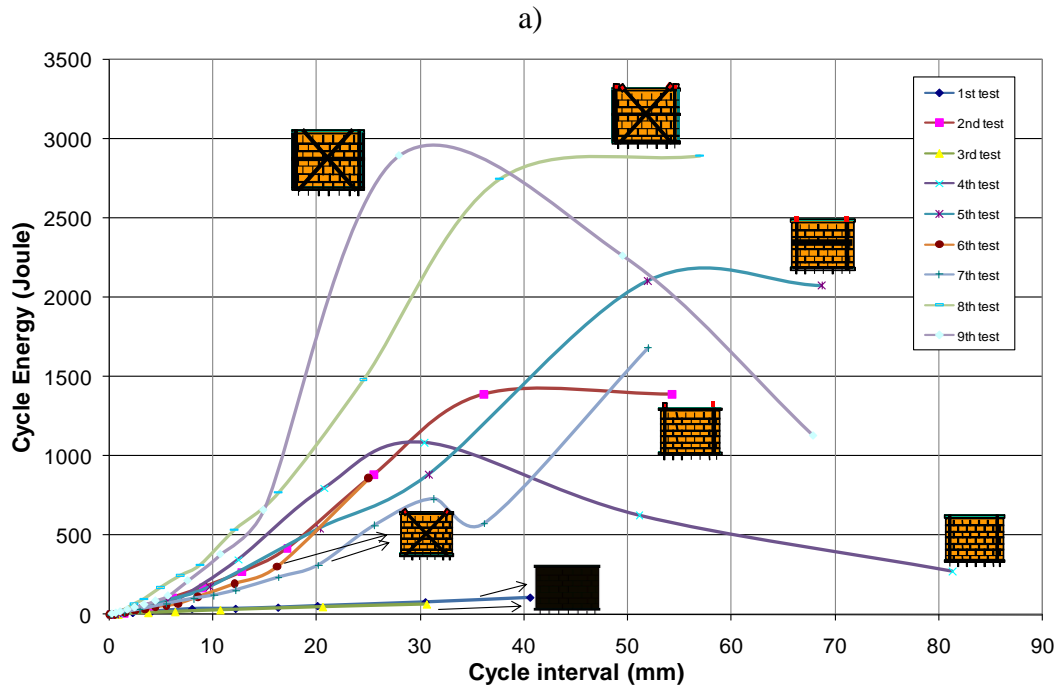


Figure 6.4 Energy Dissipation versus Total Deformation Curves of rebar post-tensioned brick masonry wall tests

Ultimate load capacities of the tests have been represented by small schematic pictures and shown in Figure 6.5. Capacity increment participation of each strengthening component used in the tests is summarized in Figure 6.6 as force and percentage contributions to the overall strength of the last capacity test, which achieved the largest horizontal force capacity of 170 kN.

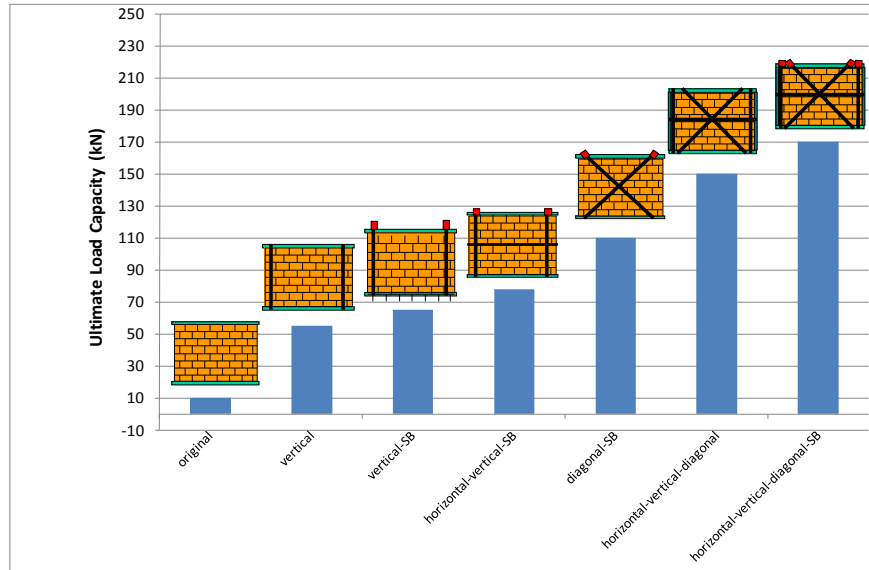


Figure 6.5 Ultimate Load Capacities of the wall tests

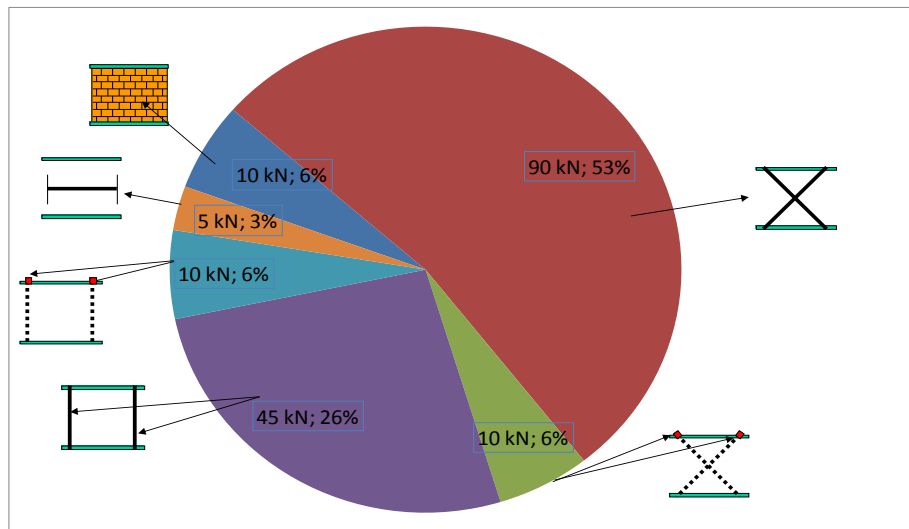


Figure 6.6 Capacity increment participation of test components

6.1.4 Damage patterns and strengthening procedures for URM walls using post-tensioning rebars

Numerous tests conducted on URM and rebar strengthened walls have shown that the failure mechanisms follow a logical pattern and ultimate capacities may be predicted using simplistic equations. Therefore, the strengthening design procedure should be first based on the existing capacity calculations and comparison against demands on each wall. If the walls need strengthening, the level of required strengthening can be checked in an iterative process by evaluating strength increase after each intervention. Vertical rebars may be adequate for some cases while diagonal bars are also needed for some other cases.

Experimental and analytical studies on walls have shown that walls with high aspect ratio (H/B) and low vertical load has a tendency to fail in flexure (rocking) mode. Increasing levels of vertical post-tensioning force application would lead to a) corner brick crushing or b) diagonal cracking (due to split + shear generated tensile stresses). If the vertical force exceeds the diagonal cracking or corner crushing capacities of the walls, diagonal rebars are also needed.

Diagonally placed rebars would start carrying load as the post-cracking deformations get larger since the masonry walls have very low cracking deformations, usually less than a millimeter. If the diagonal rebars are post-tensioned, they would start to feel the deformations at an earlier stage; nevertheless, deformations should get much larger than the cracking drifts in order to transfer forces on the diagonal rebars. Therefore, the force distribution could only be analyzed at the ultimate stage where the wall has cracked and compression strut formations are in equilibrium with the diagonally and vertically placed rebars.

When both vertical and diagonal rebars are used, the lateral force is divided between the two systems: a) vertical rebar with diagonal compression strut in masonry and b) diagonal rebar with vertical compression strut in masonry.

Experience has shown that the diagonal rebars would always yield while the vertical rebars (with the same diameter) do not exceed their yielding capacity. The capacities of the rebars should be well selected since crushing of the masonry wall corner bricks before yielding of the diagonal rebars is not a preferred mechanism. The load carried by the vertical rebar (and diagonal compression strut) may be calculated by considering the crushing capacity of the corner bricks under biaxial loading.

The procedure for strengthening of single storey brick masonry houses is given in Figure 6.7.

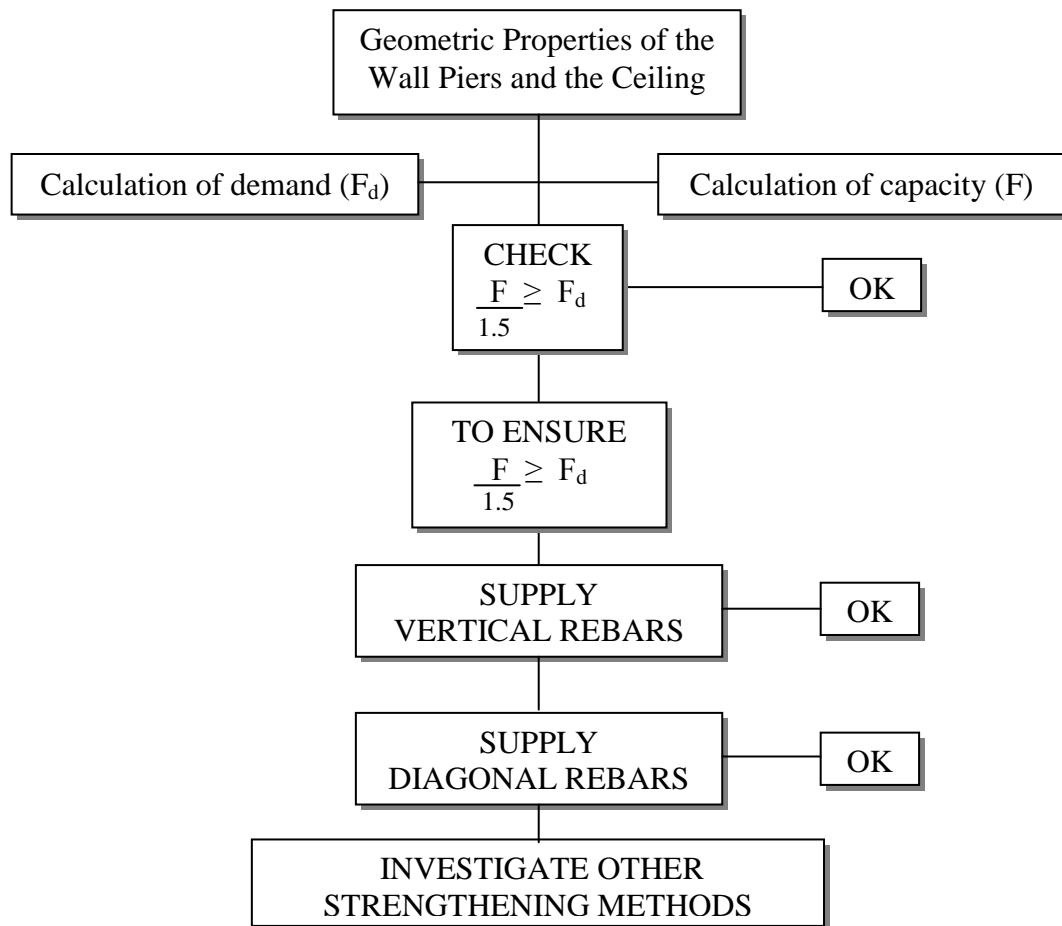


Figure 6.7 Strengthening procedure for single storey brick masonry houses

A single storey brick masonry house constitutes window and door openings placed arbitrarily on the walls. The wall segments between these openings form the piers that carry all of the mass above. Spandrels that are above and below the openings transfer the seismic forces through the piers. Failure and cracks are observed generally on the piers during a seismic activity (Figure 6.8). The pier locations and geometric properties are determined on the layout of the house as “H” refers to height, “B” refers to length and “t” refers to thickness of the pier.

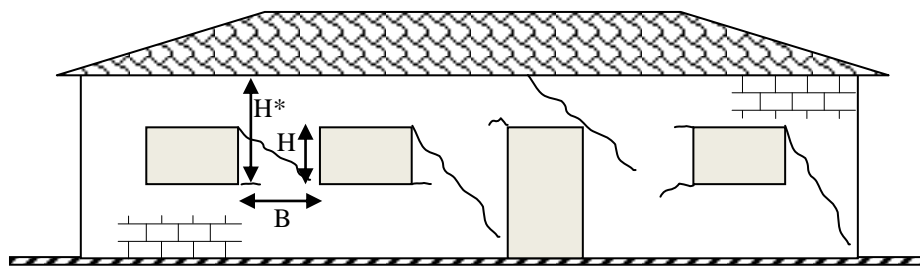


Figure 6.8 Possible crack patterns on a generic URM house

Distribution of the seismic demand force among the wall piers is calculated using Eqns. (2.10) through (2.21). The wall piers between the spandrels are assumed as fixed-fixed ended and the in-plane lateral load capacity of each wall is calculated using Eqns. (2.23) and (2.27) which are derived in Chapter 2 for rocking and diagonal shear failure, respectively. Capacity of each wall is divided by a safety factor of 1.5 and the minimum of the capacities for rocking and diagonal shear governs the failure mechanism. Rating factors of every single wall are calculated using capacities and demands of each wall. Maximum vertical load that should be applied on the house by using vertical rebars is determined from the reverse calculation of the related capacity equation of the wall that has the lowest rating factor. Final rating factors of each wall should be checked to be larger than 1.0 in order to satisfy the safety condition for rocking or diagonal shear failure.

Post-tensioning application and an example of strengthening method on Antakya house is given in the following sections.

6.1.4.1 Post-tensioning application using bolts

Bolted connections can be utilized to easily stretch post-tensioning bars using a threaded rod. Threaded rods can be welded on plain or deformed rebars and stretched using a simple nut and washer system as shown in Figure 6.9. The amount of post tensioning force can be arranged using the torque applied on the nut; however, a pre-calibration of the threaded rod – nut system is needed. The amount of torque to generate a certain amount of tensioning force in the rebar can be applied by using a torque wrench or simply measuring the applied torque using a hand wrench combined with a weighing spring placed in perpendicular direction to the wrench axis (Figure 6.9).

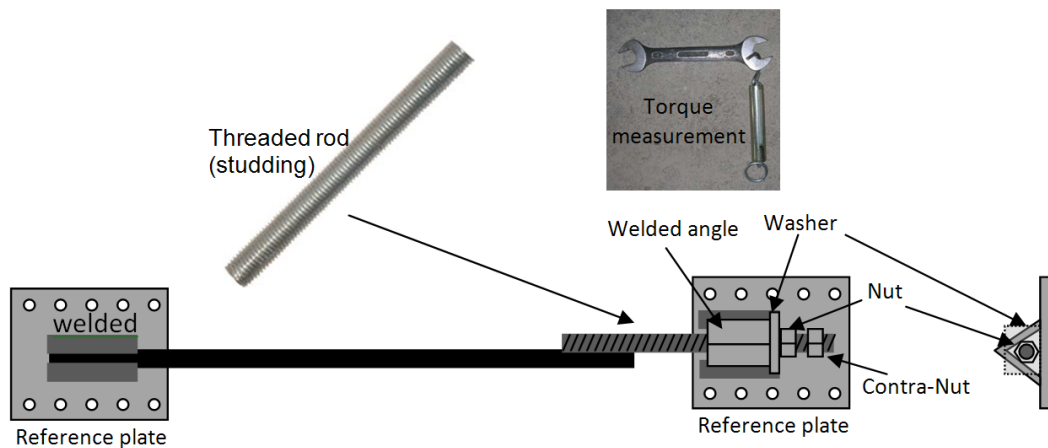


Figure 6.9 Schematic representation of post-tensioning mechanism using bolts

A general formula was developed to predict the amount of post-tensioning force as a function of the applied torque as shown in Eqn. (6.1), in which ‘f’ stands for the necessary amount of force that needs to be applied on the wrench to create torque, ‘p’ stands for the post-tensioning force in the rod, ‘s’ is the spacing between each

thread on the threaded bar, ‘r’ is the radius of the threaded bar, ‘η’ is the coefficient of friction between nut and the threaded bar, and ‘R’ is the radius of wrench between centroid of the threaded bar and wrench end where force ‘f’ is applied by hand. Calibration studies have shown that ‘η’ can be taken as 0.3; however, existence of oil on the threaded bar surface reduces the ‘η’ value. Although oil existence or application may reduce the amount of torque applied by the wrench, it is important to lock the nut in place with a contra-nut to prevent post-tensioning losses due to loosening of the nut.

$$f = p \times \left(\frac{s}{2\pi r} + \eta \right) \times \frac{r}{R} \quad (6.1)$$

6.1.4.2 Example application using Antakya house and cost evaluation

Strengthening of the URM house that is given in Figure 2.10 in section 2.1.3.1 is expressed in this section. Also approximate cost was simply calculated using the materials included in strengthening of the house and compared against the overall house value. Layout of the wall piers is given in Figure 2.11 and data of the numbered walls is tabularized in Table 6.1. Firstly, seismic acceleration was assumed to act in the longitudinal (x) direction of the house.

Table 6.1 Wall data of the example house in longitudinal direction

Wall	H (mm)	H* (mm)	B (mm)	λ	K_i (N/mm)	P_i (N)
5	1200	1800	1450	1.24	82635	31872
6	1200	1800	1750	1.20	105902	38466
7	1200	1800	1900	1.19	117391	41763
8	1200	1800	1900	1.19	117391	41763
9	1200	1800	1750	1.20	105902	38466
10	2000	2600	1450	1.41	37267	31872
11	1200	1800	1450	1.24	82635	31872
12	1200	1800	1750	1.20	105902	38466
13	1200	1800	1900	1.19	117391	41763
14	1200	1800	1900	1.19	117391	41763
15	1200	1800	1750	1.20	105902	38466
16	2000	2600	1450	1.41	37267	31872

Elastic modulus and tensile strength of the mortar was assumed as 2100 MPa and 0.3 MPa, respectively. The thickness of the brick-mortar interactions was taken as 120 mm. Stiffness of each wall was calculated using Eqn. (2.11). Total mass of the house over the wall piers was approximately obtained as 106 tons and seismic demand on the house considering $a_0=0.3$ g ground acceleration was calculated about 391 kN using Eqn. (2.17). Total weight of about 1060 kN was distributed among the wall piers according to their area ratios. Horizontal seismic demands on each wall were obtained using the stiffness ratios of the walls. Seismic demands, rocking and diagonal shear capacities (with a safety factor of 1.5), and rating factors of each wall are tabulated in Table 6.2. The lowest rating factor was found to be 0.53 and belongs to the walls numbered as “5” and “11”, which exhibits rocking motion during a seismic activity. These walls were taken as reference in strengthening of the URM house, such that even the weakest wall will remain in its elastic range during a seismic activity.

Table 6.2 Demands, strengths, and rating factors of the wall piers in longitudinal direction

Wall	Demand F_{di} (kN)	Rocking F_i (kN) (divided by 1.5)	Diagonal F_i (kN) (divided by 1.5)	RF Rocking	RF Diagonal
5	29	15	35	0.53	1.24
6	37	22	44	0.60	1.21
7	41	26	49	0.64	1.20
8	41	26	49	0.64	1.20
9	37	22	44	0.60	1.21
10	13	10	31	0.81	2.44
11	29	15	35	0.53	1.24
12	37	22	44	0.60	1.21
13	41	26	49	0.64	1.20
14	41	26	49	0.64	1.20
15	37	22	44	0.60	1.21
16	13	10	31	0.81	2.44

The necessary vertical post-tensioning force to be applied on the house using vertical rebars can be obtained by iterating the Eqn. (2.27) to safely carry the earthquake demand forces on the walls. Consequently, a total of about 1061 kN vertical post-tensioning force should be applied on the URM house to maintain the “no-crack” condition of the wall piers (Table 6.3). Diagonal shear failure was also checked with the applied additional 1061 kN of vertical force on the house in Table 6.4.

Table 6.3 Required vertical force on the URM house

Wall	Required P_i (kN)	Required total P (kN)
5	75	1061
6	68	791
7	63	673
8	63	673
9	68	791
10	20	279
11	75	1061
12	68	791
13	63	673
14	63	673
15	68	791
16	20	279

Table 6.4 Checking of the walls against diagonal shear failure due to applied vertical post-tensioning on the URM house

Wall	P_i (kN)	Diagonal F_i (kN) (divided by 1.5)	RF Diagonal
5	45	38	1.34
6	54	48	1.30
7	59	52	1.29
8	59	52	1.29
9	54	48	1.30
10	45	34	2.62
11	45	38	1.34
12	54	48	1.30
13	59	52	1.29
14	59	52	1.29
15	54	48	1.30
16	45	34	2.62

If the seismic acceleration was assumed to act in the transverse direction (y) of the URM house, the same procedure was applied by considering the walls numbered

as “1”, “2”, “3”, and “4” as in-plane resisting walls. However, the walls in transverse direction satisfy the safety condition and there is no need to improve the house in transverse direction (Table 6.5 and Table 6.6).

Table 6.5 Wall data of the example house in transverse direction

Wall	H (mm)	H* (mm)	B (mm)	λ	K_i (N/mm)	P_i (N)
1	2400	2400	7500	1.09	253836	164853
2	2400	2400	6500	1.11	217611	142873
3	2400	2400	6500	1.11	217611	142873
4	2400	2400	7500	1.09	253836	164853

Table 6.6 Demands, strengths, and rating factors of the wall piers in transverse direction

Wall	Demand F_{di} (kN)	Rocking F_i (kN) (divided by 1.5)	Diagonal F_i (kN) (divided by 1.5)	RF Rocking	RF Diagonal
1	105	302	209	2.87	1.98
2	90	227	178	2.51	1.98
3	90	227	178	2.51	1.98
4	105	302	209	2.87	1.98

Calculated post-tensioning force of 1061 kN can be applied on the house using about 27 ϕ 16mm rebars, which are all post-tensioned to 40 kN force. Total of about 16 m 200mm X 10mm steel plates which are connected to the slab using about 128 steel dowels are used. Threaded rods (Figure 6.9) about 400 mm in length (ϕ 16mm) are used at the ends of the rebars to adjust the post-tensioning force of the bar with the bolts. All of the materials used in the strengthening of the house costs about 1000 TL which can be increased up to about 2000 TL including the workmanship. On the other hand, according to the “Ministry of Public Works and Settlement”, each m^2 of the URM house costs about 114.65 TL, which results in a total of about 15000 TL (17.5m X 7.5m X 114.65 TL) only for construction of

the house. The cost of the demolishing and reconstructing of the URM house can rise up to about 20000 TL, which may lead to a reasonable result that the strengthening of the house is preferable in that case.

6.2 Conclusions

The following conclusions were derived based on the analytical and experimental studies conducted in this thesis:

- a. When masonry walls have small vertical loads acting on them, such as in the case of single storey houses, and with high aspect ratios, the walls have a tendency to separate from the base due to tension and form a failure mechanism similar to a rigid rectangle rotating over its bottom corner (flexure or rocking mode of failure).
- b. In-plane post-tensioning of masonry walls in the vertical direction would delay the tension crack formation at the base and therefore would improve the initial cracking strength of the walls in the linear range.
- c. Vertical force may be easily and economically applied using post-tensioning rebars in the vertical direction. However, when the walls exceed their cracking capacity, minor crushing of the walls would result in rapid loss of vertical post-tensioning and lead to premature failure.
- d. Spring box usage at the top ends of post-tensioning rebars had favorable effects in post-cracking performance of the masonry walls at all brick masonry wall tests, since shortening of the walls due to crushing could be better tolerated without losing majority of the post-tensioning force.
- e. Increasing the vertical load acting on masonry walls is found to be a very efficient way to improve lateral load capacity in the nonlinear range as well, especially since the URM and slender walls have very low ultimate capacity governed by the rocking mode. The ultimate capacity in the post-cracking range would linearly increase as a function of the vertical force

- since vertical force would have a resisting effect on the rotation (rocking) motion. Energy dissipation capacities are also enhanced by post-tensioning.
- f. Further increase in the vertical load would result in corner crushing and/or diagonal crack opening that would alter the governing failure mechanism.
 - g. At the ultimate loading stage of brick masonry walls, the walls were totally damaged due to excessive crushing at the base towards the corners when diagonal rebars were used. Base sliding damage was observed only when vertical rebars were used together with horizontal rebars throughout the wall tests.
 - h. Horizontally placed rebars have not significantly increased the ultimate capacity of the walls under various rebar arrangement.

6.3 Future studies

Future studies that were outside the scope of this thesis but raised interest during different phases of this study are listed below. These ideas might be investigated by future researchers.

- Optimization of the level of post tensioning and rebar inclination for the best performance of URM brick walls.
- Investigate the strengthening using rebars for different material other than brick blocks (such as adobe, stone masonry, etc).
- Investigate multiple storey masonry house strengthening techniques.
- Investigate, strengthening using different forms of steel (such as metal sheet located on the outer surface of the URM wall) or different materials (such as CFRP or wire-mesh with plaster).

REFERENCES

- [1] DİE – State Institute of Statistics Prime Ministry Republic of Turkey (2000) Building Census
- [2] Franklin L. Moon, Tianyi Yi, Roberto T. Leon, and Lawrence F. Kahn, *Recommendations for Seismic Evaluation and Retrofit of Low-Rise URM Structures*, Journal of Structural Engineering ASCE (2006) 663-672
- [3] G. Magenes, G.M. Calvi, *In-plane seismic response of brick masonry walls*, *Earthquake Engineering and Structural Dynamics*, Vol 26 (1997) 1091-1112
- [4] Miha Tomazevic, *Earthquake-Resistant Design of Masonry Buildings*, (1999)
- [5] R.Cardoso, M.Lopes, R.Bento, *Seismic evaluation of old masonry buildings, Part I: Method description and application to a case-study*, *Engineering structures* 27 (2005) 2024-2035
- [6] M. Corradi, A. Borri, A. Vignoli, *Experimental study on the determination of strength of masonry walls*, *Construction and Building Materials* 17 (2003) 325-337
- [7] Mohamed A. ElGawady, Pierino Lestuzz, Marc Badoux, *Shear strength of URM walls retrofitted using FRP*, *Engineering Structures* 28 (2006) 1658-1670
- [8] Pere Roca, *Assessment of masonry shear-walls by simple equilibrium models*, *Construction and Building Materials* 20 (2006) 229–238

- [9] Jocelyn Paquette, Michel Bruneau, *Pseudo-dynamic testing of unreinforced masonry building with flexible diaphragm and comparison with existing procedures*, Construction and Building Materials 20 (2006) 220–228
- [10] D. Benedetti, P. Carydis, and P. Pezzoli, *Shaking Table Tests on 24 Simple Masonry Buildings*, Earthquake Engineering and Structural Dynamics, Vol. 27, (1998) 67–90
- [11] N.G. Shrive, *The use of fiber reinforced polymers to improve seismic resistance of masonry*, Construction and Building Materials 20 (2006) 269–277
- [12] A. M. Holberg and H. R. Hamilton III, *Strengthening URM with GFRP Composites and Ductile Connections*, Earthquake Spectra Vol. 18 (2002) 63-84
- [13] Gustavo Tumialan and Antonio Nanni, *Strengthening of Masonry Walls with FRP Bars*, Composites Fabricator Magazine, March 2002, Arlington, VA
- [14] Istvan Kotorman and Miklos Ivanyi, *Numerical Examination of Different Masonry Strengthening Methods*, 2nd Int. PhD Symposium in Civil Engineering 1998 Budapest
- [15] Rai D.C., Goel S.C., *Seismic strengthening of unreinforced masonry piers with steel elements*, Earthquake Spectra Vol 12 (1996) 845-862
- [16] S. Altın, F. Kuran, M.E. Kara, and Ö. Anıl, *Yığma Yapıların Rehabilitasyonu İçin Bir Yöntem*, YDGA2005 - Yığma Yapıların Deprem Güvenliğinin Arttırılması Çalıştayı, 17 Şubat 2005, Orta Dogu Teknik Üniversitesi, Ankara.
- [17] C. V. R. Murtyl, Jayanta Dutta, and S. K. Agrawal, *Twin lintel belt in steel for seismic strengthening of brick masonry buildings*, Earthquake Engineering and Engineering Vibration Vol. 3 (2004) 215-222

[18] Chiara Calderini, Serena Cattari, and Sergio Lagomarsino, *In-plane strength of unreinforced masonry piers*, Earthquake Engineering and Structural Dynamics, (2008) EQE-08-0140.R1

[19] Ahmet Türer, Abdullah Dilsiz, *Yığma Yapıların Deprem Güvenliğinin Arttırılması Çalıştayı - YDGA*, February 2005, METU

APPENDIX A

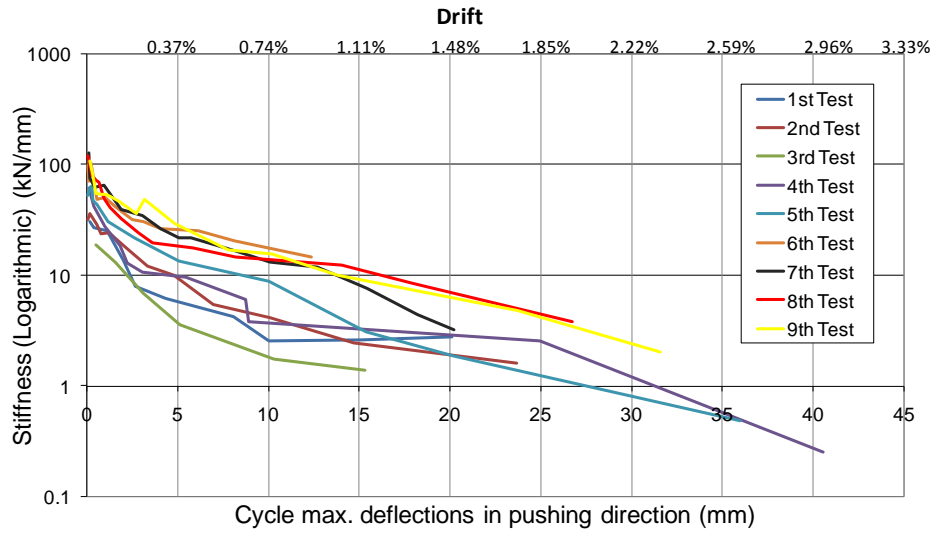


Figure a) Initial stiffness decrement of the brick wall tests (calculated using initial slopes of the force-deflection curves).

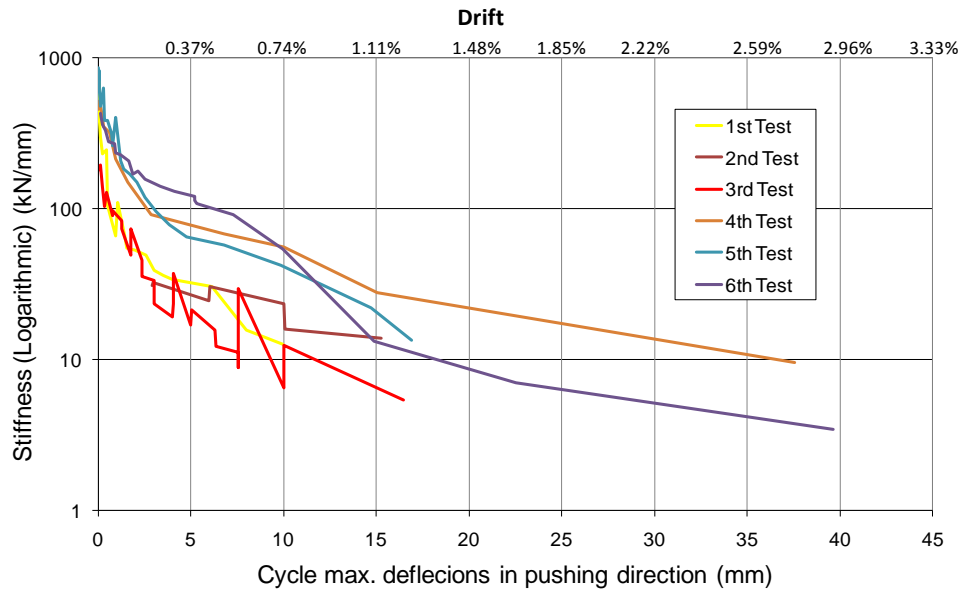


Figure b) Initial stiffness decrement of the half-scale brick house tests (calculated using initial slopes of the force-deflection curves).